ENZYMOLOGY AT THE DIMER INTERFACE OF CYTOSOLIC GLUTATHIONE S-TRANSFERASES

by

Robert Patrick Lyon

A dissertation submitted in partial fulfillment of the requirements for the degree of

Doctor of Philosophy

University of Washington

2002

Program authorized to offer degree: Medicinal Chemistry

UMI Number: 3072112

UMI Microform 3072112

ProQuest Information and Learning Company
300 North Zeeb Road
P.O. Box 1346
Ann Arbor, MI 48106-1346

Doctoral Dissertation

In presenting this dissertation in partial fulfillment of the requirements for the Doctoral degree at the University of Washington,
I agree that the Library shall make its copies freely available for inspection. I further agree that extensive copying of the dissertation is allowable only for scholarly purposes, consistent with "fair use" as prescribed in the U.S. Copyright Law. Requests for copying or reproduction of this dissertation may be referred to Bell and Howell Information and Learning,
300 North Zeeb Road, P.O. Box 1346, Ann Arbor, MI 48106-1346, or to the author.

Signature 

Date 10-28-02

University of Washington

Graduate School

This is to certify that I have examined a copy of a doctoral dissertation submitted by

Robert Patrick Lyon

and have found that it is complete and satisfactory in all respects,
and that any and all revisions required by the final
examining committee have been made.

Chair of Supervisory Committee:

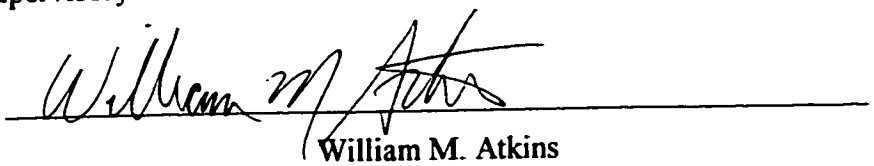

William M. Atkins

Reading Committee:

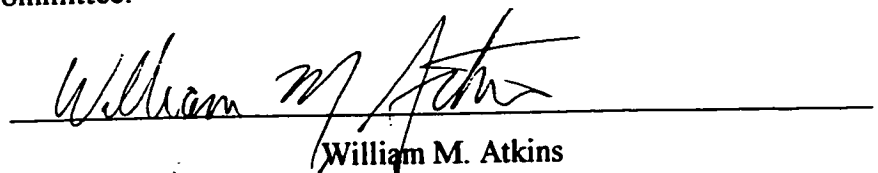

William M. Atkins

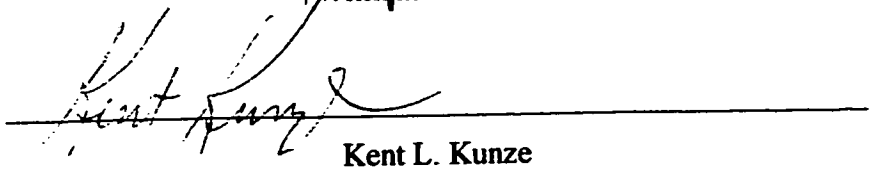

Kent L. Kunze

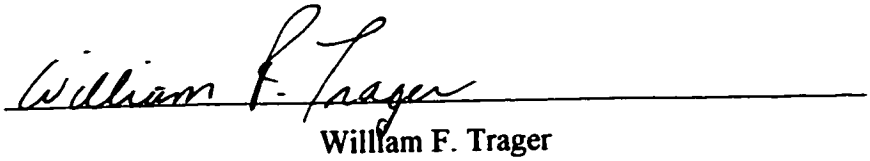

William F. Trager

Date: 10-28-02

ABSTRACT

University of Washington

Abstract

Enzymology at the Dimer Interface of Cytosolic Glutathione S-Transferases

by Robert Patrick Lyon

Chairperson of the Supervisory Committee

Professor William M. Atkins
Department of Medicinal Chemistry

The glutathione S-transferases (GSTs) represent a family of cytosolic enzymes whose primary function is the detoxification of electrophilic chemical species of endogenous and exogenous origin. As described in the introductory chapter (Chapter 1) these enzymes exist as homodimers and exhibit a broad, solvent-accessible cleft above the dimer interface. This interface region represents an area of active research in GST enzymology, as it is purported to be a ligand binding site, and it lies directly between the two active sites of the GST dimer. We exploited this geometry to design bifunctional inhibitors of this enzyme which simultaneously occupy both active sites by spanning the intersubunit cleft (Chapter 2). Such inhibitors may be desirable as adjuvants to cytotoxic tumor chemotherapy, as GSTs are believed to play a key role in acquired resistance to these important drugs. We also prepared chemically modified GST in which the chemical environment of the intersubunit cleft is altered (Chapter 3). The results of these studies suggest that many ligands which have been reported by other researchers to bind in the intersubunit cleft may actually bind at the active site. Finally, Chapter 4 describes an unusual property of the GST cofactor, glutathione, which was discovered during the above studies—in polar organic solvents, glutathione disulfide appears to self-assemble to form extensive intramolecular arrays which tangle and result in gelation of the solvent. This self-assembly property is highly specific and depends on the unusual geometry of the tripeptide glutathione.

TABLE OF CONTENTS

LIST OF FIGURES

LIST OF TABLES

GLOSSARY

List of Abbreviations

CDNB : chloro-2,4-dinitrobenzene, a substrate of many glutathione S-transferases which is employed in the most common diagnostic assay.

CNBC : 4-chloro-3-nitrobenzoyl chloride, a precursor in the synthesis of glutathionyl nitrophenyl derivatives discussed in Chapter 2.

DTT : dithiothreitol, a disulfide reducing agent.

FRET : fluorescence resonance energy transfer

GS- : prefix representing the glutathionyl moiety of a glutathione conjugate. For example, GS-benzyl and GS-hexyl are the products of glutathione conjugation with benzyl bromide and bromohexane, respectively.

GSH : glutathione, γ-glutamyl-cysteinyl-glycinyl, in its reduced state bearing a reactive thiol.

GSSG : glutathione disulfide. Also called oxidized glutathione, although this term lacks precision as there are multiple species which represent various oxidation states of glutathione. Examples include glutathione sulfenic acid (GSOH), glutathione sulfonic acid (GSO_3H), and disulfide species such as glutathione disulfide sulfoxide (GSSOG).

GST : glutathione S-transferase, an enzyme family catalyzing the conjugation of reduced glutathione to an electrophilic substrate.

HNE : 4-hydroxynonenal, a product of lipid peroxidation and GST substrate.

LCA : lithocholic acid, a bile acid.

EDS : estradiol disulfate, a steroid derivative.

EA : ethacrynic acid, (a phenoxyacetic acid derivative) a diuretic drug containing an α, β-unsaturated ketone which is a GST substrate. Its glutathione conjugate is an inhibitor of several GST isoforms.

ACKNOWLEDGEMENTS

It has been my privilege to study with Dr. Bill Atkins and I thank him for the many research opportunities which he provided me, a few which are described in the pages which follow. Our many discussions, conversations, and good-natured arguments have contributed enormously to my growth as a scientist. I also wish to thank several members of Bill's lab who have helped me in many ways throughout my time here. They include Michael Dabrowski, Dr. Eric Dietze, Dr. Catherine Ibarra, Dr. Brenda Nieslanik, Doug Lu, and Josh Pearson. I would also like to express my gratitude to Dr. Alana Upthagrove and Dr. Siddhartha Sarma for their assistance and advice. Finally, I would like to thank the Department of Medicinal Chemistry for the opportunity to study here and the many graduate students and others in the department with whom I have had the pleasure to spend much of my free time over the last several years.

DEDICATION

To Susan D. Lyon,

my wife,

whose considerable patience has made this possible.

CHAPTER 1

INTRODUCTION

1.1 Glutathione S-transferases

The glutathione S-transferases (GSTs) are a family of cytosolic proteins with multiple known functions (Mannervik, 1985). The family takes its name from their most well-documented function, the catalytic activity wherein the nucleophilic tripeptide glutathione (GSH, γ-glu-cys-gly) is conjugated to structurally diverse hydrophobic electrophiles. Examples of the substrates for GSTs and the products of glutathione conjugation catalyzed by these enzymes are shown in Figure 1.1. This glutathione conjugation activity serves to detoxify foreign electrophiles as well as reactive products of oxidative stress (Mannervik, 1988). Moreover, some of the reactions catalyzed by GSTs are part of the biosynthetic pathway of endogenous compounds including leukotriene A4 and prostaglandin H2 (Armstrong, 1994). The GSTs are a remarkably ubiquitous enzyme family amongst aerobic organisms, having been identified in plants, fungi, yeast, bacteria, and of course in all manner of animals (Wilce and Parker, 1994). This occurrence across kingdoms throughout the biosphere underscores their relevance as detoxification enzymes, particularly with respect to reactive oxygen species.

Several different isoforms of these enzymes have been characterized and grouped by sequence similarity into classes A, P, M, T, K, Z, and S [1] (Mannervik *et al.*, 1992);

each class contains multiple subclasses identified numerically (e.g. A1, A2, P1, etc.). The enzymes exist as dimers wherein each subunit contributes a catalytically independent

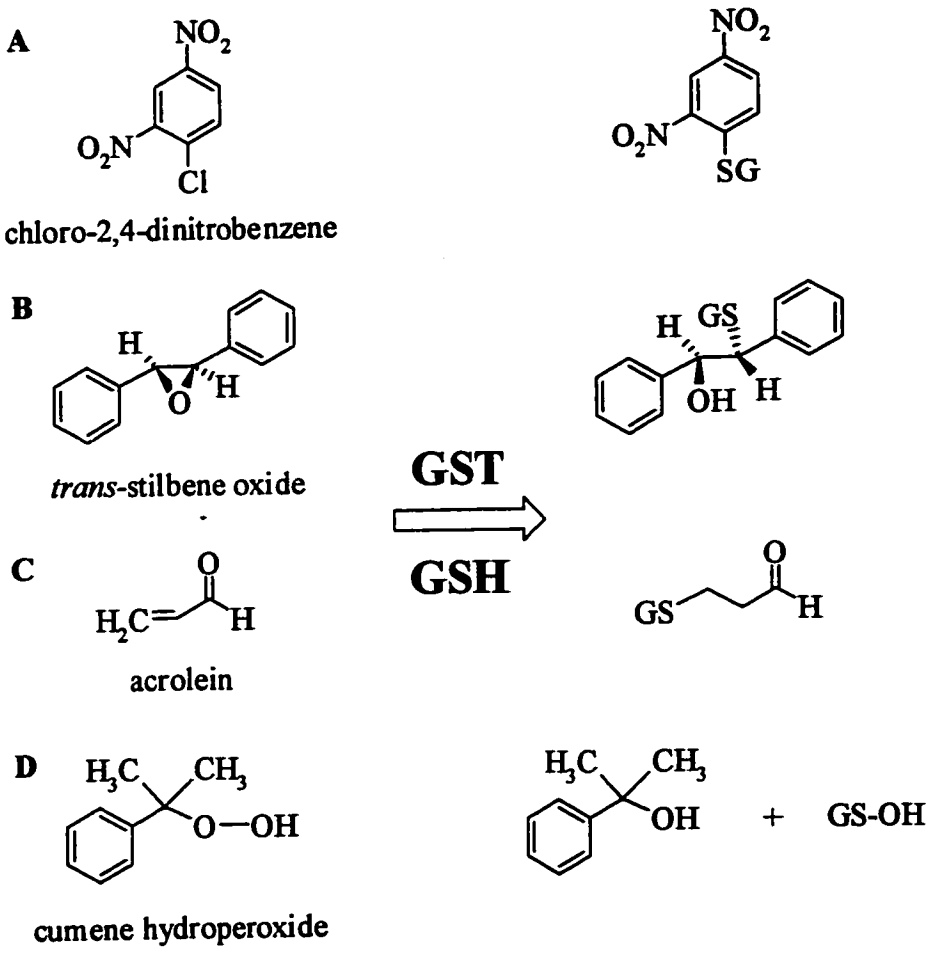

Figure 1.1: Representative GST substrates and products; A, nucleophilic substitution of CDNB is the most widely used GST assay; B, nucleophilic addition to epoxides such as *trans*-stilbene oxide is catalyzed with effeciency by M-class GSTs; C, conjugate addition to α, β-unsaturated carbonyls such as acrolein; D, cumene hydroperoxide is rapidly metabolized by class A GSTs, producing glutathione sulfenic acid (GS-OH) which undergoes further reaction with GSH to generate GSSG and water.

active site, and the intact dimer is thus properly designated by the class as well as the subclass of the two monomers. For example, GST A1-1 is a homodimer consisting of two monomers of GST A1. The formation of heterodimers within a given class (but not between classes) is possible; for example, GST A1-2 consists of one monomer of A1 and one monomer of A2. Despite the existence of such a large number of isoforms, only a handful have been found to be expressed at high levels in human tissues (Armstrong, 1997). The major human isoforms (and the tissues in which they are expressed) are A1 (liver, kidney), P1 (brain, lung, placenta), and M1(liver). It should be noted that there also exists a non-cytosolic GST which is localized to the membrane of the endoplasmic reticulum. This 'microsomal' GST is structurally unrelated to the cytosolic GSTs and appears to be a product of convergent evolution; that is, the microsomal and cytosolic GSTs independently evolved a glutathione transferase enzymatic activity. This dissertation deals only with the cytosolic GSTs and no further discussion will be made of the microsomal enzyme.

1.1.1 GST Structure

Despite a sequence homology of less than 30% between the GST classes, they all share a canonical protein fold which is illustrated in Figure 1.2. The homodimer of GST P1-1 in complex with glutathione-dinitrobenzene (GS-DNB) is shown, and the C2 symmetry of the complex is evident when viewed along the twofold symmetry axis (Figure 1.2, top). When viewed perpendicular to this axis (Figure 1.2, bottom), the most

notable feature of the structure is the large, V-shaped cleft between the two subunits. Each subunit possesses a catalytically independent active site, consisting of a glutathione binding subsite ('G-site') and a hydrophobic substrate site ('H-site'). In Figure 1.2, these sites are occupied by the glutathione (yellow) and dinitrobenzyl (red) moieties, respectively, of GS-benzyl. Numerous crystallographic studies (Sinning *et al.*, 1993; Cameron *et al.*, 1995; McTigue *et al.*, 1995; Oakley *et al.*, 1999) have clearly identified these sites, with the observation that the residues contributing to the G-site are well conserved across GST classes, whereas those of the H-site are highly variable and thus produce the varying hydrophobic substrate specificities of the different isoforms.

Each subunit folds in such a way as to produce two distinct domains, referred to simply as the C-terminal and N-terminal domains. The C-terminal domain, which contains the majority of the protein sequence, is comprised of five separate α-helices. Two of these helices (4 and 5) are greater than 40 Å in length and extend along the dimer interface to form the sides of the V-shaped intersubunit cleft (Figure 1.2). Helix 4 also contains several residues which define the hydrophobic binding site. For nearly 3 turns of this helix, the residues approximate a repeating hydrophobic-hydrophilic-hydrophobic motif; the first hydrophobic residue is buried, the hydrophilic residue lines the intersubunit cleft, and the second hydrophobic residue lies in the H-site. Since most of the residues which make up the H-site are in the C-terminal domain, it is largely sequence variations within this domain which result in the different substrate specificities of individual GST isoforms.

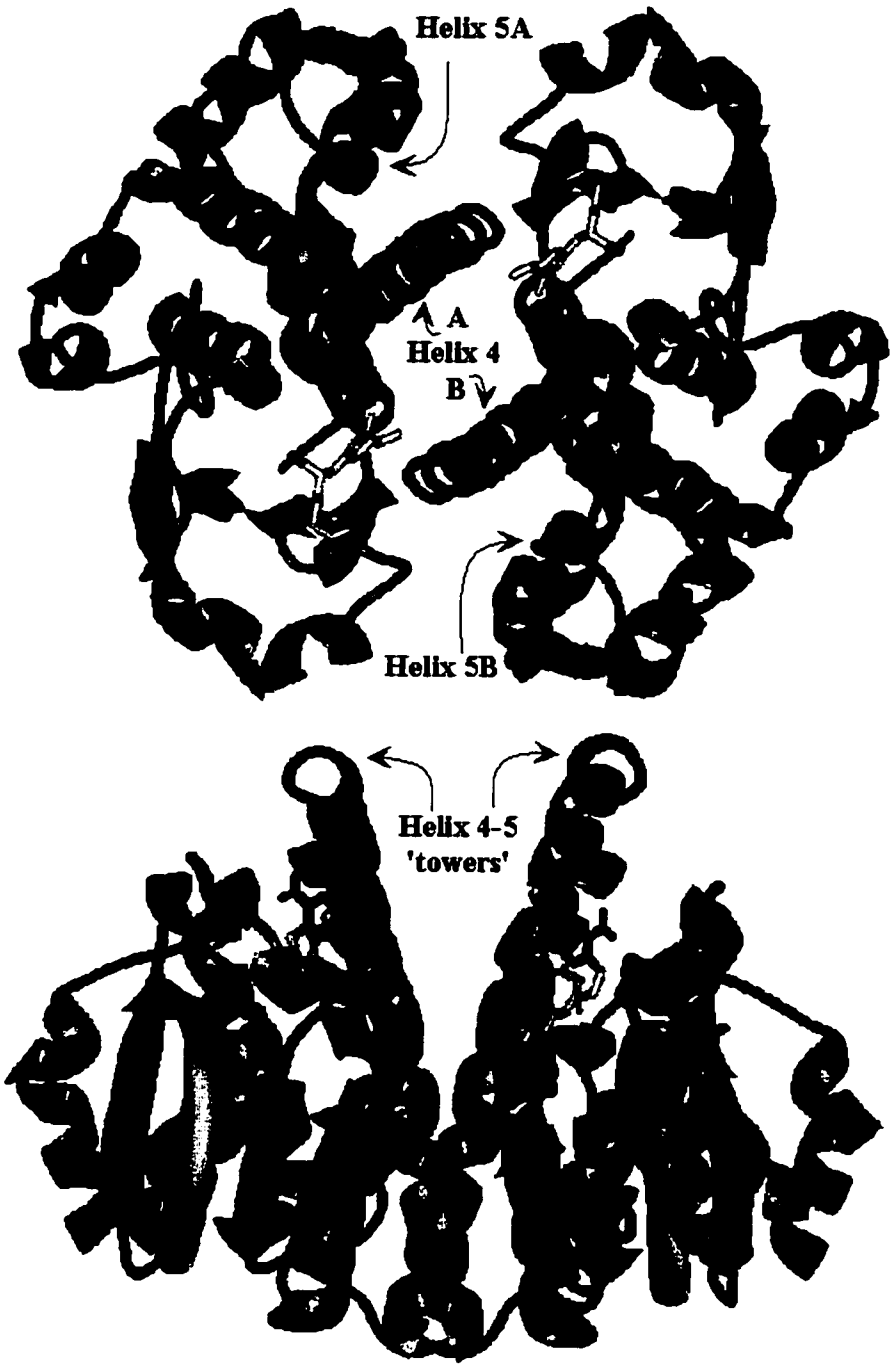

Figure 1.2: Crystal structure of GST P1-1 in complex with glutathione-dinitrobenzene. Glutathione moieties are shown in yellow, dinitrophenyl moieties in red. Top, the intact dimer viewed along the C2-symmetry axis; bottom, viewed perpendicular to this axis.

The N-terminal domain represents about 30% of the protein and is a mixed α-helix and β-sheet structure. The amino acid residues which comprise the G-site are contained within this domain. As would be expected for such a hydrophilic and highly charged species as glutathione, these residues bind GSH via hydrogen bonding and electrostatic interactions (Figure 1.3). The free amino group of glutathione forms a salt bridge with an aspartyl residue which resides on helix 4 of the opposite subunit, a feature conserved across GST isoforms. Thus, proper dimerization and the environment of the dimer interface contribute to glutathione binding and are important to the catalytic function of this enzyme. This has been confirmed by one study in which structured monomers were isolated as unfolding intermediates, but these species exhibited no glutathione transferase activity (Wilce and Parker, 1994).

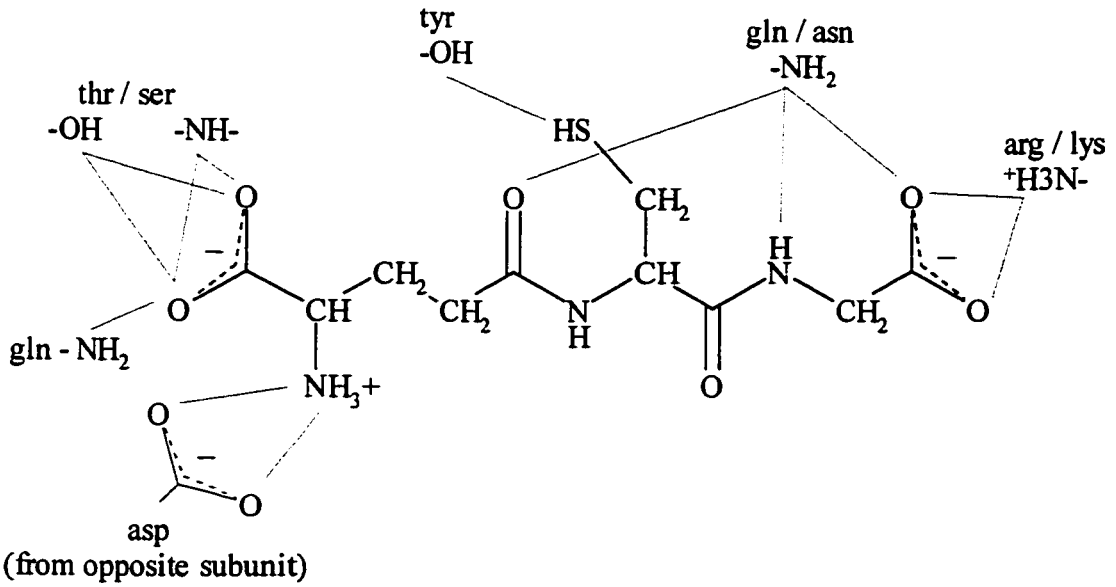

Figure 1.3: Electrostatic interactions involved in GSH binding to GST. These G-site residues are well-conserved across GST isoforms, with three conservative mutations as shown. Specific interactions are shown in magenta for clarity.

The dimerization of GST subunits is driven by interactions between the C-terminal domain of one subunit and the N-terminal domain of the adjacent subunit. These interactions include both electrostatics (salt bridging and hydrogen bonding) as well as hydrophobic interactions. In the latter category, one particular interaction is observed which has been aptly described as a ball-and-socket joint (Armstrong, 1997). A conserved phenylalanine residue in the N-terminal domain represents the ball, and in the intact dimer it inserts into a hydrophobic socket located between the long helices 4 and 5 of the C-terminal domain on the other subunit. In GST A1-1 (Figure 1.4), this socket is formed by the confluence of several structural features: two small residues, gly 98 and ala 135, which face each other and create space between the helices; the presence of pro 134 on the outside of helix 5 which induces a kink adjacent to this space; and two aromatic residues, tyr 132 and phe 136, on consecutive turns of helix 5 between which the 'ball' (phe 52) intercalates. The geometry of this arrangement may be a major contributor to the class recognition such that heterodimers within a class (e.g. A1-2) are possible but heterodimers between classes (e.g. P1-A1) are not. This ball-and-socket joint is only observed in the major human isoforms (A, M, and P); the dimer interfaces of the S and T classes are more hydrophilic in character, while structures of the other GST classes have not yet been solved.

In the major human isoforms the total surface area which is buried upon dimerization (and thus stabilizing the dimeric state) is about 1500 $Å^2$, which represents a modest 13% of the solvent-accessible surface area (Wilce and Parker, 1994; Armstrong, 1994). This value would be greater if not for the fact that helices 4 and 5 (which

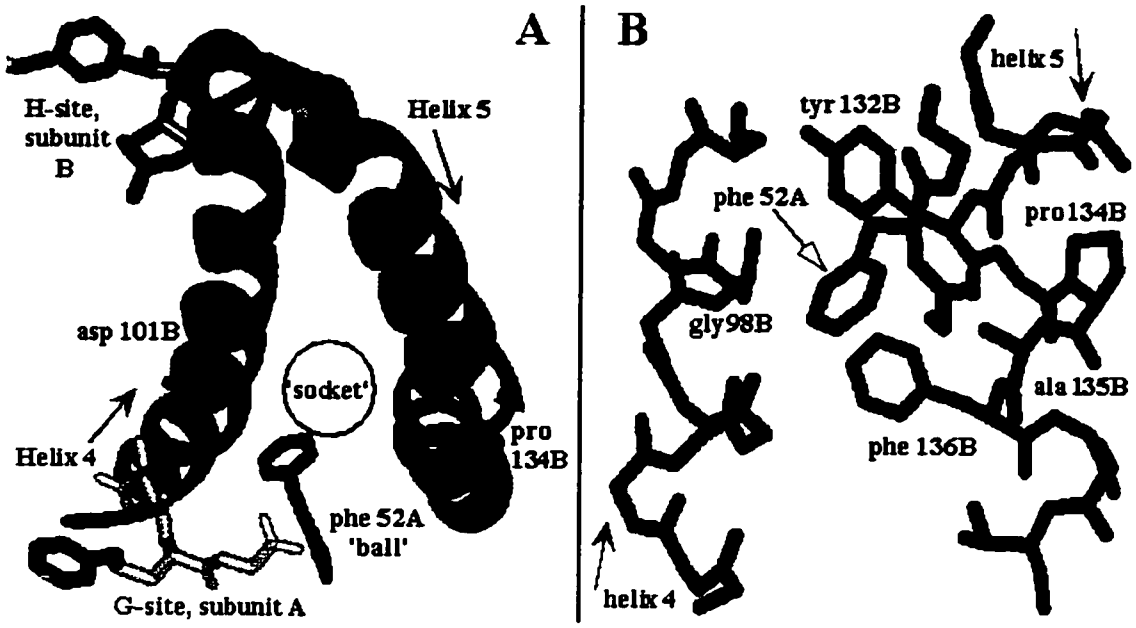

Figure 1.4: The 'ball and socket' interface of GST A1-1. **A**, an overall view of the helix 4-5 tower showing the position of the 'ball' (phe 52A[2], magenta) and 'socket' with respect to other structural features: asp 101B (blue), which forms a salt bridge with glutathione (yellow) bound to subunit A, denoted by short green dashes; several hydrophobic residues on helix 4 which contribute to the H-site on subunit B (red); pro 134 (cyan), which helps to form the kink in helix 5. **B**, detailed view of the residues on helices 4 and 5 which contribute to the 'socket;' the side chains are shown for the residues in cyan (see text for discussion).

contribute much of the buried surface area) diverge away from the dimer interface, thus creating the large V-shaped cleft and the helical 'tower' structures which are such a striking feature of the cytosolic GSTs. Without this divergence, greater dimerization energy could be achieved, but the intersubunit cleft would not exist. This fact, coupled with the observation by crystallography that the helix 4-5 towers are among the most

dynamic structural elements on the protein, suggests that the towers and/or the cleft which they create have specific functional consequences.

In summary, the intact dimer presents an interface which is integral with the active site of each subunit, and the two subunits are separated by the solvent-accessible V-shaped intersubunit cleft formed by the helix 4-5 towers of each subunit. It is the geometry of these features about the dimer interface which forms the basis of the project described in Chapter 2 of this dissertation.

1.1.2 GST Functions

As already noted, the most well-characterized function of the GSTs is their ability to catalyze glutathione conjugation reactions. This catalytic function serves both a detoxification and a biosynthetic role. However, GSTs have been found to have other functions as well, the significance of which are still being studied. A second, and only recently appreciated, GST function is in the modulation of signal transduction via binding to protein kinases involved in cell proliferation and apoptosis. Specifically, GST isoforms P1-1 and M1-1 have been reported to modulate the phosphorylation activity of JunK and ASK1, respectively (Wang *et al.*, 2001). No structural models have been reported for these complexes, and nothing is known about which domains of the GST are involved in the protein-protein interaction. However, it appears likely that GST – JunK or GST – ASK1 interactions are important contributors to the cellular antioxidant response.

A third function of GSTs is their capacity to reversibly bind, without catalytic turnover, a variety of hydrophobic ligands. Historically, this binding capacity has been referred to as the 'ligandin' activity (Litwack *et al.*, 1971). The GST isoform with the most extensively studied 'ligandin' behavior is GST A1-1, the structure of which is shown in Figure 1.5. This isoform is particularly abundant in the liver, comprising about 3% of all cytosolic protein in human hepatocytes. Prototypical ligands for this enzyme are aromatic and contain at least one anionic functional group; examples include

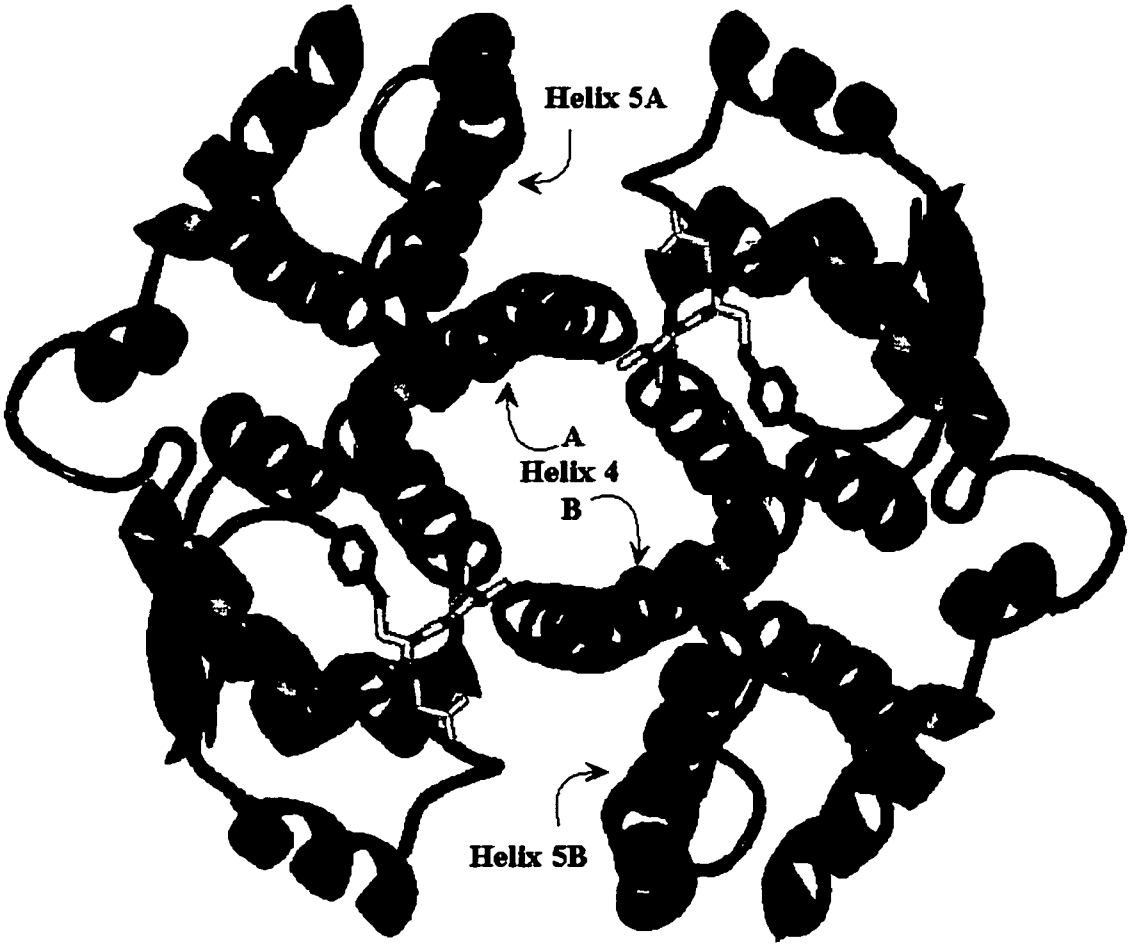

Figure 1.5: GST A1-1 in complex with glutathione-benzyl. As in previous Figures, the glutathione moieties are shown in yellow, benzyl moieties in red.

endogenous compounds such as porphyrins, steroids, and bile acids (Ketley *et al.*, 1975). Such a high concentration of this enzyme in an organ responsible for the metabolism of many of the compounds which bind to it with high affinity suggests some physiological role. These non-substrate ligands are inhibitors of the glutathione conjugation activity, and early investigators of the 'ligandin' activity reported that they inhibit non-competitively, suggesting that they bind at a site distinct from the H-site (Ketley *et al.*, 1975; Kamisaka *et al.*, 1975; Ohl and Litwack, 1977). Furthermore, early reports also indicated that in some cases, complete inhibition could be attained at a stoichiometry of 1 mol ligand / mol GST dimer, suggesting the existence of only one binding site per dimer for some non-substrate ligands (Ketley *et al.*, 1975; Kamisaka *et al.*, 1975). These observations led to speculation that the 'ligandin' site may lie within the large, V-shaped intersubunit cleft near the two-fold symmetry axis (Figures 1.2, 1.5). This hypothesis seemed to be confirmed when the structure of a cytosolic GST from *Schistozoma japonicum* was solved, and the antihelmenthitic drug praziquantel was observed to be bound within the solvent-accessible intersubunit cleft (McTigue *et al.*, 1995). Furthermore, this hypothesis has been supported by affinity labeling studies and fluorescence resonance energy transfer studies with rat and human GST A1-1, respectively (Barycki and Colman, 1997; Vargo and Colman, 2001; Sluis-Cremer *et al.*, 1996). However, no crystal structures of GST A1-1 in complex with a non-substrate ligand have been solved, and the binding modes of non-substrate ligands therefore remain uncertain. This uncertainty and the continued interest in the interaction between GST A1-1 and non-substrate ligands is the basis for chapter 3 of this dissertation.

1.1.3 GST Enzymology

In order to fulfill their function in the detoxification of foreign electrophiles, GSTs must by their very nature possess rather amorphous active sites capable of binding structurally diverse compounds. As with other detoxification enzymes, this results in broad substrate selectivity, with considerable overlap between different GST isoforms. However, the trade-off for the ability to metabolize a large variety of substrates is the relatively low affinity for nearly all of them, reflected in relatively high K_m values.

The residues which define the hydrophobic binding site are of course the major determinate in binding affinity for a given substrate. Beyond exhibiting simple affinity for substrates, catalysis requires that these residues must bind substrates in the proper orientation such that their electrophilic centers are properly positioned and adjacent to the glutathionyl sulfur. In some GST isoforms (including A1-1), most of the amino acid residues which comprise the H-site possess purely aliphatic side chains (leu, ile, val); others, such as P1-1, have aromatic residues which stack with aromatic substrates. An illustrative example of how these residues affect substrate specificity is in the turnover by P1-1 of the two α, β-unsaturated carbonyls shown in Figure 1.6, the diuretic drug ethacrynic acid and 4-hydroxynonenal, a product of lipid peroxidation. With its aromatic ring adjacent to the electrophilic center, ethacrynic acid stacks with a phenylalanine residue in the H-site of P1-1 and is rapidly metabolized. In contrast, the purely aliphatic species 4-hydroxynonenal is a poor substrate for this isoform (Mannervik, 1998). It is, however, turned over very rapidly by A4-4.

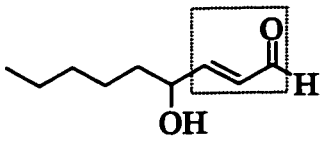

4-hydroxy-2-nonenal

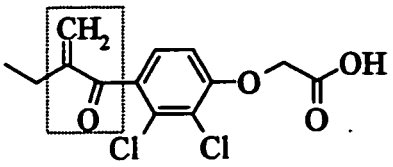

ethacrynic acid

Figure 1.6: Two α, β-unsaturated carbonyls (highlighted) with dramatically different K_ms for P1-1, reflecting the importance of the hydrophobic moieies of subsrates in addition to their electrophilic centers.

Of course, substrate selectivity is affected not only by binding, but also by the efficiency of chemical catalysis as indicated by k_{cat} or V_{max}. To understand this contributor to substrate selectivity, much effort has been made to determine the mechanism of GST catalysis. These studies have identified a conserved tyrosine residue near the N-terminus as a key catalytic residue (Armstrong, 1997). Through hydrogen bonding interactions with bound GSH, this residue appears to lower the pK_a of the thiol of bound glutathione. In this manner, the tyrosine serves to generate the thiolate anion, which is a superior nucleophile to the thiol. However, the mechanism by which this is achieved is unclear, and may differ between GST isoforms. The two competing models have tyrosine acting as a hydrogen bond donor (I) or as a general base (II):

$$\text{tyr-O-H} + \text{H-SG} \longleftrightarrow \text{tyr-O-H}\cdots{}^{-}\text{SG} + \text{H}^{+} \qquad \text{(I)}$$

$$\text{tyr-O}^{-} + \text{H-SG} \longleftrightarrow \text{tyr-O}^{-}\cdots\text{H-SG} \qquad \text{(II)}$$

$$\text{tyr-O}^{-}\cdots\text{H-SG} \longleftrightarrow \text{tyr-OH}\cdots{}^{-}\text{SG}$$

Note that mechanism II requires the formation of tyrosinate prior to any interaction with GSH. Several studies have measured the pK_a of the catalytic tyrosine of different GST isoforms and have indeed found that some (notably A1-1) have pK_as in the physiological range. However, these two mechanisms really represent the two ends of a continuum of electrostatic interactions between GSH and the conserved tyrosine residue. Different isoforms may lie at different points along this continuum, and thus vary in the degree of proton transfer and the extent to which they generate GS^-. Indeed, this characteristic may contribute to the efficiency with which different isoforms conjugate GSH to different electrophilic species. The electrophilic centers of GST substrates vary widely, and include among others epoxides, peroxides, aromatic and aliphatic halides, and α, β-unsaturated carbonyls. These electrophilic species exhibit marked differences in their degree of 'hardness' or 'softness,' a characteristic which affects their reactivity with different nucleophiles ('hard' and 'soft' nucleophiles react most readily with 'hard' and 'soft' electrophiles, respectively). Since the thiolate anion is a significantly 'harder' nucleophile than the thiol, the electrostatic nature of GSH when bound to different GST isoforms may make it inherently more reactive with certain electrophilic centers than with others. Moreover, residues in the active sites of the various GST isoforms may better stabilize the transition states generated from some electrophilic centers than from others. For example, M1-1 exhibits particularly high activity toward peroxides, which may be explained by the presence of an additional active site tyrosine residue. It is believed that this residue stabilizes the oxyanion which develops during the nucleophilic attack of GSH upon the peroxide (Armstrong, 1997). In support of this view, mutation of

this residue to phenylalanine lowers the k_{cat} by nearly 100-fold (Johnson, 1993). This mutant is also impaired in its metabolism of α, β-unsaturated carbonyls, suggesting that the tyrosine residue in the native enzyme is also capable of stabilizing the enolate formed during conjugate addition (Ji, 1994).

The observed catalytic efficiencies of different GST isoforms toward various substrates are therefore dependent upon both K_m and k_{cat} effects. The K_m effects are largely dictated by interactions between the hydrophobic moieties of a given substrate and the highly variable H-site residues. The variations in k_{cat} may be rationalized by specific interactions which stabilize the intermediates formed during the conjugation of a given electrophilic species. Furthermore, GST isoforms may differ in the extent to which they generate the glutathione thiolate anion, which may in turn affect the intrinsic reactivity toward a given electrophilic center.

In contrast, the Km for glutathione across the GST family appears quite consistent, with values around 250 μM having been reported for most isoforms. Although this value may seem high for a cofactor which is required to carry out the catalytic function of the enzyme, it must be considered that the intracellular concentration of reduced glutathione is typically about 5 mM, or 20-fold above the Km for GST. The enzyme should therefore be considered saturated with its cofactor. It is interesting to note that evolution has produced such large family of enzymes, differing in their hydrophobic substrate binding affinities but consistent with respect to GSH binding. Indeed, given the high intracellular concentration of GSH, there is no selective pressure to favor enzymes with lower GSH K_ms than those which these enzymes exhibit.

1.2 Biomedical Relevance of GSTs

The multifunctional nature and broad substrate specificity of the GSTs makes them a complicated and multifaceted enzyme system for biomedical researchers. The GSTs have been found to be involved in so many biochemical processes that they have become of interest to researchers in many different disciplines. Researchers in the fields of toxicology and drug metabolism are intensely interested in the ability of these enzymes to conjugate glutathione to foreign compounds. Glutathione conjugation serves to both detoxify electrophilic species and to render them more hydrophilic, facilitating their excretion in the urine. A vast array of environmental toxins as well as drugs and new drug candidates are known to undergo glutathione conjugation. Moreover, the reactive electrophilic species formed during periods of oxidative stress (for example, products of lipid peroxidation) are also detoxified via this pathway.

It has become evident that in addition to the detoxification of potentially harmful electrophiles, glutathione conjugation can also form toxic metabolites or precursors. Numerous examples of such 'bioactivation' are now known in which glutathione conjugates undergo further metabolism to form toxins. In the case of α, β-unsaturated carbonyls, which form reversible nucleophilic addition products, glutathione conjugation may serve to transport toxins from one tissue or cellular compartment to another, whereupon the addition product undergoes elimination to release the toxin. Due to the thermodynamic mandate that enzymes must catalyze a reaction in both directions, this

release of toxin may even be catalyzed by GST. In this manner, a glutathione conjugate formed in the liver may be transferred to the kidney or bladder and become a GST substrate for the release of the parent compound.

The role of GSTs in the detoxification of reactive electrophiles has a complex relationship with carcinogenesis and cancer chemotherapy. Various GST isoforms detoxify many potential carcinogens and thus provide a protective benefit. However, other examples are known (including benzopyrene) in which glutathione conjugation leads to a product more carcinogenic than the original compound. Furthermore, the treatment of cancer often involves the administration of electrophilic compounds designed to damage the DNA of malignant cells. These alkylating agents are often substrates for GSTs, thus being detoxified without exerting their antitumor effects. The finding that GSTs, particularly P1-1, are upregulated in many tumor cell lines suggests that this is one mechanism by which malignant cells acquire drug resistance.

GSTs, then, present a double-edged sword to human health: they indiscriminately detoxify undesirable toxins as well as lethal but necessary antitumor agents; they bioactivate some electrophilic species into more toxic or carcinogenic metabolites; and they have the potential to facilitate the transport of toxins from one tissue to another. A better understanding of their activities as intracellular binding proteins and their participation in signal transduction will almost certainly yield a similarly complex picture. The study of GSTs is therefore likely to continue to hold interest well into the future.

1.3 Dissertation Outline

This dissertation contains four chapters. Following this introduction, Chapter 2 addresses efforts to design high affinity, isoform-selective GST inhibitors. We hypothesized that the structure of the GST dimer, with its two active sites at opposite ends of the intersubunit cleft, presents an opportunity for the design of a bifunctional molecule which occupies both sites simultaneously. The design and preparation of these molecules will be presented together with the results of kinetic assays to characterize their behavior as inhibitors of the major human GST isoforms.

Chapter 3 deals with the enzymatic effects of chemical modifications made to a cysteine residue within the intersubunit cleft of GST A1-1. The location of this residue on helix 4 is very near the twofold symmetry axis, adjacent to what is believed to be the binding site of non-substrate ligands. This residue is also near the hydrophobic substrate binding site. For these reasons, be believed that modifications to this residue may have effects on the 'ligandin' function as well as catalytic turnover. One of the modifications we prepared is a mixed disulfide with glutathione, which has been shown to modulate the activity of several enzymes, including the microsomal GST isoform. We also prepared enzyme which is crosslinked across the intersubunit cleft to probe the mobility of the helix 4-5 tower in solution and to assess the potential relevance of this mobility to catalysis or non-substrate ligand binding.

Chapter 4 departs from the enzymology of GSTs and describes a striking feature of its cofactor, glutathione, which was discovered during the investigations covered in

Chapters 2 and 3. During the course of work on these other projects, an unexpected observation was made of non-aqueous solutions of glutathione. In polar organic solvents including dimethylsulfoxide, dimethylformamide, and methanol, the disulfide form of glutathione appears to self-assemble to form a transparent, rigid gel. This previously undocumented behavior is quite surprising for a peptide as small as glutathione. Based on intriguing results from an NMR study, we hypothesized that the unusual structural feature of glutathione, the side-chain δ-glu-cys linkage, is responsible for this behavior. Through analog studies and spectroscopic techniques, we have probed this hypothesis and present a model of glutathione self-assembly.

Notes to Chapter 1

1. The nomenclature of the GSTs has undergone multiple changes in the thirty years since they were first characterized, creating considerable confusion in the literature. The family notation A, P, M, T, K, and S has replaced the use of the Greek designations α, π, μ, θ, κ, ζand σ, respectively, and will be used throughout this dissertation.
2. Where descriptions of subunit interactions are critical, residues are labeled by their appropriate number followed by 'A' or 'B' to denote which subunit they are located on. Note, however, that equivalent residues, such as phe 52A and phe 52B, are symmetry related.

CHAPTER 2

A Novel Class of Bifunctional Inhibitors of Glutathione S-Transferases Designed to Span the Intersubunit Cleft and Occupy both Active Sites

2.1 Introduction

Among the substrates for GSTs are the alkylating agents used in the cytotoxic chemotherapy of many cancers. Because of this, these enzymes have been of interest to the biomedical community for many years. Interest in the GSTs has been increased by the observation that many isoforms are upregulated in malignant cell lines. Specifically, it has been found that the P1-1 isoform is expressed in all of the tumor cell lines maintained by the National Cancer Institute, while the A1-1 and M1-1 isoforms are present in subsets of these cells (Tew *et al.*, 1996). Since these enzymes catalyze the detoxification of several drug classes employed to combat these cancers, it has been hypothesized that GST overexpression in malignant cells is a mechanism of acquired resistance to these antitumor agents (Waxman, 1990; Tew, 1994; Hubert *et al.*, 1995). Evidence in support of this hypothesis has emerged from both *in vitro* and *in vivo* studies in which sensitivity to alkylating agents has been restored to previously resistant cell lines by exposure to P1-1 antisense RNA or GST inhibitors (Niitsu *et al.*, 1998). Therefore, the coadministration of potent, selective GST inhibitors as adjuvants to cytotoxic chemotherapy has emerged as a strategy to restore the drug sensitivity of

resistant cells, thereby extending the usefulness of many first-line anticancer agents and improving clinical outcomes.

Toward this end, many groups have been pursuing the development of GST inhibitors for more than a decade (Lyttle et al., 1994; Flatgaard et al., 1993; Morgan et al., 1996). The currently existing GST inhibitors tend to fall into three classes, determined by their binding site on the protein and mechanism of inhibition. The first of these are hydrophobic substrate analogs, which bind in the H-site and competitively inhibit the binding of hydrophobic substrates. Second are glutathione conjugates, which occupy both the G-site and at least part of the H-site, and are typically competitive with respect to both glutathione and the hydrophobic substrate. Such conjugates include S-hexyl glutathione, S-benzyl glutathione, and the glutathione conjugate of ethacrynic acid. Third, a collection of compounds referred to as non-substrate ligands are noncompetitive inhibitors of the GSTs; this type of inhibitors will be discussed at length in Chapter 3. These inhibitors are typically hydrophobic anions and include endogenous compounds such as porphyrins and bile acids and such exogenous compounds as sulfated organic dyes. The binding site of this group of inhibitors remains uncertain, but it may lie at one edge of the H-site or within the wide cleft between the two subunits of the GST dimer. They are unique among the GST inhibitors in that they elicit non-competitive inhibition with respect to both glutathione and the electrophilic substrate.

A common feature of these existing inhibitors is relatively low affinity, with the very best compounds exhibiting K_is on the order of 100 nM. Furthermore, many of these compounds inhibit multiple GST isoforms with little selectivity. Consequently, little

progress has been made in validating the concept of GST inhibition as a means of restoring sensitivity to drug resistant malignancies. For this reason, we wished to design a novel class of GST inhibitors which exhibited both greater affinity and selectivity for specific GST isoforms.

The approach that we took in our inhibitor design is based on the concept of polyvalency, which has recently been applied to many enzyme systems to achieve considerable increases in both affinity and selectivity (Pang *et al.*, 1996; Rao *et al.*, 2000; Schaschke *et al.*, 2001). Briefly, the underlying principle of the approach is that by incorporating multiple binding domains within a single molecule, great improvements in affinity can be achieved due to the additivity of enthalpic binding terms without the additional entropic price associated with binding many individual molecules. Furthermore, because the geometry of the polyvalent molecule must be appropriate for presenting each binding domain to its proper binding site, very high selectivity can also be attained. To illustrate these effects, the cartoon in Figure 2.1 represents a macromolecule with two identical binding sites (analogous to the GST dimer), both of which are occupied by some generic, aromatic ligand. In Figure 2.1 A, these ligands are two separate molecules, and the equation describing the binding energy of these two monovalent ligands (ΔG_{2m}) is shown at right to be twice the enthalpy and entropy of binding the ligands singly (this of course assumes no cooperativity of binding). The entropic contribution includes positive factors (favorable to binding) such as dispersal of ordered solvent from a hydrophobic surface,

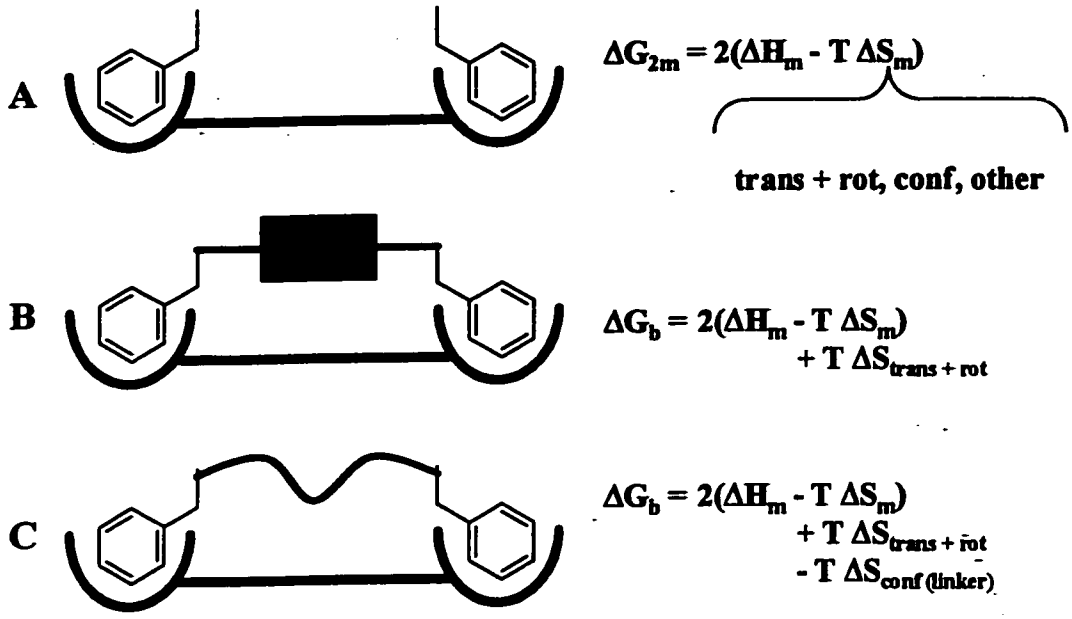

Figure 2.1. Representation of the entropic advantage of bivalency. The entropic terms include negative contributions such as the loss of translational, rotational, and conformational degrees of freedom; see text for discussion.

as well as negative factors which are unfavorable to binding. These unfavorable entropic 'costs' of binding include the loss of translational and rotational entropy of the ligand through solvent upon binding, and the loss of internal entropy of the ligand in the form of rotatable bonds which, when in the bound state, must adopt a specific conformation. When the two ligands shown are tethered together with a rigid linker (Figure 2.1 B), the free energy of binding of the resulting bivalent ligand (ΔG_b) still benefits from the favorable enthalpic and entropic contributions of the two binding events, but instead of losing two sets of translational and rotational entropy, only one set is lost (as only one molecule is binding). Consequently, the equation to the right of Figure 2.1 B includes the 'return' of one set of translational and rotational entropies. If, however, the linker that

tethers the two binding domains together possesses significant internal entropy (such as rotatable bonds), then binding to the macromolecule may result in a forfeiture of this additional entropy. This situation is illustrated in Figure 2.1 C, and the equation which describes the binding energetics includes an additional entropic term to reflect the lost conformational entropy of the linker. Therefore, the ideal linker is one of the proper size and geometry to place the binding domains at their respective binding sites without inducing strain in the linker or sterically clashing with the macromolecule; furthermore, minimizing the number of rotatable bonds within the linker consistent with the aforementioned factors will result in the least loss of internal entropy upon binding.

While Figure 2.1 attempts to quantify the advantage of bivalency in terms of binding energy, Figure 2.2 relates these effects to the binding constants of a bivalent molecule in a stepwise fashion. In the initial binding event (the equilibrium between 2.2 A and 2.2 B), the dissociation constant (K_{d1}) is dominated by the energetics of the binding of a single binding domain, and so would be expected to be approximately the same as the binding of a monovalent ligand. With this initial binding, the translational and rotational entropy of the bivalent ligand is lost, as would be the case for its monovalent counterpart. The factors which increase the affinity of the bivalent molecule arise from the second binding event (the equilibrium between 2.2 B and 2.2 C), in which another set of favorable enthalpies and entropies are gained without an additional loss of translational and rotational entropies. This has the effect of producing a dissociation constant (K_{d2}) which is significantly lower than K_{d1}. How much lower certainly depends on many factors, including the loss of conformational entropy within the linker as shown

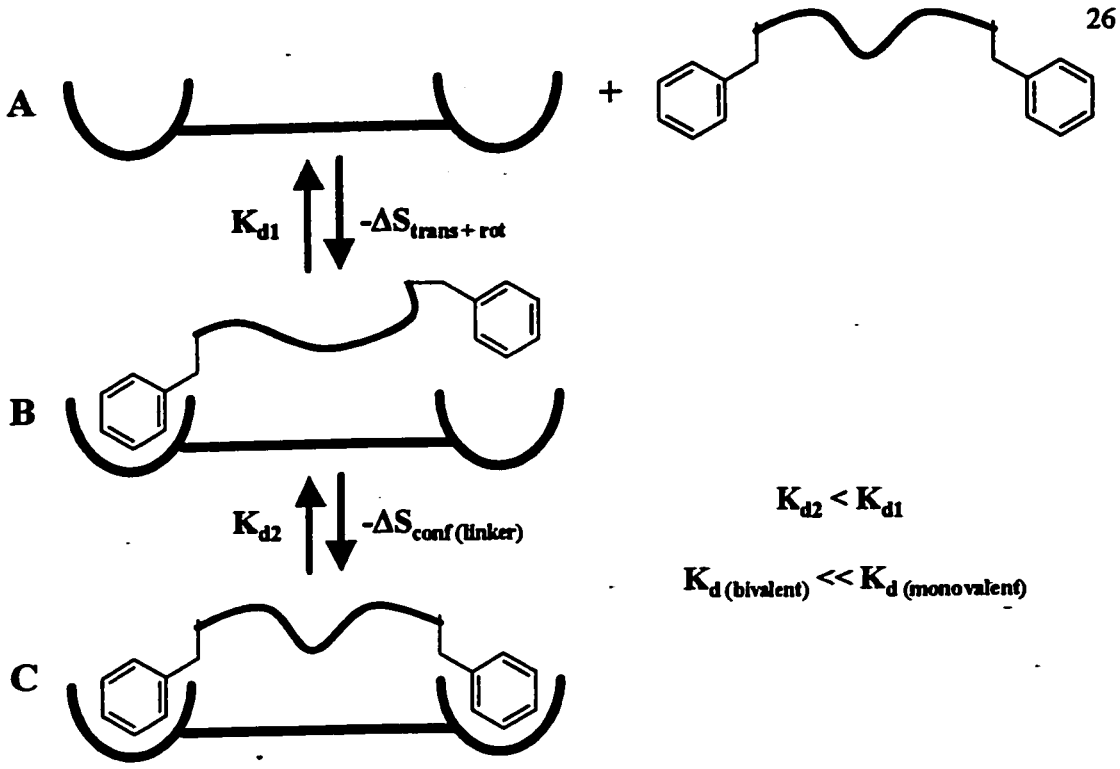

Figure 2.2. Microscopic binding constants of bivalent ligands. Since the initial binding event (A → B) is driven by the same enthalpic and entropic contributors (including the loss of translational and rotational entropy) that drive the binding of a monovalent ligand, K_{d1} is similar in magnitude between the bivalent and monovalent ligands. During the second binding event (B → C), the internal conformational entropy of the linker is lost, but no further translational or rotational degrees of freedom are lost; K_{d2} is therefore lower than K_{d1}. The macroscopic result is a K_d for the bivalent ligand significantly lower than that for the monovalent ligand.

in the figure. However, the relationship $K_{d2} < K_{d1}$ is perhaps the best general definition of what makes a 'bivalent' ligand. Moreover, this relationship has the effect of producing

observed, macroscopic dissociation constants which can be much lower for bivalent ligands than their monovalent analogs; K_ds more than 5 orders of magnitude lower have been reported (Schaschke *et al.*, 2001).

We believe that the geometry of the GST dimer (see Chapter 1 for details), with its two active sites at opposite ends of the solvent-accessible intersubunit cleft, presents an opportunity to design bivalent inhibitors to occupy both active sites simultaneously, thus realizing the benefits of bivalency. Since each active site contains a glutathione binding subsite and a hydrophobic subsite, the binding domains of these inhibitors can be designed to occupy either or both of these sites, and thus be expected to exhibit competitive or non-competitive inhibition kinetics with respect to the two substrates. We present here the design and synthesis of four classes of symmetrical, bifunctional compounds and their kinetic characterization as inhibitors of GST isoforms P1-1 and A1-1.

2.2 Experimental Procedures

2.2.1 Materials

Reduced glutathione and S-hexyl glutathione were purchased from Sigma. The crosslinking agents ethylenediol *bis*-ethylamine and tetraethyleneglycol *bis*-amine were purchased from Molecular Biosciences. N-BOC-1,3-diaminopropane was purchased from Fluka. All other small molecule starting materials were purchased from Aldrich.

Recombinant human glutathione S-transferase A1-1 was expressed in E. *coli* and purified as described previously (Ibarra *et al.*, 2001). The enzyme was incubated with 10 mM dithiothreitol to ensure complete reduction of cysteine residues, followed by extensive dialysis to remove the reducing agent. Recombinant human glutathione S-transferase P1-1 was expressed and purified by the same protocol.

2.2.2 GST assays

Assays of GST activity and inhibition were performed with chloro-2,4-dinitrobenzene (CDNB) as the electrophilic substrate. Except where otherwise stated, GST concentration was 20 nM. For IC_{50} determinations, the concentration of GSH and CDNB were at their respective K_ms for each enzyme: 250 μM GSH for both enzymes, 750 μM CDNB for GST A-1, and 1.5 mM CDNB for GST P1-1. Rates were determined by measuring absorption at 340 nm (λ_{max} of glutathione-dinitrobenzene) for 1 minute on a Beckman DU 7400 spectrophotometer. For IC_{50} determinations, assays were performed at inhibitor concentrations ranging over at least five orders of magnitude (from 100-fold above the IC_{50} to 100-fold below). Data were fit to a sigmoidal dose-response function using GraphPad Prism to determine the 50% inhibitory concentration.

For variable substrate concentration assays with the *bis*-Uniblue A compound 7, five CDNB concentrations (250 μM, 500 μM, 1 mM, 1.5 mM, 2 mM) were paired with 3 mM GSH at five inhibitor concentrations (0, 25 nM, 50 nM, 100 nM, 200 nM). For the variable enzyme concentration assays with this compound, three GST P1-1

concentrations (5 nM, 15 nM, 40 nM) were matched with twelve inhibitor concentrations (2.5 nM, 5 nM, 10 nM, 25 nM, 50 nM, 100 nM, 250 nM, 500 nM, 1 μM, 2.5 μM, 5 μM, 10 μM) at a CDNB concentration of 1.5 mM and a GSH concentration of 3 mM. Data from these assays were fit to the appropriate equations (as discussed in Section 2.3.2, Kinetics) by global nonlinear regression using Microcal Origin.

Fluorescence titrations were performed using a SLM-AMINCO 8000 fluorometer. With the excitation monochromator at 280 nm the emission was monitored from 295 nm to 415 nm, and the fluorescence peak was integrated over this range after addition of each aliquot of ligand.

2.2.3 Molecular modeling

Modeling of protein structures, including determination of geometrical arrangements within protein-ligand complexes and manual 'docking' of proposed synthetic targets, was performed using UCSF MidasPlus. All protein crystal structures were retrieved from the Brookhaven Protein Data Bank. Geometry optimization and conformational analysis of small molecules for use in modeling protein-ligand interactions was performed using Spartan.

2.2.4 Preparation of Inhibitors

Electrospray ionization mass spectra of all compounds were obtained with a Fisons VG Quattro II mass spectrometer fitted with a Z-spray ESI source. Purified compounds were analyzed by direct injection into the instrument.

Preparation of N-substituted S-hexyl glutathione.

N-benzyl-S-hexyl glutathione was prepared by the reductive amination of benzaldehyde with the amino terminus of S-hexyl glutathione. S-hexyl glutathione (2.5 mmol, 980 mg) was added to10 mL methanol to which 2.5 mmol (349 μL) triethylamine had been added, and stirred until dissolved. Benzaldehyde (0.5 mmol, 51 μL) was added and the solution stirred for one hour, followed by addition of sodium cyanoborohydride ($NaBH_3CN$: 0.625 mmol, 39.4 mg) which had been dissolved in 1 mL methanol. This solution was stirred overnight, then evaporated to dryness *in vacuo*. Upon addition of water (5 mL), a flocculent white precipitate was produced, which was filtered and washed sequentially with water, acetonitrile, and ether. The washed precipitate was dried *in vacuo*, yielding 35 mg (3%).

N-ethyl-S-hexyl glutathione was prepared as above, but acetaldehyde (0.5 mmol, 28 μL) was substituted for benzaldehyde. After evaporation, the residue was dissolved in 5 mL water, then placed on ice and acidified with dropwise 1 M HCl until a white precipitate was produced. Ethyl acetate (5 mL) was then added and the solution shaken to produce an emulsion. Saturated Na_2CO_3 was then added dropwise until the lower aqueous layer was again transparent; at this point, the emulsion had re-separated, leaving a white precipitate at the interface of the aqueous and organic layers. This precipitate

was removed, filtered, and washed sequentially with water, acetonitrile, and ether. The washed precipitate was dried *in vacuo*, yielding 160 mg (15%).

The electrospray mass spectra of these compounds are shown in Figure 2.3; assignments of the major peaks are shown. Frequently observed MS fragments of glutathione conjugates result from loss of the γ-glu group, which is cleaved at peptide bond for a loss of 129 from the molecular ion or at the N-C_α bond for a loss of 146. In these compounds, the N-substitution of the glutamyl amine means that these losses are 157 and 174, respectively for the ethyl derivative and 219 and 236 for the benzyl derivative. These fragments give rise to the peaks at 246 and 263 seen in both spectra.

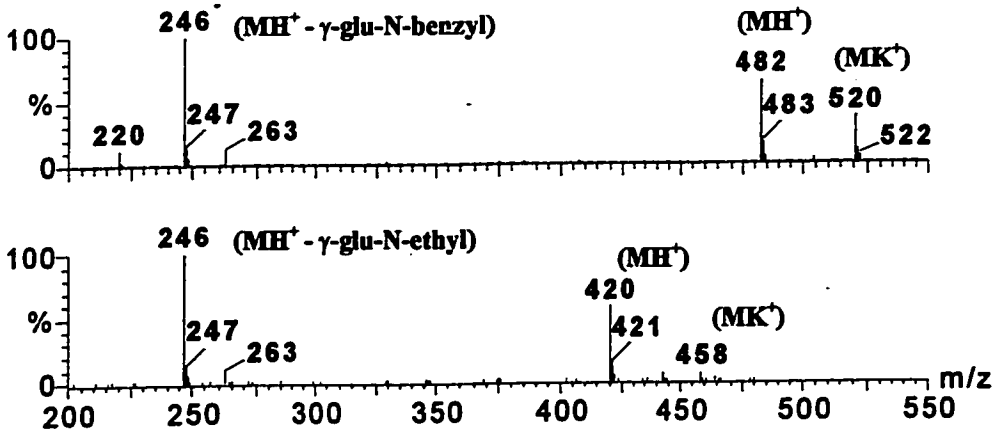

Figure 2.3. Electrospray mass spectrum of N-benzyl-S-hexyl glutathione (top) and N-ethyl-S-hexyl glutathione (bottom).

Preparation of *bis*-glutathionyl bisphenol A glycerolate

This section describes the preparation scheme outlined in Figure 2.9. Bisphenol A glycerolate diacrylate (2.5 mmol, 1.2114 g) was dissolved, with considerable patience,

in 75 mL ethanol. Reduced glutathione (7.5 mmol, 2.3 g) was dissolved in water, and 1250 μL of 6 M NaOH were added (7.5 mmol). This basified glutathione solution was added dropwise to the diacrylate solution. After stirring for 24 hours, TLC (ethyl acetate development, UV visualization) indicated no remaining diacrylate (the limiting reagent). The solution was evaporated under vacuum to about 10 mL of predominately aqueous solution. This solution was placed on ice, then 1M HCl was added dropwise to produce a white precipitate at pH 3. This precipitate was filtered and washed sequentially with water, acetonitrile, and ether. The washed precipitate was dried *in vacuo*, yielding 1.5 g.

Verification of complete glutathione conjugation was obtained by electrospray mass spectrometry (Figure 2.4). A striking feature of this spectrum is the prominence of the doubly-charged parent ion (M + 2H) at m/z 551. This feature would prove to be common among the bis-glutathionyl conjugates prepared as GST inhibitors. The singly charged molecular ion at m/z 1099 is also observed.

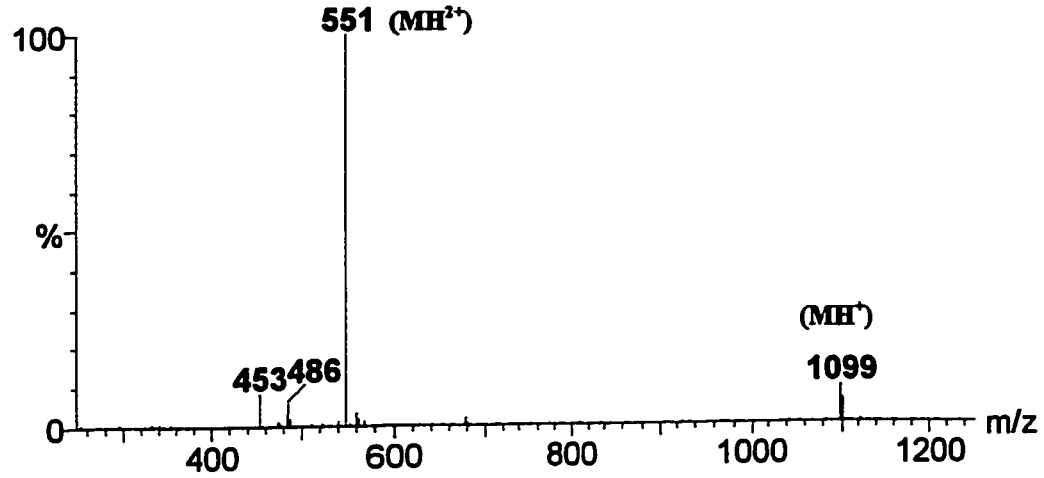

Figure 2.4. Electrospray mass spectrum of *bis*-glutathionyl bisphenol A glycerolate

Preparation of a series of *bis*-glutathionyl alkyl esters

This section describes the preparation scheme outlined in Figure 2.11. Dibromo alkyl esters were prepared by the acid-catalyzed esterification of 8-bromooctanoic acid with a series of five ω-bromo alkyl alcohols; the length of the alkyl chains of these alcohols ranged from 8 to 12 carbons, inclusive. An additional monobromo ester was prepared by esterification of 8-bromooctanoic acid with methanol. In each of five pre-dried vials, 8-bromooctanoic acid (0.6 mmol, 133.8 mg) was dissolved in freshly distilled toluene. To each of these vials was added *para*-toluenesulfonic acid (0.05 mmol, 9.5 mg), followed by 0.5 mmol of one of the ω-bromo alcohols (or 2.5 mmol methanol). These solutions were refluxed for one hour with a Dean-Stark trap containing 4A molecular sieves to remove the water formed during the esterification. At this time, TLC (methylene chloride development, iodine stain) indicated no remaining 8-bromooctanoic acid (the limiting reagent). The solutions were allowed to cool, then washed sequentially with 5% aqueous sodium bicarbonate, water, and saturated sodium chloride. The toluene was evaporated under a stream of dry air, producing a pale yellow oil. This oil was dissolved in ethyl acetate, and the bicarbonate / water / sodium chloride wash cycle was repeated. The separated ethyl acetate layer was dried with anhydrous magnesium sulfate, filtered, and evaporated under vacuum to yield colorless oil. TLC for each of the six reactions indicated pure products had been isolated.

To prepare the glutathione conjugates of these bromoesters, a 1 M reduced glutathione solution was prepared by dissolving 6 mmol GSH (1.842 g) in 4.0 mL water plus 2.0 mL 6 M NaOH (12 mmol NaOH). Aliquots of this solution (0.75 mL, 0.75

mmol GSH) were placed in each of six vials, then 95% ethanol added until a slight cloudiness appeared (total volume about 4 mL). Each ester (0.25 mmol) was placed in a separate vial and dissolved in 0.5 mL of 95% ethanol, then added dropwise to the glutathione solution. These reactions were stirred for 24 hours, then evaporated under a stream of dry air to a volume of about 1 mL of predominately aqueous solution. This volume was increased to about 4 mL by addition of water, then placed in an ice bath and acidified to pH 3, in each case producing a white precipitate. These precipitates were filtered and washed sequentially with water, acetonitrile, and ether. The washed precipitates were then dried *in vacuo*. Verification of complete glutathione conjugation of these compounds was again achieved by electrospray mass spectrometry; Figure 2.5 illustrates a representative spectrum, the C_{18} ester (*bis*-glutathionyl decyloctanoate). Again, the doubly charged molecular ion (m/z 455) is a prominent peak in this spectrum.

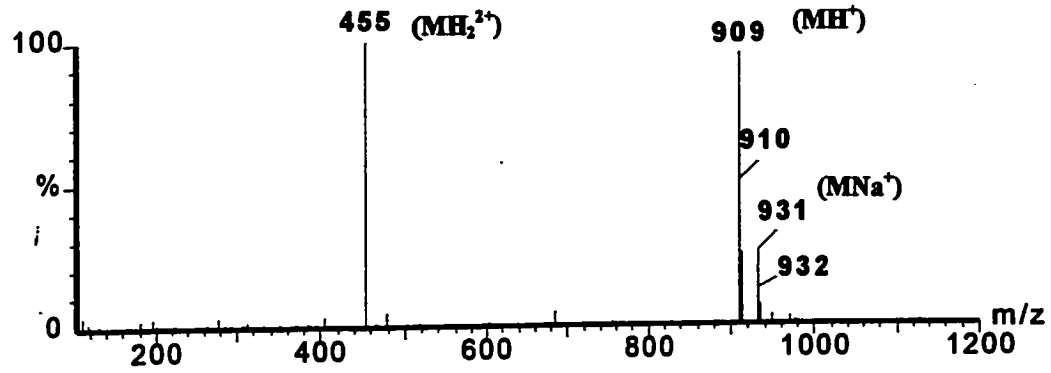

Figure 2.5. Electrospray mass spectrum of *bis*-glutathionyl decyloctanoate, a representative member of the series of *bis*-glutathionyl alkyl esters.

Preparation of a series of *bis*-glutathionyl nitrophenyl derivatives

This section describes the preparation scheme outlined in Figure 2.15. This series of three compounds (plus the monofunctional reference compound) is based on esters of 4-chloro-3-nitrobenzoyl chloride (CNBC). The alcohols required for the esterification are diols which represent the linker of each compound, and are thus different for each compound in the series. One of the diols, tetraethyleneglycol, is commercially available, as is the alcohol (ethanol) used to prepare the monofunctional reference compound; the other two are based on diesters of isophthalic acid which had to be prepared separately.

To prepare the isophthalate diesters, isophthaloyl chloride was esterified to ethylene glycol or 1,3-propanediol. Due to the two equivalent reactive groups of isophthaloyl chloride and the diols, large excesses of the diols were necessary to prevent formation of polymeric species. Ethylene glycol and 1,3-propanediol (4 mL, about 60 mmol) were placed in two separate pre-dried vials. Isophthaloyl chloride (0.5 mmol, 101.5 mg) was placed in each of two separate pre-dried vials and dissolved in 1 mL of dry, freshly distilled THF. Using a dry syringe, the isophthaloyl chloride solution was added dropwise to each diol with vigorous stirring. Stirring was continued for 12 hours, at which time TLC (ethyl acetate development, UV visualization) indicated no remaining isophthaloyl chloride (the limiting reagent). Water (8 mL) was added to each reaction, then the solutions were extracted with 10 mL of toluene. The toluene extract contained a highly non-polar species observed by TLC, but little of the major product. The aqueous solutions were then extracted with 10 mL of either ethyl acetate (ethylene glycol ester) or diethyl ether (1,3-propanediol ester), repeated four times. The five extracts for each

product were combined and washed sequentially with water and saturated sodium chloride, then dried with anhydrous magnesium sulfate and evaporated under vacuum. The *bis*-ethanolisophthalate evaporated to a white solid which was recrystallized from anhydrous diethyl ether; the *bis*-propanolisophthalate evaporated to a colorless oil.

To prepare the linkers, tetraethyleneglycol, *bis*-ethanolisophthalate, and *bis*-propanolisophthalate were esterified to two equivalents of CNBC. Each of the diols plus ethanol for the monofunctional reference compound (0.25 mmol) were placed in pre-dried vials and dissolved in 1 mL of dry, freshly distilled pyridine. Four portions of CNBC (1.5 mmol) were placed in separate pre-dried vessels and dissolved in 1 mL of dry pyridine. The diol (or ethanol) solutions were added dropwise to the CNBC solutions with stirring, producing an exothermic reaction and an immediate precipitate of pyridine hydrochloride. After 30 minutes, TLC (ethyl acetate development, UV visualization and iodine staining) indicated no remaining diols (the limiting reagents) in any of the reaction media. The precipitates were removed by filtration, leaving pale yellow solutions in each case. Icewater (10 mL) was added to each solution, resulting in immediate clouding of the solutions. Centrifugation resulted in the formation of off-white solid pellets in the case of the ethyl ester (monofunctional reference) and *bis*-ethanolisophthalate diester; the other reactions (tetraethyleneglycol diester and *bis*-propanolisophthalate diester) yielded pale yellow oils. The solid products were filtered, washed with water, and dried *in vacuo*. Addition of 95% ethanol to the tetraethyleneglycol diester oil resulted in the formation of a nearly white precipitate which was filtered, washed sequentially with

water and ethanol, and dried *in vacuo*. However, the *bis*-propanolisophthalate diester remained oily after washing with water and 95% ethanol.

The final step in the preparation of this series of compounds was glutathione substitution of the aryl chlorides. The monofunctional CNB ethyl ester (0.5 mmol, 115 mg) was dissolved in 2 mL of ethanol. GSH (1 mmol, 307 mg) was dissolved in 2 mL water plus 334 μL 6M NaOH (2 mmol NaOH). To this solution 95% ethanol was added until a slight cloudiness appeared (total volume about 6 mL). The CNB ethyl ester solution was then added dropwise to the GSH solution and allowed to stir for 48 hours, producing a yellow solution. Each of the *bis*-CNB bifunctional diesters (0.075 mmol) were dissolved in 1 mL acetonitrile. In three separate vials, GSH (0.375 mmol) was dissolved in 1 mL water plus 125 μL 6M NaOH (0.75 mmol NaOH), then acetonitrile (2 mL) was added to this solution. The *bis*-CNB bifunctional diester solutions were then each added to one of the GSH solutions. These mixtures were stirred for 48 hours, producing yellow solutions in each case. All four of the above reaction mixtures were then evaporated under a stream of dry air to a volume of about 1 mL of predominately aqueous solution. These were placed in an ice bath and acidified to pH 3 by dropwise addition of 1 M HCl, producing yellow precipitates. After standing for 30 minutes, these mixtures were centrifuged and the supernatants discarded. The solid precipitates were resuspended in dilute HCl, filtered, and washed sequentially with water, acetonitrile, and diethyl ether, then dried *in vacuo*. Confirmation of complete glutathione conjugation of these compounds was again achieved by electrospray mass spectrometry; Figure 2.6 illustrates a representative spectrum.

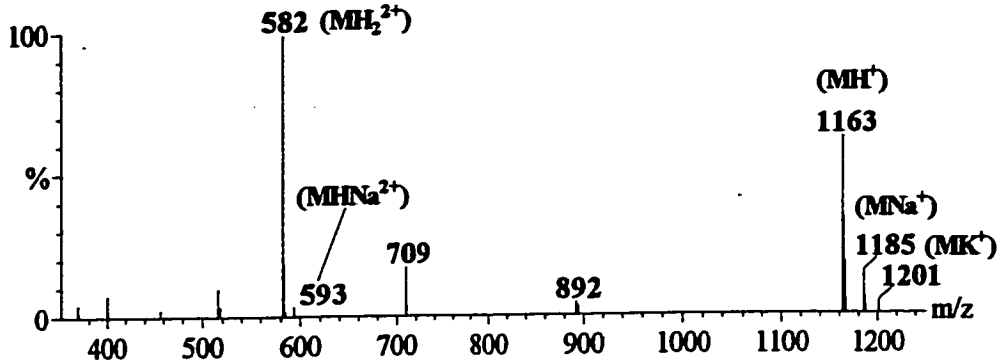

Figure 2.6. Electrospray mass spectrum of compound **3**, *bis*-glutathionylnitrobenzoyl ethylisophthalate. Assignments of major peaks are labeled; the peak at m/z 709 arises from fragmentation of the nitrobenzoyl ester. Partially unreacted intermediate (the mono-glutathionyl, mono-chloro species) gives rise to the small peak at m/z 892 along with its isotopic peak at m/z 894.

Preparation of a series of *bis*-Uniblue A derivatives

This section describes the preparation scheme outlined in Figure 2.19. This series of three compounds is based on a series of diamines conjugated to the α,β-unsaturated sulfone moiety of the commercially available dye Uniblue A; the monofunctional reference is the ethylamine conjugate of this dye. Two of the diamines, ethylenediol *bis*-ethylamine (EDBEA) and tetraethyleneglycol *bis*-amine (TEGBA), are commercially available; the third is a diamide of isophthalic acid which had to be prepared separately.

To prepare the isophthalamide, isophthaloyl chloride (0.1 mmol, 20.3 mg)was placed in a pre-dried vial and dissolved in 3 mL of dry, freshly distilled THF. Neat N-BOC-1,3-diaminopropane (0.286 mmol, 50 μL) was added dropwise from a dry syringe, producing an immediate white precipitate. After stirring for 30 minutes, the precipitate

was filtered and the THF solution evaporated under vacuum, leaving an oily residue. This oil was dissolved in 10 mL of ethyl acetate and extracted sequentially with 10 mL each of water, 5% $NaHCO_3$, water, dilute HCl, and saturated NaCl. The washed ethyl acetate was then dried with anhydrous magnesium sulfate and evaporated under vacuum, leaving a colorless oil. This oil was then dissolved in $CHCl_3$ (3 mL) and 300 μL trifluoroacetic acid added to effect cleavage of the BOC protecting group and yield the *bis*-propylamineisophthalamide. After stirring for 30 minutes, TLC (alumina plate, methanol development, UV visualization) indicated complete cleavage had been effected. The solution was then evaporated under vacuum to a colorless oil, which was washed with hexane and dried *in vacuo*.

Conjugation of the diamines with Uniblue A was effected by dissolving each diamine (0.1 mmol) in 1 mL of water, then adding this to a solution of Uniblue A (0.3 mmol) in 4 mL of water. The pH of these solutions was found to be about 10.5 for the EDBEA and TEGBA solutions, but about 2.0 for the *bis*-propylamineisophthalamide. The pH of this solution was raised to 10.5 with saturated Na_2CO_3. The solutions were stirred for 2 days and the *bis*-Uniblue A products were purified from the reaction medium by preparative HPLC. The products were the final species to elute from a 10 mm i.d. C_{16} reversed phase column eluted with 30% acetonitrile / 70% water. For each product, the pooled dark blue fractions were evaporated under a stream of air; as the acetonitrile was removed, a dark blue precipitate formed. When little color remained in solution, the precipitate was filtered and dried *in vacuo*. Conjugation of Uniblue A with ethylamine to prepare the monofunctional reference compound was performed similarly to the above

procedure, but 0.1 mmol of Uniblue A (50 mg) was mixed with 0.1 mmol of ethylamine (6.5 μL of a 70% aqueous solution). HPLC purification was performed as above. The electrospray mass spectrum of a representative member of this series of compounds is shown in Figure 2.7.

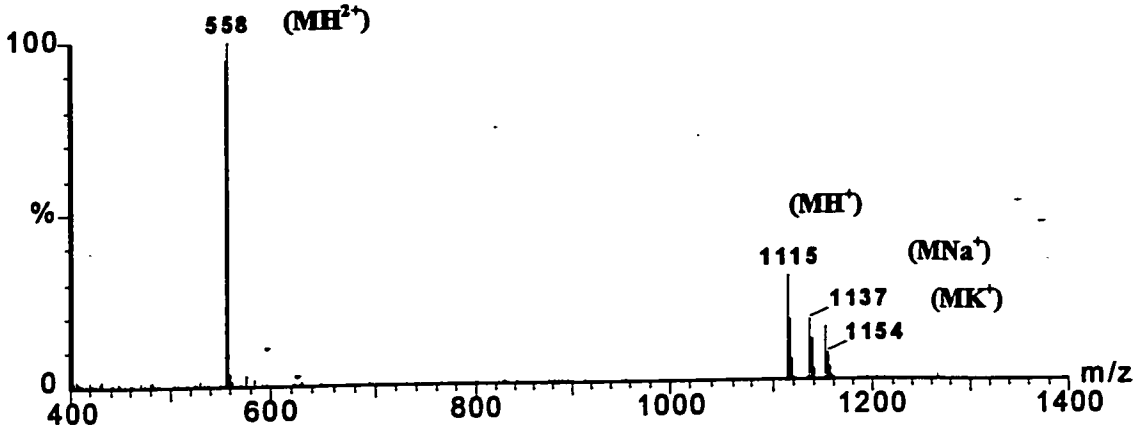

Figure 2.7. Electrospray mass spectrum of compound **6**, *bis*-Uniblue A ethylenediolethylamine.

2.3 Results

Due to the observation that P1-1 is the GST isoform most commonly overexposed in malignant cells, much of the interest in the role of GST in alkylating agent resistance is centered on this isoform. We therefore used the structure of GST P1-1 as the basis for designing bivalent inhibitors in order to maximize selectivity for this isoform. The crystal structure of GST P1-1 in complex with glutathione-2,4-dinitrobenzene (GS-DNB) shown in Figure 2.8 (PDB entry 18GS) illustrates the location of the H- and G-sites of

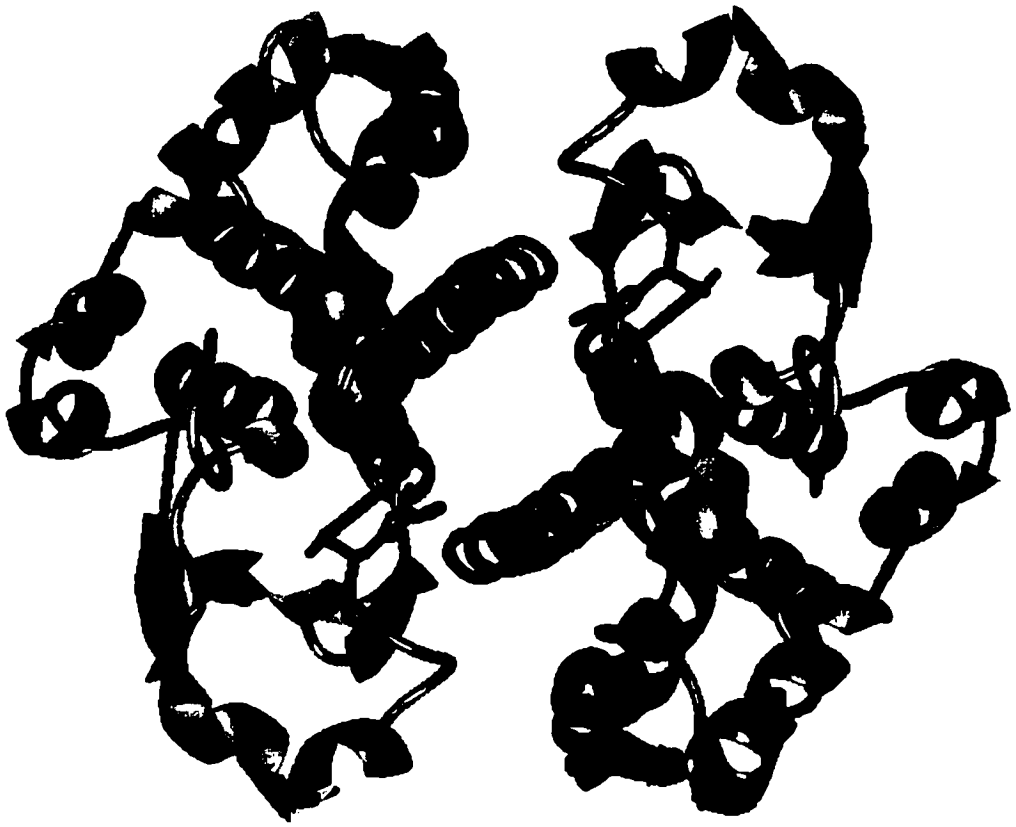

Figure 2.8. Complex of GST P1-1 and GS-DNB. Glutathione moieties are shown in green, with the amino termini in blue; dinitrophenyl moieties in red.

each monomer and the positions of the two active sites relative to each other. As discussed in Chapter 1, these active sites are positioned at the ends of the deep, solvent-accessible cleft which lies above the subunit interface. Due to the proximity of the two active sites of the GST dimer and their location at opposite ends of the solvent-accessible intersubunit cleft, we reasoned that bifunctional inhibitors could be designed which would simultaneously occupy both active sites. The binding domains of such a molecule require a linker which would bridge and thus partially occupy the intersubunit cleft. Given that this cleft is postulated to be a ligand binding site[1] and two crystal structures of

different GST isoforms have been reported with ligands bound within the cleft, it seems reasonable that a linker could occupy this region without inducing significant changes in the protein architecture.

The design considerations of bifunctional inhibitors can be divided into two elements: the binding domains and the molecular linker between them. We have designed two classes of inhibitors which differ in their binding domains. These two classes of compounds and the molecular linkers used for each will be presented separately.

2.3.1 Glutathione-based bifunctional inhibitors

Inspection of Figure 2.8 reveals that the two glutathione moieties bind to GST in such an orientation that the free amino ends of the peptides (blue) are pointed toward the intersubunit cleft, and hence toward each other. Consequently, the span between these nitrogens (12 Å) is shorter than the span between any other pair of atoms in the two bound glutathione molecules. These atoms therefore appeared to be good candidates as attachment points for a linker, as a linker between these two atoms could be shorter than a linker between the two thiols. Since this nitrogen is involved in a salt bridge when bound to the enzyme (with an aspartyl residue from the opposite subunit), it would be desirable to retain the amine functionality, rather than derivatize it to produce an amide or other uncharged functional group.

In order to determine the effect of converting this nitrogen into a secondary amine on its GST binding affinity, two such derivatives were prepared. Employing S-hexyl glutathione as the parent molecule, acetaldehyde and benzaldehyde were coupled to the nitrogen via reductive amination as described in section 2.2.4. The IC_{50}s of the resulting compounds and the parent compound were determined with GST P1-1 and are shown in Table 2.1. Both of the derivatives exhibit an IC_{50} an order of magnitude higher than the unmodified S-hexyl glutathione. This large loss of affinity suggests that derivatization of the glutathionyl amine terminus, even with the small ethyl group, significantly impairs binding to the enzyme.

Table 2.1. IC_{50}s of N-substituted S-hexyl glutathione (GS-hexyl).

Inhibitor:	GS-hexyl	N-ethyl GS-hexyl	N-benzyl GS-hexyl
IC_{50}:	15μM	190 μM	120 μM

Given this result, all further efforts with glutathione-based inhibitors were based on linkers which couple the glutathione moieties via the thiols. Conjugation at this site with hydrophobic compounds often results in binding affinities higher than that of reduced glutathione. However, linkers which exploit the thiols as attachment points need to be considerably longer to account for the fact that in the bound conformation, these groups are 27Å apart, twice as far as the space between the nitrogens. In the current study, three classes of such linkers were employed which will be described separately.

A. *bis*-glutathionyl bisphenol A glycerolate

Design and Preparation.

As an initial attempt to determine the feasibility of bifunctional glutathione conjugates as GST inhibitors, a commercially available precursor compound was desired. Therefore, a molecule was sought which bore a reactive electrophilic center at each end of the compound, separated by a space of approximately 27 Å for conjugation to the glutathionyl thiols. Regions of hydrophobic functionality were also desired, particularly near the two electrophilic sites which would lie adjacent to the glutathionyl thiols in the resulting bis-conjugate (and therefore in the H-site when bound to the enzyme). To

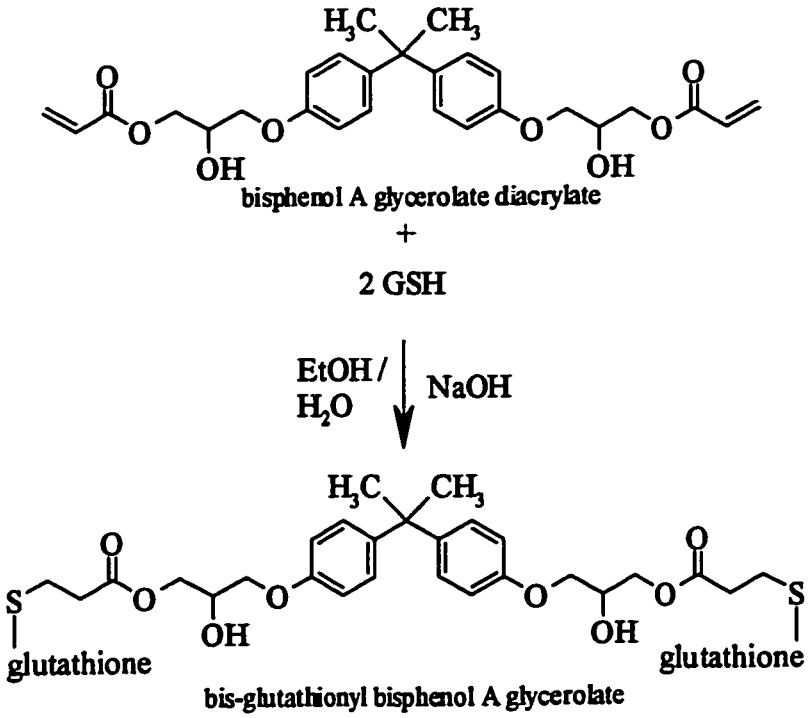

Figure 2.9. Scheme for the preparation of *bis*-glutathionyl bisphenol A glycerolate

satisfy these requirements, bisphenol A glycerolate diacrylate was chosen. By the straightforward one-step synthesis shown in Figure 2.9 and described in section 2.2.4, the bis-glutathionyl conjugate of this compound was prepared and purified by HPLC.

Kinetics.

The concentrations of *bis*-glutathionyl bisphenol A glycerolate required to produce 50% inhibition (IC_{50}) of GST isoforms P1-1 and A1-1 were determined using the CDNB assay. These values were determined to be 0.4 μM and 0.9 μM, respectively. These sub-micromolar EC_{50}s suggest that bifunctional glutathione conjugates can bind effectively to GST. However, we have no monofunctional analog of this compound with which to compare relative affinities, and thus determine the advantage of the bifunctional molecule. The results of this preliminary study were therefore not conclusive about the benefits of the bifunctional approach, but did suggest that *bis*-glutathione conjugates may be feasible as higher affinity GST inhibitors.

B. *bis*-glutathionyl alkyl esters

Design.

One of the classic and most well characterized classes of GST inhibitors is the S-alkyl glutathione conjugates. Alkyl chains from one to nine carbons in length have been conjugated to glutathione and shown to be inhibitors of considerable affinity. However, these compounds tend to be rather non-selective with respect to different GST isoforms. Given the well-studied nature of S-alkyl glutathione conjugates and the relative ease with

which alkyl chains of variable length can be prepared from commercially available precursors, we believed that this class of compounds could be easily modified to test the bifunctional inhibitor concept. A monofunctional conjugate, representing 'half' of the bifunctional molecules could easily be prepared to serve as a benchmark in assessing the advantage of bifunctionality. Using straightforward chemistry, alkyl chains of various length can be prepared with glutathione substituents at each end. By varying the length of this chain, it was hypothesized that the resulting compounds would exhibit greater isoform selectivity than the monofunctional counterpart, due to the varying distances between the G-sites of different GST isoforms. To illustrate this, Figure 2.10 shows the intersubunit cleft regions of GST isoforms A1-1 and P1-1 as observed in the crystal structures of their respective complexes with glutathione. In these crystal structures, the distance between the two glutathionyl thiols differs by 3 Å for the two isoforms.

Preparation.

The strategy chosen to produce a series of alkyl linkers of various lengths was to start with a single ω-bromo carboxylic acid and esterify to it a series of ω-bromo alcohols, followed by displacement of the bromo substituents with two equivalents of glutathione. By esterification with methanol, a monofunctional glutathione conjugate representing half of the bifunctional compounds could be easily prepared. As shown in Figure 2.11, 8-bromooctanoic acid was esterified to a series of alcohols ranging from 8 to 12 carbons; this gives rise to a series of dibromo esters 16 to 20 carbons in length.

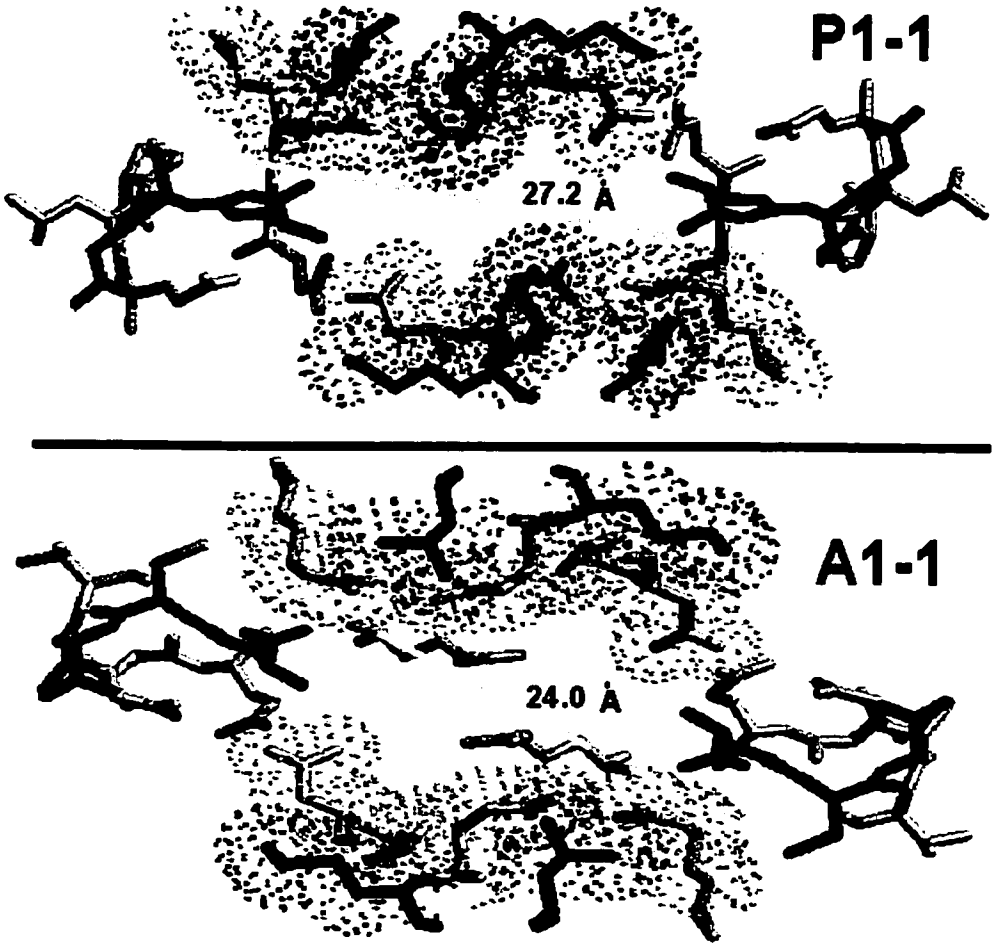

Figure 2.10. Intersubunit cleft residues of GST P1-1 and A1-1. The two bound glutathione moieties are green, with their cysteinyl thiols in yellow and their amino termini in blue. The yellow dashes and corresponding distances represent the crystallographically observed separation of the two glutathionyl sulfurs. The residues in magenta lie at approximately the same 'depth' within the cleft as the glutathionyl sulfurs; the residues in gray lie deeper within the cleft.

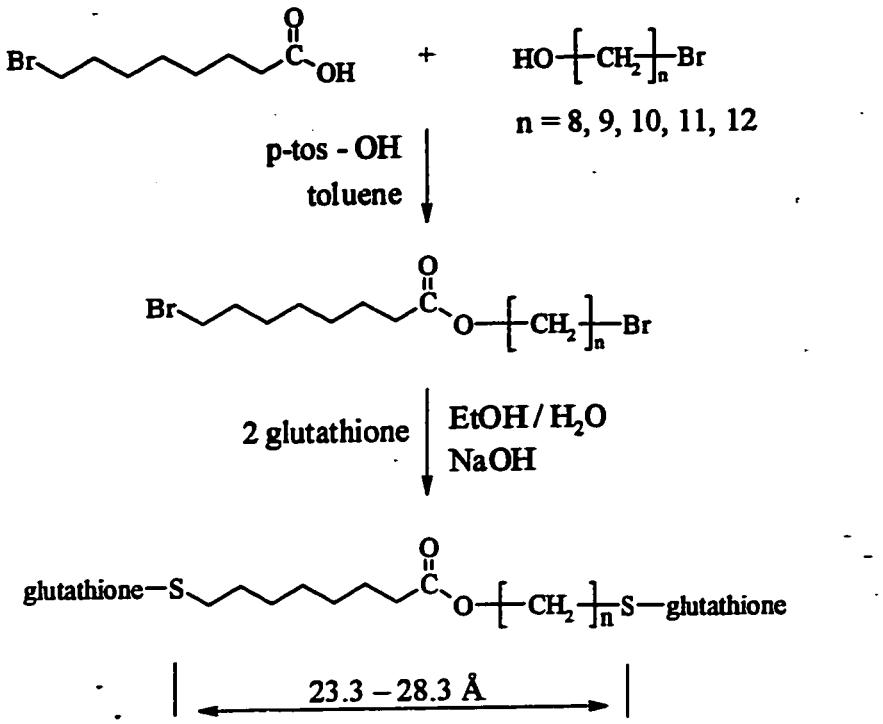

Figure 2.11. Scheme for the preparation of a series of *bis*-glutathionyl alkyl esters.

Following the glutathione substitution, the span of the resulting linkers between the glutathionyl sulfurs, when modeled in an extended conformation, ranges from 23.3 Å to 28.3 Å. This range brackets the thiol-thiol distances observed between the two glutathionyl sulfurs in isoforms A1-1 and P1-1 (Figure 2.10).

Kinetics.

Using CDNB as the hydrophobic substrate, IC_{50}s were determined for each of the 16 to 20 carbon *bis*-glutathionyl alkyl esters with GST isoforms A1-1 and P1-1. An IC_{50} was also determined for the monofunctional methyl ester to serve as a benchmark. The

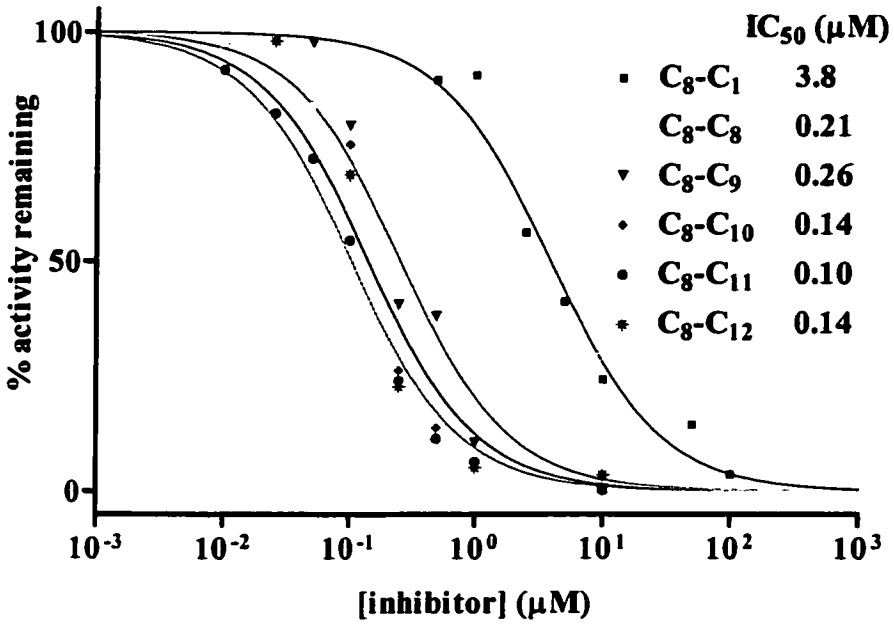

Figure 2.12. Inhibition of GST A1-1 by *bis*-glutathionyl alkyl esters. Inset table reports the IC_{50} found for each chain length; C_8-C_1 refers to the mono-glutathionyl methyl ester.

data from the assays with A1-1 are plotted in Figure 2.12, with the IC_{50} values derived from these plots shown in the inset. Notably, each of the *bis*-glutathionyl alkyl esters exhibits an IC_{50} more than one order of magnitude lower than the monovalent benchmark compound; however, there is only about a twofold difference between the highest and lowest values for the bifunctional compounds. Similar results were obtained for GST P1-1 (not shown), and the IC_{50}s with both enzymes were plotted as a function of alkyl chain length (Figure 2.13). From this plot, it is evident that somewhat greater variation in the *bis*-glutathionyl alkyl ester IC_{50}s is observed with P1-1 than with A1-1, and in both cases the bifunctional compounds exhibit between 10- and 100-fold lower values than the monofunctional methyl ester. The bifunctional compounds are typically slightly better

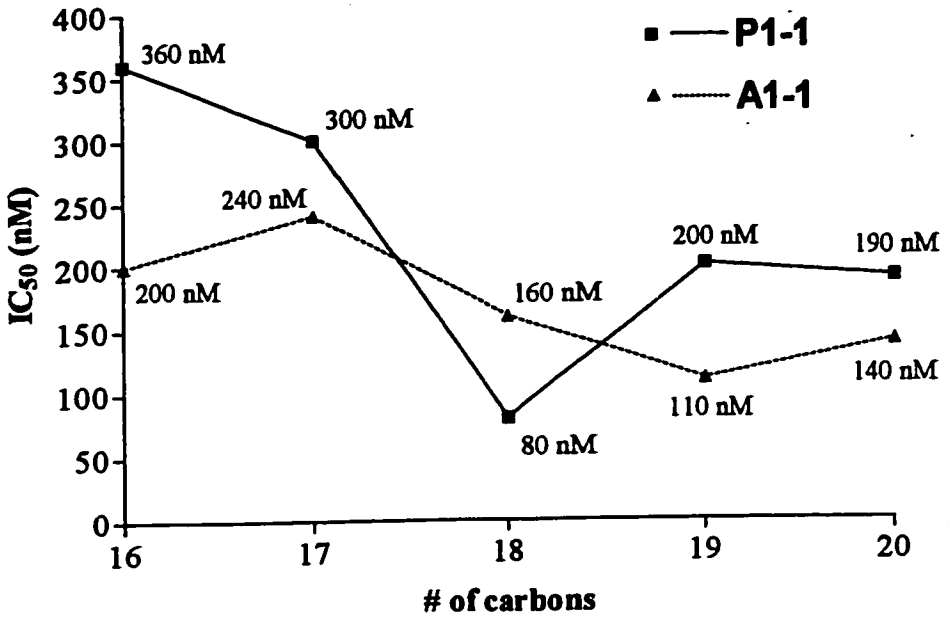

Figure 2.13. *Bis*-alkyl ester IC_{50}s by chain length for GST P1-1 and A1-1.

inhibitors of the A1-1 isoform, however this relationship is reversed at C-18, which exhibits a slightly lower IC_{50} for P1-1; moreover, this value is two- to four-fold lower than that for the other bifunctional inhibitors of P1-1. On the whole, it therefore appears that significant increases in affinity have been achieved with the bifunctional approach, however little isoform selectivity has been gained.

C *bis*-glutathionyl nitrophenyl derivatives

Design. A close examination of the crystal structure of the complex between GST P1-1 and GS-DNB (Figure 2.14) suggested that S-phenyl glutathione conjugates may be

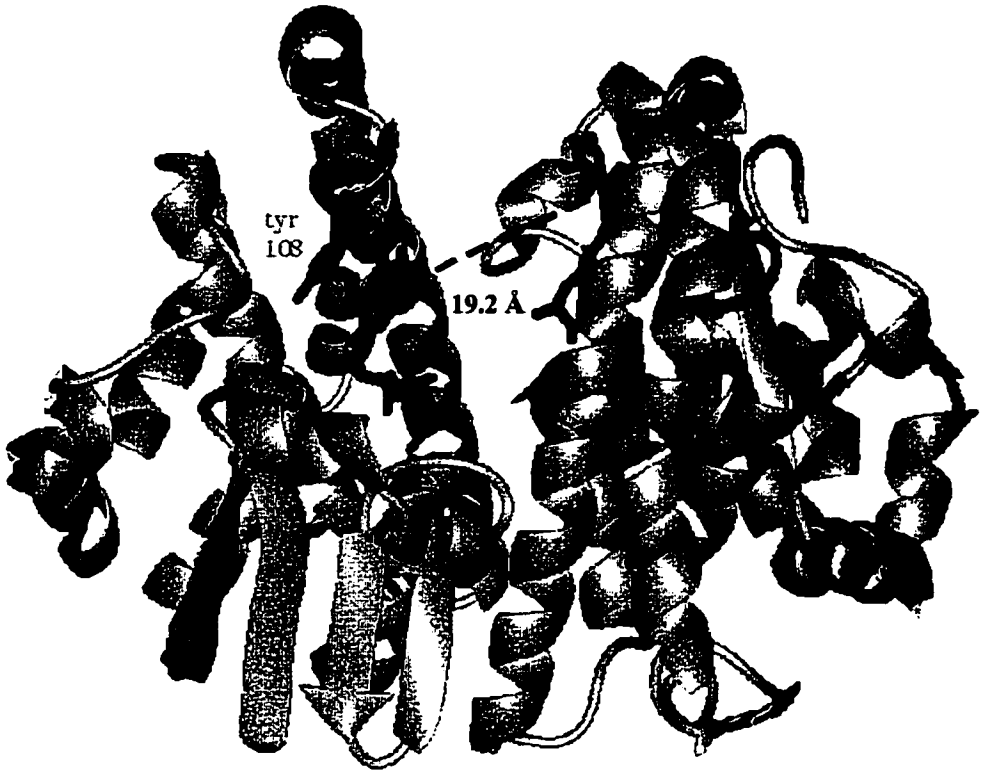

Figure 2.14. GST P1-1 complex with GS-DNB, illustrating the aromatic stacking interaction between tyrosine 108 and the phenyl moiety of the bound ligand. In this bound conformation, the span between the two carbons *para-* to the glutathione substituents of the two GS-DNB ligands is 19.2 Å.

superior to S-alkyl glutathione conjugates in their ability to anchor the binding moiety in an appropriate orientation for bivalent binding in the manner which we have envisioned. Within the H-site of P1-1, the phenyl moiety of the GS-DNB ligand is stacked with the side chain of tyr 108. This aromatic interaction, which does not exist in A1-1 due to the exclusively aliphatic residues along the side of the H-site of that isoform, orients the ring such that the *para-* nitro group is pointed toward the intersubunit cleft and its counterpart

bound to other subunit. We hypothesized that this interaction may therefore produce a better (and more P1-1 specific) anchorage than the highly flexible alkyl chains employed previously. The *para-* carbon of this ring seemed a reasonable attachment point for a linker which would join two analogs of GS-DNB.

To prepare bifunctional analogs of GS-DNB we selected 4-chloro-3-nitrobenzoyl chloride (CNBC) as a precursor. This reagent presents a reactive acyl halide in place of the *para-* nitro group and is thus easily crosslinked at this position. However, it retains the highly electron withdrawing nitro group *ortho-* to the chloro substituent, thus retaining the reactivity at this site (for ensuing substitution with glutathione) and the electron deficient nature of the aromatic ring in the final product.

Preparation. The distance between the *para-* carbons of the two GS-DNB moieties observed in the P1-1 crystal structure is 19.2 Å (Figure 2.14). We employed linkers of varying lengths to bracket this observed separation. We also employed linkers with varying degrees of internal flexibility, from fully rotatable polyethylene glycol (PEG) polymers to aromatic diesters of isophthalic acid. As described in section 2.2.4, each of these crosslinkers was esterified to two equivalents of CNBC, followed by conjugation with two equivalents of glutathione to create the set of compounds (**2 - 4**) illustrated in Figure 2.15. The length of the resulting compounds (between the *para-* carbons) when modeled in an extended conformation is also shown in Figure 2.15. As a monofunctional benchmark to assess the relative advantage of bifunctionality, the ethyl ester of CNBC was also prepared, then conjugated with one equivalent of glutathione (Figure 2.15, **1**).

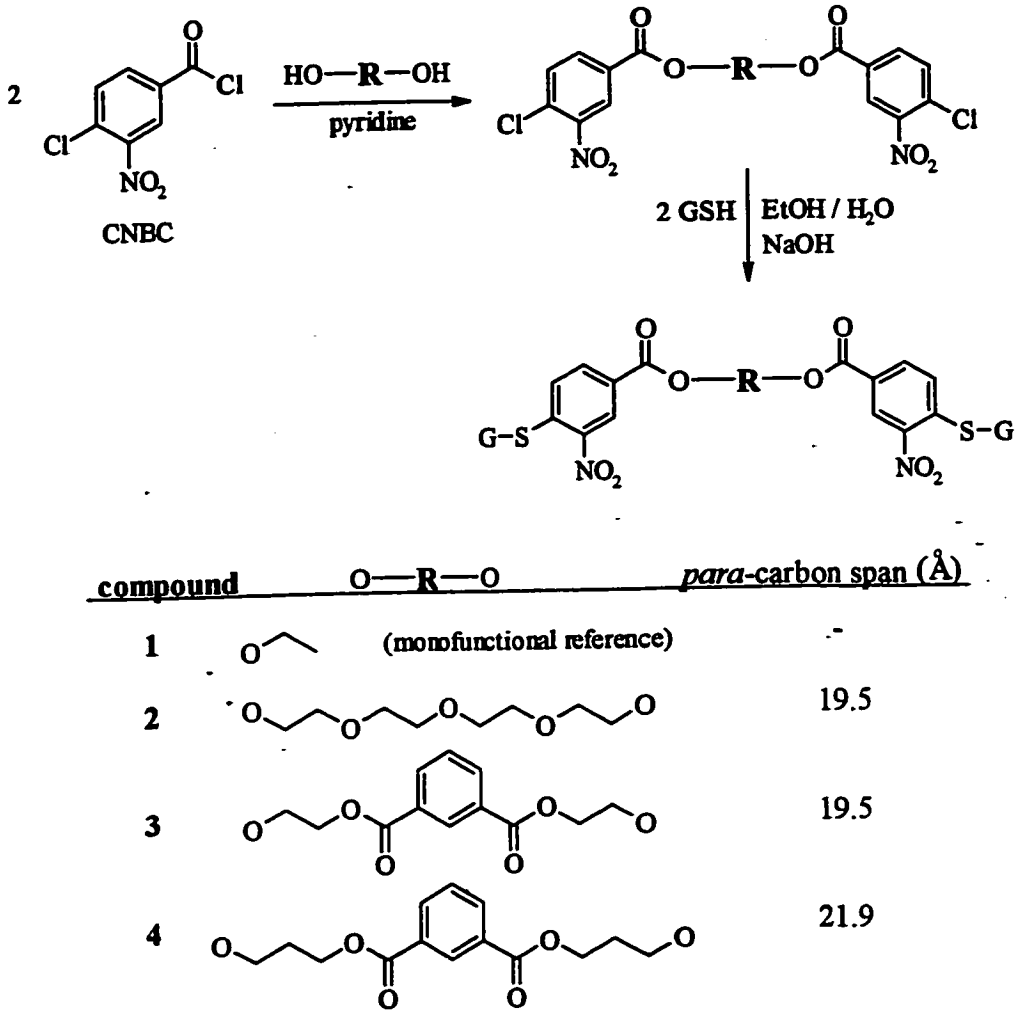

compound	O—R—O	*para*-carbon span (Å)
1		(monofunctional reference)
2		19.5
3		19.5
4		21.9

Figure 2.15. Scheme for the preparation of a series of bis-glutathionyl nitrophenyl derivatives. Compound **1** is the monofunctional reference prepared by the esterification of ethanol with only one equivalent of CNBC.

Kinetics. The concentration required for 50% inhibition (IC_{50}) of GST isoforms P1-1 and A1-1 was determined for compounds **1** - **4** using the CDNB assay. These data are plotted in Figure 2.16 and the resulting IC_{50}s are tabulated in Table 2.2. Although the

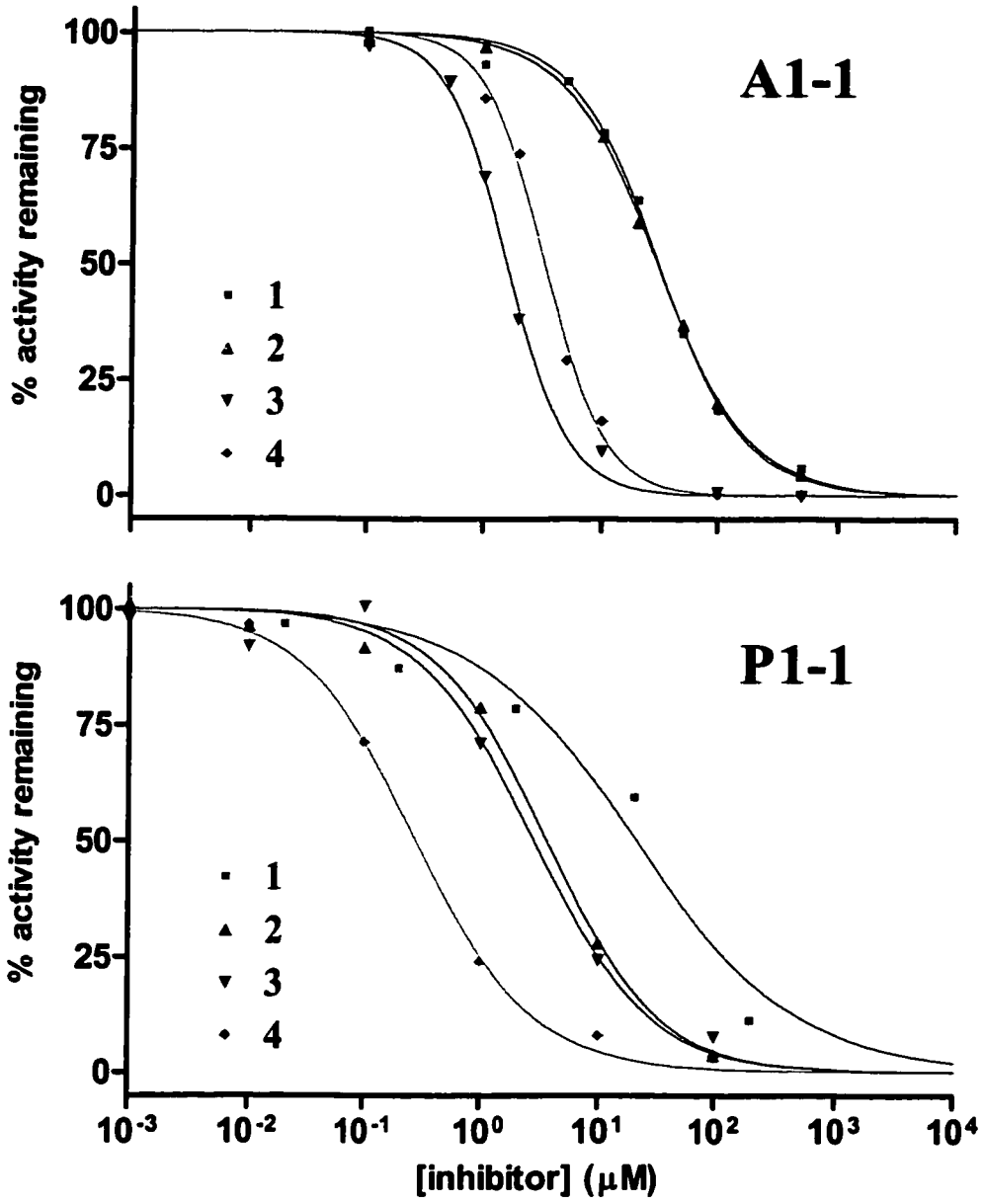

Figure 2.16. Inhibition of GST A1-1 and P1-1 by *bis*-glutathionyl nitrophenyl derivatives. See Figure 2.15 for structures of compounds **1** – **4**. Numerical IC_{50} values are tabulated in Table 2.2.

Table 2.2. IC_{50}s of *bis*-glutathionyl nitrophenyl derivatives with GST A1-1 and P1-1; values are derived from the plots shown in Figure 2.16.

compound	A1-1 IC_{50} (μM)	P1-1 IC_{50} (μM)
1	30	21
2	29	4.5
3	1.6	2.9
4	3.3	0.28

IC_{50} experiment does not yield information about inhibition mechanism, these compounds are almost certainly competitive with respect to both GSH and CDNB. These assays were performed with concentrations of GSH and CDNB equal to their respective K_ms. Since $IC_{50} = 2\ K_i$ for competitive inhibitors under these assay conditions (Cheng and Prusoff, 1973), the K_i of these compounds can be expected to be about half the determined IC_{50} values.

2.3.2 Non-substrate ligand-based bivalent inhibitors

Design. A recently published crystal structure (PDB entry 20GS) of GST P1-1 in complex with cibacron blue was used as the basis for the second set of inhibitors. In this structure (Figure 2.17), only the anthraquinone sulfonate moiety was crystallographically observed, with no electron density seen for approximately half of the molecule. The anthraquinone sulfonate thus seems to be the binding determinate for the relatively high

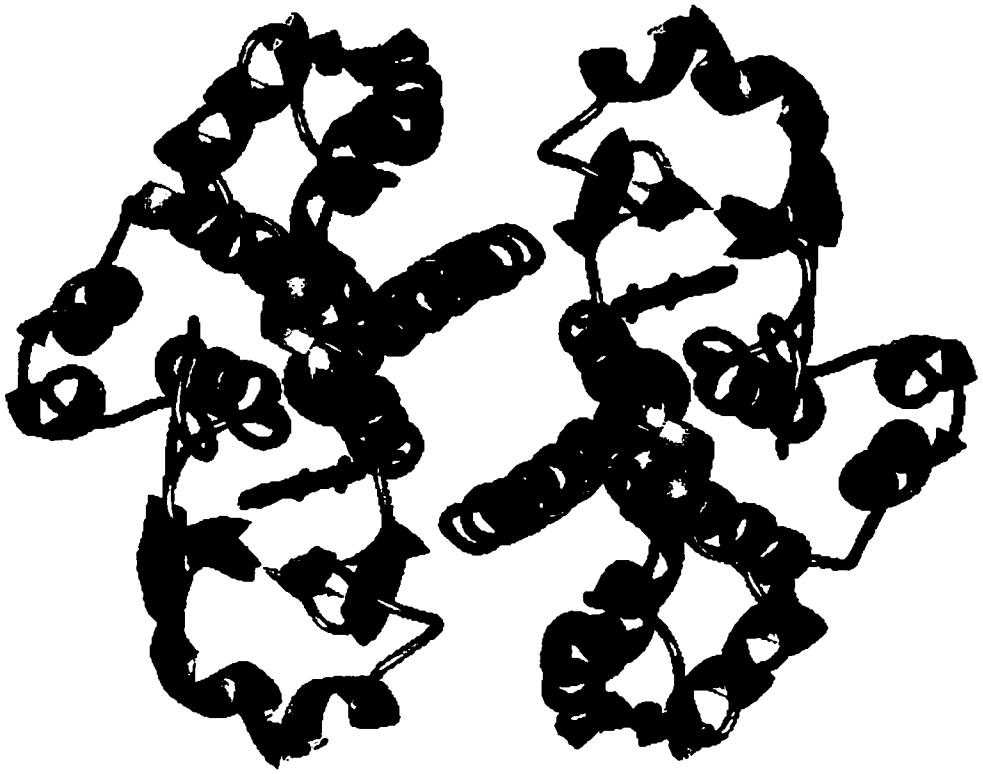

Figure 2.17. Structure of the complex between GST P1-1 and Cibacron Blue; only the anthraquinone sulfonate moiety of the ligand is crystallographically observed (green).

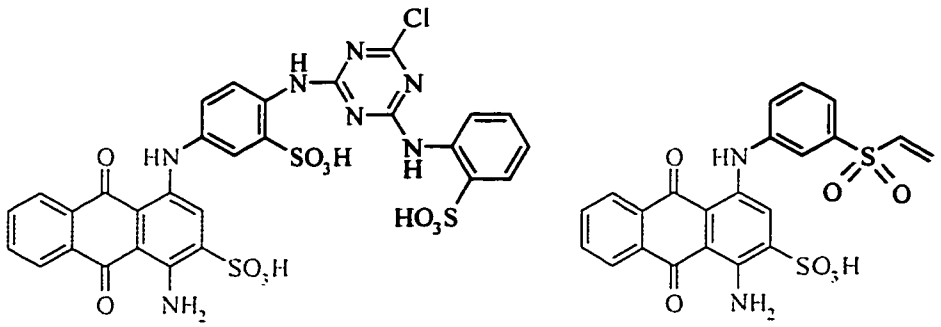

Cibacron Blue Uniblue A

Figure 2.18. Structures of Cibacron Blue and Uniblue A. The anthraquinone sulfonate moiety of Cibacron Blue shown here in green corresponds to that portion of the structure which is crystallographically observed in the P1-1 complex (Figure 2.17). This binding moiety is preserved in Uniblue A as shown at right.

affinity interaction between Cibacron Blue and GST P1-1. We reasoned that an analog of Cibacron Blue which contained this binding determinate but which possessed a reactive handle appropriately positioned for crosslinkage with a second moiety would be a good candidate for a bifunctional inhibitor. We therefore selected Uniblue A as the binding moiety, which possesses all of the structural elements observed in the cibacron blue – GST P1-1 complex and has a reactive α,β-unsaturated sulfone moiety for crosslinkage (Figure 2.18). When two molecules of Uniblue A are overlaid with the observable anthraquinone moieties of Cibacron Blue in the GST P1-1 complex, their reactive β-carbons are 16.2 Å apart. We again employed linkers to bracket this distance and to vary the degree of internal flexibility.

Preparation. As with the *bis*-glutathionyl nitrophenyl derivatives discussed above, we employed linkers with varying degrees of internal flexibility, including two polyethylene glycol (PEG) polymers and an aromatic diamide of isophthalic acid. As described in section 2.2.4, these diamino linkers were conjugated to the α,β-unsaturated sulfone moieties of two equivalents of Uniblue A to prepare the bifunctional compounds **6 - 8** shown in Figure 2.19. The length of the resulting compounds (between the β- carbons) when modeled in an extended conformation is also shown in Figure 2.19. The monofunctional derivative **5** (Figure 2.19) was prepared with ethylamine to serve as a benchmark compound.

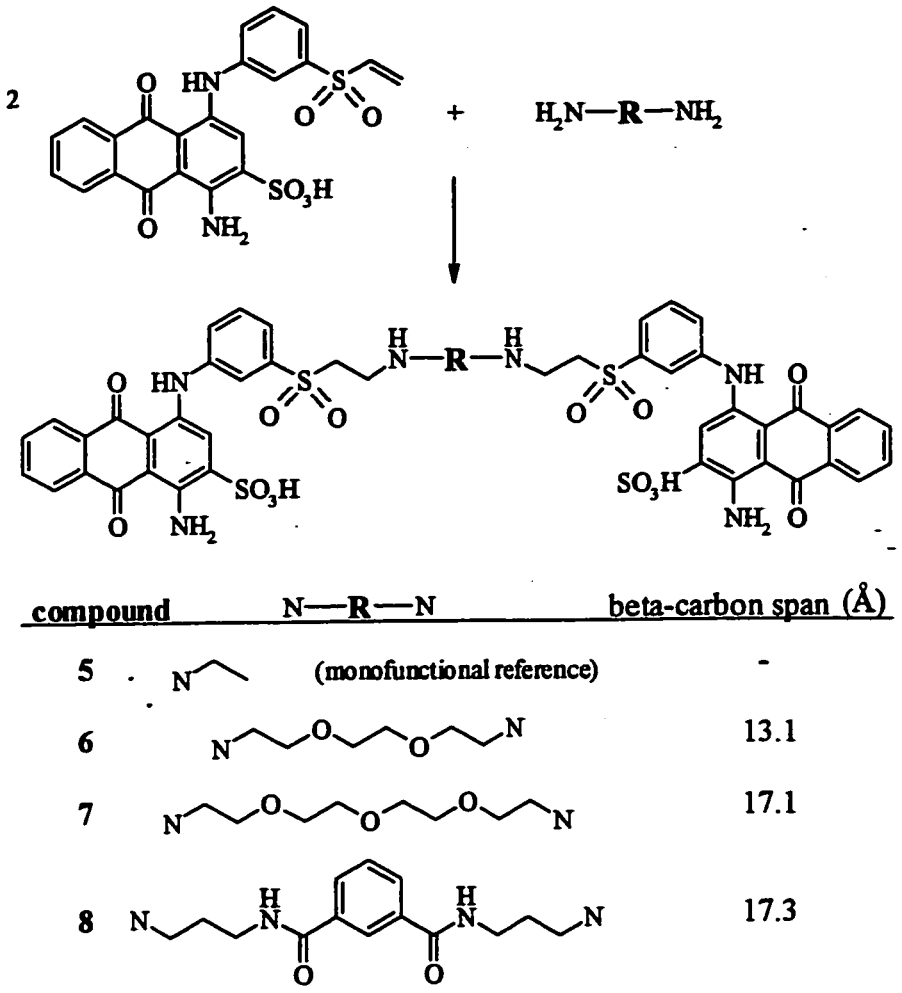

Figure 2.19. Scheme for the preparation of a series of *bis*-Uniblue A derivatives.

Kinetics. Again, the CDNB assay was employed to determine IC_{50}s for compounds **5** - **8** with GST isoforms P1-1 and A1-1. However, these compounds (including the monofunctional ethyl ester **5**) did not exhibit any inhibition of GST A1-1 at the highest inhibitor concentration tested (100 μM). The inhibition data for P1-1 are plotted in Figure 2.20, and the resulting IC_{50}s are tabulated within the figure. As with the *bis*-glutathionyl

nitrophenyl derivatives, the highest affinity compound (**6**) exhibits an IC_{50} approximately two orders of magnitude lower than that of the monofunctional reference compound, **5**.

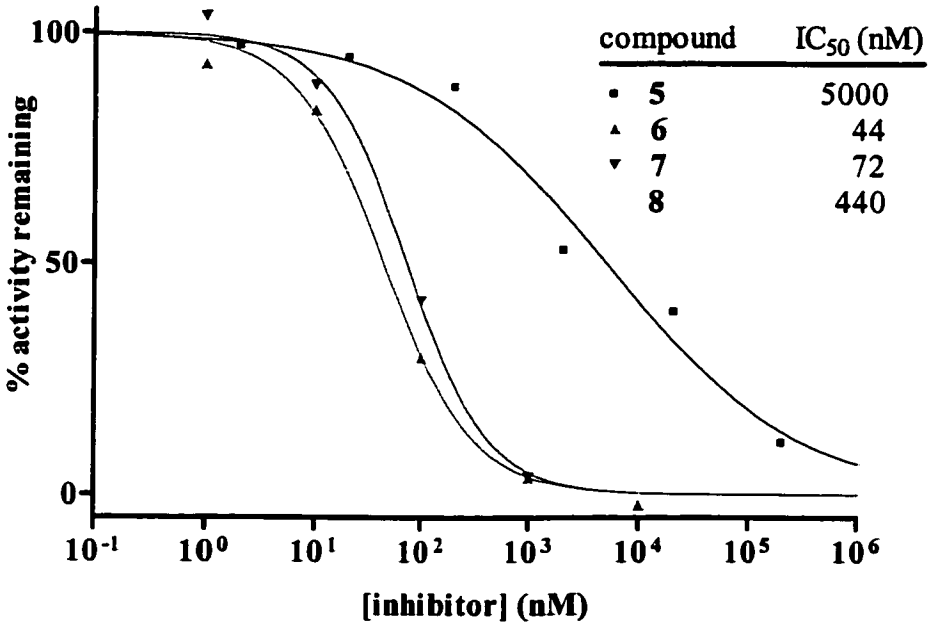

Figure 2.20. Inhibition of GST P1-1 by *bis*-Uniblue A derivatives. See Figure 2.18 for structures of compounds **5** – **8**. Numerical IC_{50} values are tabulated at upper right.

Interestingly, in this series of compounds, the two members with the flexible, ethylene glycol-based linkers both exhibit higher affinity than the isophthalamide-based compound, which is in contrast to the results seen in A1-1 inhibition by the *bis*-glutathionyl nitrophenyl derivatives.

Many 'non-substrate ligands' such as Cibacron Blue have been reported to be non-competitive inhibitors of the GSTs. Since the mechanism by which **5** – **8** elicit inhibition cannot be discerned from the IC_{50} determination, we selected the highest

affinity compound of this series (**6**) and performed assays at variable CDNB concentrations to determine the K_i and inhibition mechanism. The data from these studies were fit to the equation

$$v = \frac{V_{max} \cdot [S]}{K_m \cdot \left(1 + \frac{[I]}{K_i}\right) + [S] \cdot \left(1 + \frac{[I]}{\alpha \cdot K_i}\right)}$$

by global nonlinear fitting. This rate equation, which is discussed at greater length in Chapter 3, yields a K_i for the inhibitor plus the value α, which is a quantitative measure of the mechanism along the continuum from pure competitive to pure noncompetitive inhibition. Convergence on an α value of 1 reduces this equation to the rate equation for a non-competitive inhibitor, while expansion of α to infinity reduces it to the competitive model. Values between 0 and 1 or between 1 and infinity imply mixed inhibition with positive or negative cooperatively, respectively, in the binding of substrate and inhibitor.

The results of this global nonlinear treatment of the inhibition data are shown in Figure 2.21. The convergence values for the fitting parameters, as shown in the figure, are an α value of 6 and a K_i of 50 nM. The α of 6 suggests that compound **6** exhibits mixed inhibition of GST P1-1, neither purely competitive nor non-competitive. The determined K_i is in close agreement with the observed IC_{50} of 44 nM, suggesting that **6** is one of the highest affinity GST inhibitors to have been reported.

However, these assays (and the IC_{50}) assays were conducted at a GST concentration of 20 nM, meaning that the assays at the lowest inhibitor concentrations

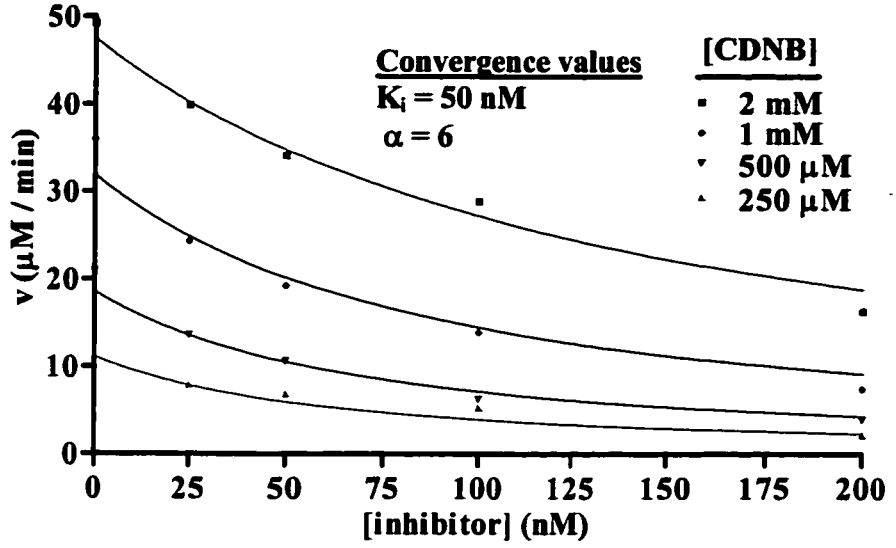

Figure 2.21. Global non-linear fit of P1-1 inhibition data by compound **6**. The best fit values for the K_i and α are 50 nM and 6, respectively; see text for the fitting equation.

contained a concentration of **6** scarcely above that of GST. Under such 'inhibitor depletion' conditions, the equations describing Michaelis-Menten kinetics do not neatly apply, as these assume that the total concentration of inhibitor (which is known) is equal to the concentration of free, unbound inhibitor (which is unknown). Compounds with such high affinity as to produce these conditions are often referred to as 'tight-binding' inhibitors. Although some may not consider that a 50 nM K_i suggests a tight-binding inhibitor, from an experimental point of view the only relevant factor is the ratio of the values of K_i and the enzyme concentration which must be employed in the assay. To more accurately determine the inhibition constants of tight-binding inhibitors, a more complex treatment needs to be employed. The equation

$$v_i = v_o \frac{[E] - [I] - K_i + \sqrt{([E] - [I] - K_i)^2 + 4[E]K_i}}{2[E]}$$

describes the reaction rate in the presence of inhibitor (v_i) as the product of the uninhibited reaction rate (v_o) and the fraction of free enzyme (Williams and Morrison, 1979; Kuzmič *et al.*, 2000). The quadratic term in the equation is derived from the expression of the inhibitor binding equilibrium, and the inhibitor concentrations are stated as total [I] rather than free [I] as in equations based on Michaelis-Menten kinetics. Note that substrate concentration is not a variable in this equation, but enzyme concentration is. Therefore, to perform an analysis by this method, inhibition data must be obtained at a single substrate concentration and multiple enzyme concentrations. We performed

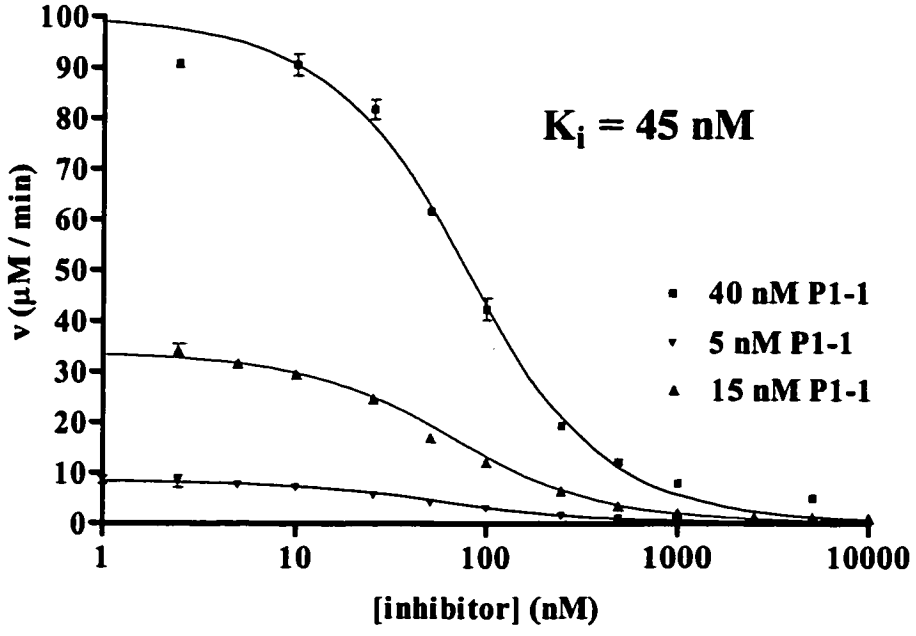

Figure 2.22. Global nonlinear fit of variable P1-1 concentration inhibition data by compound **6**. See text for the fitting equation.

assays at 5 nM, 15 nM, and 40 nM GST P1-1 and have plotted the resulting data in Figure 2.22. The data were again fit by global non-linear regression to the above equation, yielding a K_i of 45 nM, only slightly lower than the value obtained from the Michaelis-Menten analysis. However, this method does not provide insight as to inhibition mechanism, and the K_i which it produces is actually an apparent K_i, equal to the true K_i only in the case of noncompetitive inhibitors; for purely competitive inhibitors the true K_i is derived by dividing the apparent K_i by the factor $1 + [S] / K_m$ (Greco and Hakala, 1979). Because the previous analysis suggested mixed inhibition is operative in this case, it appears probable that the true K_i is lower than the apparent K_i; however, regardless of this uncertainty the observed value of 45 nM may be considered an upper limit for the K_i of compound 7.

2.3.3 Binding studies of bifunctional inhibitors

Several of the bifunctional compounds discussed above exhibit affinities two orders of magnitude greater than the relevant monofunctional reference compounds. However, the basis for this improved inhibition cannot be determined from the kinetic studies. If these compounds are indeed binding to GST in the fashion we envision, then they should bind at a stoichiometry of 1 per GST dimer; that is, the binding curves for these compounds should be saturated at a ligand:dimer ratio of 1:1.

One common method for determining binding stoichiometry is by titration of the intrinsic tryptophan fluorescence of the protein. Upon ligand binding, tryptophan

fluorescence is often observed to undergo a change in intensity and/or emission wavelength; this property can be exploited to follow the ligand binding curve. If the protein is present at high concentration relative to the K_d of the ligand (at least 10-fold above the K_d), then low concentrations of ligand will be essentially completely bound to the protein. Thus, the serial addition of small quantities of ligand will initially produce a linear response in the tryptophan fluorescence. As further ligand is added, the protein reaches its binding saturation point, and any additional ligand produces no further change in fluorescence. The resulting binding curve is therefore hyperbolic, and the fluorescence level of the saturation plateau and an extension of the initial linear part of the curve should intersect at the ligand concentration required for saturation.

GST P1-1 contains a tryptophan residue within its glutathione binding site and is therefore amenable to study by this technique. We performed a fluorescence titration with the highest affinity *bis*-glutathionyl alkyl ester for this isoform, the C_{18} compound (Figures 2.8, 2.11). Addition of this ligand produces a significant quenching of tryptophan fluorescence, which is plotted in Figure 2.23. Although the saturation plateau is very evident in this binding curve, the initial linear region appears to be biphasic. The earliest ligand additions, up to about 0.4 equivalents of ligand per dimer, produce dramatic linear tryptophan quenching which, when extended to the saturation plateau suggests that the ligand is binding at a stoichiometry of 1 per dimer. However, between about 0.4 and 1.5 equivalents, a second, less steep linear region prevails, which appears to intersect the saturation plateau at a stoichiometry of 2 per dimer. It thus appears that the enzyme is clearly capable of binding 2 equivalents of this ligand, as saturation is not

reached until after 2 equivalents have been added. However, the twofold change in the slope of the linear region suggests that at low ligand concentrations, 1 equivalent of ligand is eliciting quenching of both active site tryptophans. Note that at about 0.6

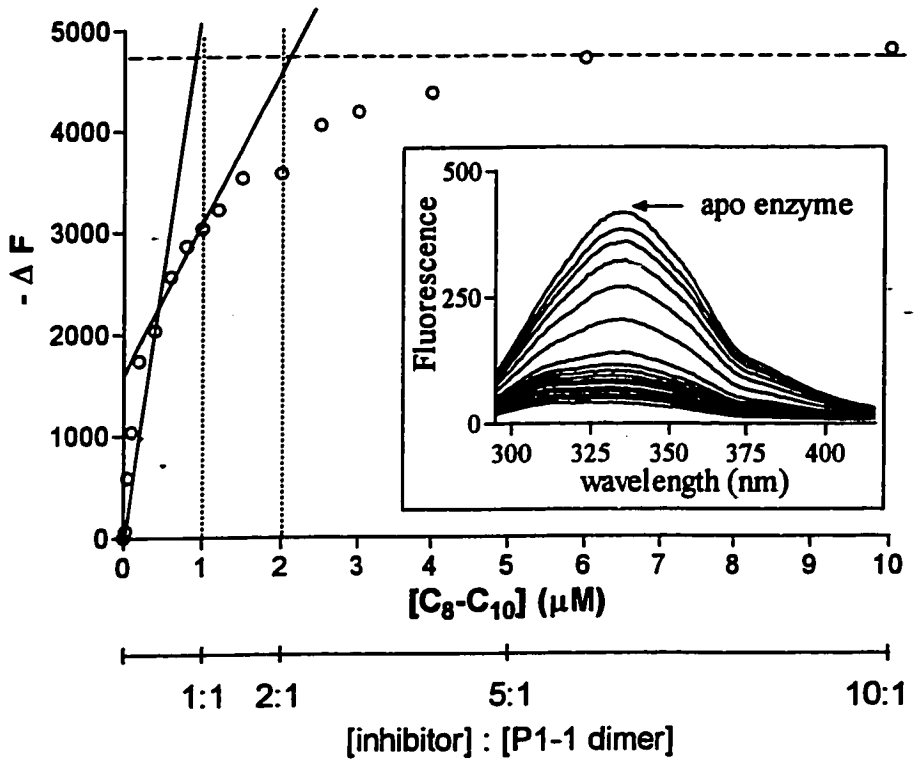

Figure 2.23. Fluorescence titration of GST P1-1 with *bis*-glutathionyl decyloctanoate. P1-1 concentration was 1 μM. Vertical dashed lines indicate points of 1:1 and 2:1 inhibitor : P1-1 ratios; horizontal dashed line represents saturation plateau. Solid lines indicate two linear regions of the titration. Raw fluorescence spectra acquired during the titration are shown in the inset.

equivalents of ligand, half of the total fluorescence quenching observed at saturation had already been attained.

A similar experiment was conducted with compound 4, the highest affinity bis-glutathionyl nitrophenyl derivative (Figures 2.13 and 2.15) for GST P1-1; the data are shown in Figure 2.24. This experiment was complicated by the fact that 4 absorbs at 280

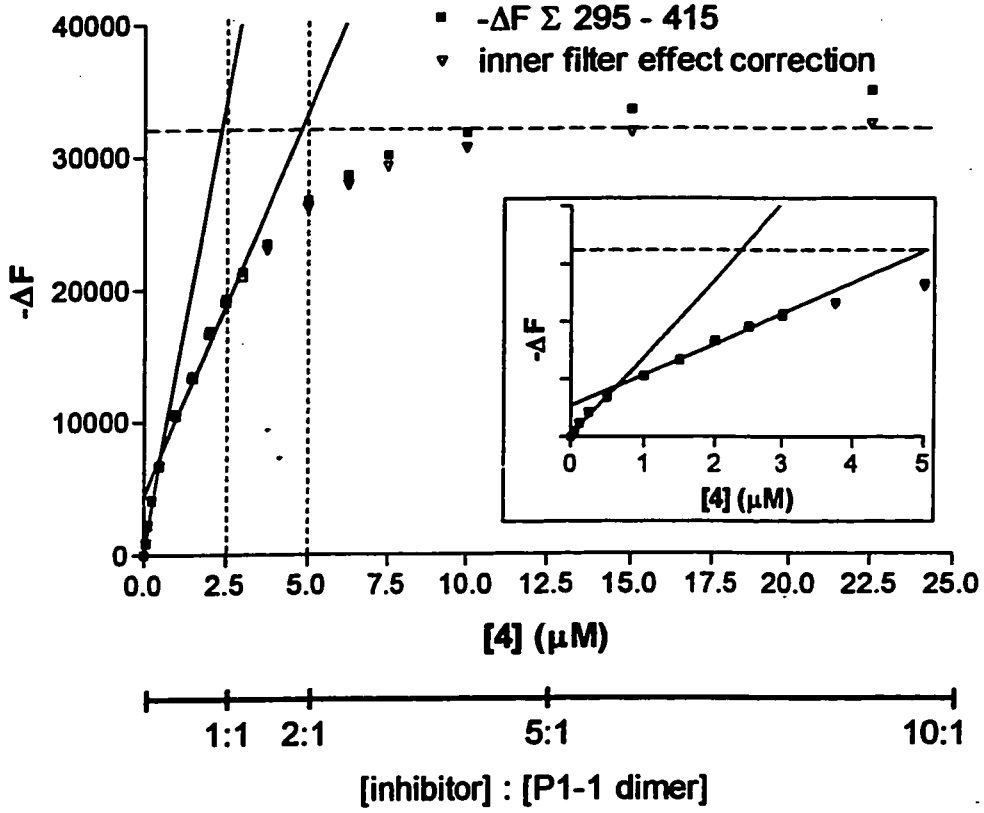

Figure 2.24. Fluorescence titration of GST P1-1 with compound 4. Correction for the inner filter effect is shown; inset details the biphasic nature of the linear region.

nm, the excitation wavelength used for the assay. Thus, some of the observed decrease in fluorescence is due not to quenching of tryptophan, but rather decreased intensity of the excitation beam due to the ligand acting as a partial filter. This 'inner filter effect' was compensated for by preparing a curve of the fluorescence decrease when ligand was

added to a cuvet placed between the excitation source and the protein sample. A 5 mm cuvet was chosen for the ligand solution, as in the actual titration experiment in a 10 mm path length cuvet, 5 mm is the average distance through which the excitation photons travel in the solution prior to striking the protein. The curve resulting from this filtration experiment was applied to the actual titration data shown in Figure 2.24; both the raw data and the corrected data are shown. It is evident that the inner filter effect is dramatic only at high ligand concentrations, where the applied correction greatly assists in identifying the saturation plateau. At low ligand concentrations, a biphasic linear response is again observed; from 0 to about 0.4 equivalents, the slope extends to a saturation stoichiometry of 1:1, but a second linear segment from 0.4 to 1.2 equivalent extends to a stoichiometry of 2:1.

A similar experiment with bifunctional non-substrate ligand **6** was attempted, but the absorbance of that compound at 280 nm was so great that the inner-filter effect is very large relative to the fluorescence quenching; useful data were therefore not obtainable. However, there are currently two experiments underway with our collaborators to further elucidate the binding mode of these bifunctional compounds to GST. One of these efforts is an isothermal calorimetry experiment with GST A1-1 comparing the thermodynamics of binding of the bis-glutathionyl nitrophenyl derivative **3** and its monofunctional counterpart **1**. If successful, this experiment will yield information about the binding stoichiometry of **3** as well as the differences in the enthalpic and entropic binding contributions between the bifunctional and monofunctional compounds. The second effort is crystallographic, with our collaborators currently trying to produce

crystals of A1-1 in complex with **3** and P1-1 in complex with **6**. If successful, the resulting structures could obviously shed enormous light on how these compounds interact with GST.

2.4 Discussion

The goals of this project have been to develop bifunctional inhibitors which exhibit significantly higher affinity and isoform selectivity than appropriate monofunctional analogs. Toward this end, we prepared several compounds based on the theme of two glutathione moieties separated by a spacer of appropriate length to place these moieties at the two glutathione binding sites of a GST dimer. By varying the length of these linkers, we hoped to find optimal sizes for two GST isoforms, P1-1 and A1-1, and thus attain isoform selectivity while simultaneously improving affinity through bivalent binding (Figures 2.1 and 2.2). It was imagined that if the length of a linker were too short to achieve bivalent binding, a *bis*-glutathionyl compound would bind with an affinity similar to that seen for a structurally related mono-glutathione compound, as both compounds would occupy only a single binding site. Our first series of compounds, based on linkers consisting of alkyl chains of varying lengths, did not produce these results. All of the bis-glutathionyl compounds exhibited similar affinity (Figure 2.10), and little isoform selectivity was observed (figure 2.11). However, these compounds did possess significantly higher affinities than the monovalent reference compound, although this may be due to the longer alkyl chains rather than the presence of the second

glutathione moiety. Subsequent to our preparation of these compounds, a crystal structure of GST P1-1 in complex with S-nonyl glutathione was published (PDB entry 12GS; Oakley et al., 1999). In this structure (Figure 2.25), the alkyl chain attached to the glutathionyl sulfur is oriented away from the intersubunit cleft, and therefore away from

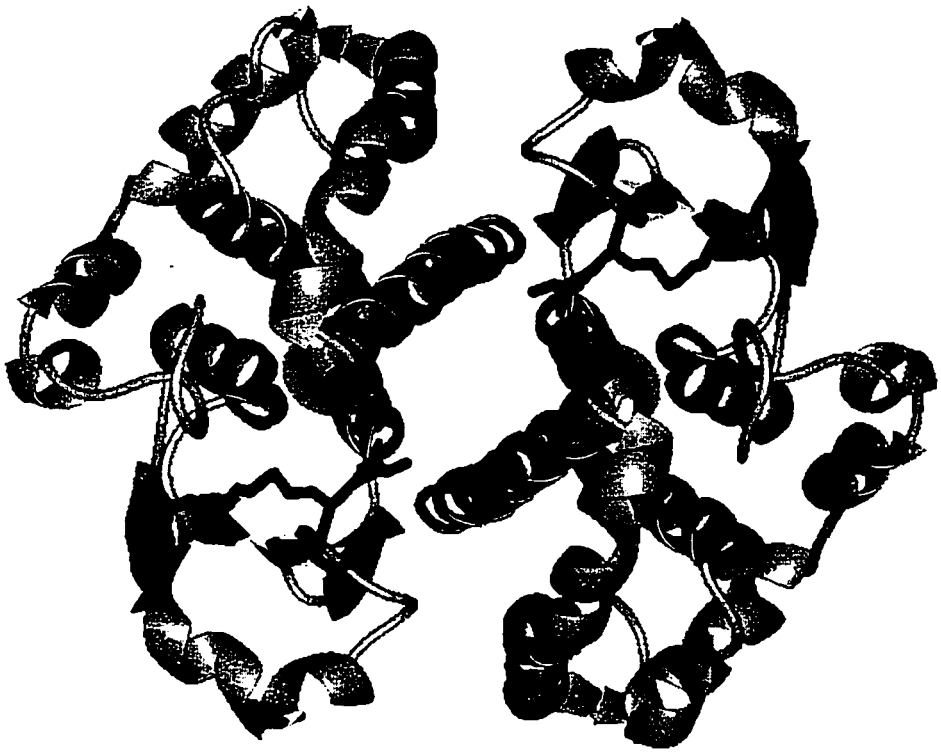

Figure 2.25. Crystal structure of the GST P1-1 complex with S-nonyl glutathione. Glutathione moieties are shown in green; nonyl moieties (red) extend from the glutathionyl attachment point in a direction away from the intersubunit cleft.

the other active site. If this is indeed the thermodynamically favored orientation of the alkyl chains of S-alkyl glutathione conjugates, it may be a significant barrier to achieving bivalent binding in the *bis*-glutathionyl alkyl ester series of compounds. In such a

binding orientation, these compounds may have one of the glutathione moieties profitably bound in one G-site, with the alkyl chain extended away from the intersubunit cleft and the second glutathione moiety extruding from the active site and into bulk solvent. This may explain the 2:1 saturation stoichiometry observed in the fluorescence titration curve of one of these compounds.

The second series of *bis*-glutathionyl compounds we prepared (**2** – **4**, figure 2.13) appear to exhibit more of the characteristics expected of bivalent ligands. For example, compounds **3** and **4**, which differ in length by only two methylene units, differ in their P1-1 IC_{50}s by an order of magnitude (Figure 2.15). For the P1-1 isoform, **4** is the highest affinity bifunctional compound, exhibiting an IC_{50} about two orders of magnitude lower than the monofunctional benchmark. Thus, with this series of compounds there appears to be greater discrimination between slightly longer or shorter linkers than was observed with the *bis*-alkyl esters. This is also seen in the results for A1-1, in which the bifunctional compound **2** exhibits no advantage over the monofunctional benchmark **2**, while the other two bifunctional compounds are each about an order of magnitude better. Also, while both isophthalate-based compounds (**3** and **4**) exhibited better inhibition of A1-1 than the more flexible ethylene glycol-based compound **2**, compounds **2** and **3** are nearly identical in their inhibition of P1-1. Finally, note that the highest affinity compound in this series (**4**) exhibits an approximately 10-fold selectivity for GST P1-1 over A1-1. The *bis*-glutathionyl nitrophenyl derivatives we have prepared therefore appear to have much more potential as bivalent GST inhibitors than the alkyl ester series,

owing to their higher affinity and isoform selectivity. These results seem to validate the approach of bivalency as we have applied it to designing inhibitors of GST.

However, the goal of designing GST inhibitors is eventually their use in cell- or animal-based models to assess their effectiveness in restoring alkylating agent sensitivity to resistant tumor cells, and ultimately as drugs in clinical use. It is probable that glutathione-based compounds would make poor drugs for several reasons. First, their ability to cross cellular membranes is likely very poor due to the highly charged and hydrophilic nature of glutathione. Second, even if they managed to diffuse into a cell, the presence of glutathione conjugate efflux pumps would result in the active transport of the compound out of the cell. Furthermore, they would likely be subject to rapid degradation by γ-glu-cys peptidase, the first enzyme in the mercapturic acid excretion pathway for glutathione conjugates. Finally, any glutathione conjugate inhibitor would almost certainly be competitive with respect to glutathione, which is present at intracellular concentrations greater than 20-fold above its K_m with GST. Therefore, to effectively compete (and thus inhibit the enzyme), an inhibitor would need to reach free, unbound intracellular concentrations at least 20-fold above its K_d; due to the difficulties stated above, this would appear to be very difficult to achieve. For all of these reasons, we chose to pursue inhibitors which are based on binding domains which occupy the hydrophobic substrate site. This represents a move away from purely *in vitro* enzyme inhibitors and toward molecules which are more 'drug-like.'

Compounds **6** – **8** (Figure 2.18) are the products of this effort to employ 'non-substrate ligands' as the binding domains of a series of bifunctional inhibitors. Two of

these compounds (**6** and **7**) exhibit P1-1 IC_{50}s two orders of magnitude lower than the monofunctional analog **5** (Figure 2.20). However, none of these compounds (including the monofunctional reference) exhibited inhibition of A1-1, so no statements can be made about how the bifunctional approach in this case affected isoform selectivity. However, it should be noted that compound **6**, with a K_i on the order of 45 nM, is the tightest-binding GST P1-1 inhibitor of which we are aware.

It is notable that in each of the three series of compounds discussed above, the highest affinity inhibitors exhibited IC_{50}s two orders of magnitude higher than the monovalent reference compounds. The consistency of the improvements in affinity observed in these series suggest a common mechanism; however, it remains unclear whether 1:1 binding in a bivalent fashion is that mechanism. Discovering the basis for this improved affinity is the subject of ongoing work on this project. Some useful information however may be found in experiments already completed.

It is interesting to note that many of the compounds which exhibit significantly higher affinities than their respective monofunctional references also exhibit significantly steeper slopes in their inhibition curves. This is best exemplified by the inhibition data for the *bis*-glutathionyl nitrophenyl derivatives with A1-1 (Figure 2.15, top). In these data, the two inhibitors (**3** and **4**) which exhibit IC_{50}s significantly lower than the monfunctional reference (**1**) possess very steep curves; the span of inhibitor concentrations between essentially no inhibition to essentially complete inhibition is little more than two orders of magnitude. In contrast, the monofunctional reference (**1**) and the low affinity bifunctional inhibitor (**2**) exhibit a concentration range of more than three

orders of magnitude between the 0% and 100% inhibition levels. These data were fit to the equation

$$v = \frac{100}{1 + 10^{B(\log IC_{50} - [I])}}$$

where B is a factor which varies the slope of the curve to achieve the best fit. The values of B (and standard errors) for compounds **1** – **4** with A1-1 were found to be –1.17 (0.06), -1.09 (0.03), -1.67 (0.13), and -1.71 (0.11), respectively. The high affinity bifunctional compounds **3** and **4**, then, exhibit B factors not quite twofold higher than those of the lower affinity compounds. Although the inhibition of P1-1 by these compounds (Figure 2.15, bottom) did not produce such a clear trend of increased slope with increased affinity, the inhibition of this isoform by the *bis*-Uniblue A derivatives (Figure 2.20) did yield dramatic differences in curve slope. The B factors (and standard errors) for compounds **5** – **8** with P1-1 were found to be –0.50 (0.06), -1.03 (0.08), -1.14 (0.16), and –0.87 (0.18), respectively. Again, slopes about twofold greater are observed for the high affinity bifunctional compounds relative to the monofunctional reference.

Such differences in the slope of a binding curve are generally attributed to cooperativity. In this case, the concept of cooperativity does not precisely apply, as cooperative binding is generally considered to be induced by a change in the protein or receptor rather than in some property of the ligand. Nonetheless, one of the principles of cooperativity does apply to bivalent ligands—that the dissociation constant of the second binding moiety of a bivalent ligand is lower than than that of the first. It is therefore not unreasonable to expect that the binding (or inhibition) curve of a bifunctional ligand to

resemble cases of positive cooperativity. The case of a bifunctional ligand is also complicated by the fact that one equivalent of ligand possesses two equivalents of binding (or inhibitory) potential. Since binding (or inhibition) curves are plotted against ligand concentration (rather than binding moiety concentration), it may be reasonable to expect a steeper curve for bifunctional ligands *if they are binding in a bivalent fashion.* The situation is analogous to performing a titration of a basic solution with 1M HCl or 1M H_2SO_4; the diprotic acid will neutralize the solution more quickly, producing a steeper titration curve if the pH is plotted against molar quantity of added acid. Therefore, the appearance of steep inhibition slopes in the data presented here may arise from the cooperative aspect of bivalent binding, the polyfunctionality of the ligands, or from an amalgamation of the two effects. Whatever the source, the slope of the curves exhibited by many of the highest affinity compounds would seem to suggest that they are indeed binding in a bivalent fashion.

The fluorescence titration curves (Figures 2.23 and 2.24) clearly indicate that bis-glutathionyl ligands are capable of binding to GST at a stoichiometry of 2:1; such a 'monovalent' binding mode probably involves one glutathione moiety bound at the G-site and second moiety extruding from the active site. However, these titrations produce an initial linear response, the slope of which is consistent with 1:1 binding. Since the GST concentration in these titrations is high relative to the Kd (at least 20-fold above), it can be assumed with confidence that essentially all of the ligand is bound to protein at the early titration points (hence the linear response). However, rather than plateauing after the addition of one equivalent of ligand, the fluorescence titration curves exhibit a second

linear region between about 0.5 and 1.5 equivalents, with a slope about one-half that of the initial linear region, suggesting 2:1 binding. A possible explanation of this biphasic behavior is that at very low ligand concentrations, the ligands do in fact bind in a bivalent, 1:1 fashion (i.e., occupying both glutathione binding sites of the dimer). As additional ligand is added, the presence of free ligand may be competing with one half of the bound ligand for the glutathione binding site. At this point, the relationship between K_{d1} and K_{d2} (Figure 2.2) would determine the population of bivalently bound and monovalently bound ligand. If K_{d2} is far lower than K_{d1}, one would expect an initial saturation plateau at a stoichiometry of 1:1, but as free ligand concentration increases, a point will be reached where a second ligand effectively competes with one end of the bivalently bound ligand. The greater the difference between K_{d1} and K_{d2}, the more pronounced this plateau would be expected to be. If K_{d1} and K_{d2} are quite close, then this plateau may be reduced to the biphasic linear regions shown here. However, these interpretations of the fluorescence quenching are predicated on the assumption that one molecule of bifunctional ligand bound in a bivalent fashion will elicit the same degree of fluorescence quenching as two molecules of bifunctional ligand bound in a monovalent fashion. Given the sensitivity of tryptophan fluorescence to its chemical environment, it is unlikely that this assumption is precisely true. Caution is therefore called for in the interpretation of these fluorescence titration spectra, and certain conclusions should not be drawn.

Notes to Chapter 1

1. The relevance of the intersubunit cleft as a binding site for non-competitive inhibitors discussed at length in Chapter 3.

CHAPTER 3

Kinetic Characterization of Native and Cysteine 112-modified Glutathione S-Transferase A1-1: Reassessment of Non-Substrate Ligand Binding[1]

3.1 Introduction

An intriguing aspect of GSTs is their multifunctional character, which stands in stark contrast to classical enzymology in which a given protein has evolved to carry out a precise task with high specificity. Within the broad function of glutathione transferase activity, substrates include both endogenous toxins resulting from oxidative stress and electrophilic species of environmental origin. Moreover, some reactions catalyzed by GSTs are part of a larger biosynthetic route toward prostaglandins and leukotrienes (Mannervik and Danielson, 1988; Armstrong, 1997).

GSTs also possess less well-characterized functions beyond the glutathione transferase activity. Recent studies have demonstrated a role for GST P1-1 in the regulation of Jun kinase, an important pathway in cellular apoptosis (Wang *et al.*, 2001; Yin *et al.*, 2000). Some isoforms, particularly A1-1 which is expressed at such high levels in the liver, may serve important functions as binding proteins for a variety of intracellular ligands. In this capacity, they may be cytosolic analogs of serum albumin. An hepatic protein with high binding capacity was identified in 1971 and termed 'ligandin' (Litwack *et al.*, 1971); subsequent research revealed that this protein was

identical to GST A1-1 (Kamisaka *et al.*, 1975; Ketley *et al.*, 1975). The physiological consequences of this binding has been a subject of debate for years and remains uncertain. Hypotheses for its significance include storage and transport of ligands, and tissue localization of ligands. It has also been suggested that this binding may have no physiological significance; the affinity for hydrophobic compounds may simply be a by-product of the non-specific active site which GSTs must possess in order to function as xenobiotic detoxification enzymes. However, many early studies with so-called non-substrate ligands found that these compounds inhibit the enzyme non-competitively, suggesting a binding site apart from the H-site (Bhargava *et al.*, 1978; Vander Jagt *et al.*, 1982; Ohl and Litwack, 1977). Moreover, many of these reports also indicated a binding stoichiometry of 1 per dimer (Kamisaka *et al.*, 1975; Ketley *et al.*, 1975), while substrates and glutathione conjugates clearly bind at 2 per dimer. For these reasons, the binding of non-substrate ligands remains an active area of GST research.

These observations have suggested a distinct non-substrate ligand binding site, which has been called various terms including the 'ligandin site' and 'L-site.' When the first crystal structure of a GST was published, the large, V-shaped intersubunit cleft near the two-fold symmetry axis immediately suggested itself as a binding site. As discussed in Chapter 1, this cleft is a very prominent feature common to all GST isoforms, and it quickly became a favorite candidate for the L-site. This hypothesis seemed to be confirmed when the structure of a cytosolic GST from the flatworm *Schistozoma japonicum* was found to include the antihelmenthitic drug praziquantel bound in the cleft (McTigue *et al.*, 1995). However, no crystal structures of GST A1-1 in complex with a

non-substrate ligand have been published, despite the fact that this isoform is most closely associated with the 'ligandin' function. Several studies employing indirect methods, such as affinity labeling (Barycki and Colman, 1997; Vargo and Colman, 2001) and fluorescence resonance energy transfer (FRET - Sluis-Cremer *et al.*, 1996), have supported the hypothesis that these ligands bind in the cleft.

Human GST A1-1 contains a single cysteine residue per monomer (cys 112) which lies within the intersubunit cleft (Figure 3.1). This residue is in the loop region between helices 4 and 5, adjacent to the hydrophobic substrate binding site. Its side chain thiol inserts into the intersubunit cleft, very near the twofold symmetry axis. We have prepared enzyme in which both cysteine residues of the dimer are involved in mixed disulfides with glutathione. Such 'glutathiolation' has recently attracted considerable research interest as an emerging regulatory mechanism for the modulation of protein activity. The observation that GST A1-1 is glutathiolated at cys 112 in many of our enzyme preparations prompted us to undertake the current study to determine if this modification affects the function of the enzyme. Work in several laboratories has demonstrated a variety of functional effects of protein glutathiolation, including protein aggregation and cellular heat-shock response, transcription factor-DNA binding, enzyme activation, and enzyme inactivation (McDuffee *et al.*, 1997; Klatt *et al.*, 1999; Ward *et al.*, 1998; Cabiscol and Levine, 1996; Chu *et al.*, 2001; Marshall *et al.*, 1997; Okamoto *et al.*, 2001; Demasi *et al.*, 2001). Because formation of a mixed disulfide from reduced cysteine is an oxidative modification, many of these researchers have postulated that glutathiolation of proteins may represent a regulatory event in response to oxidative

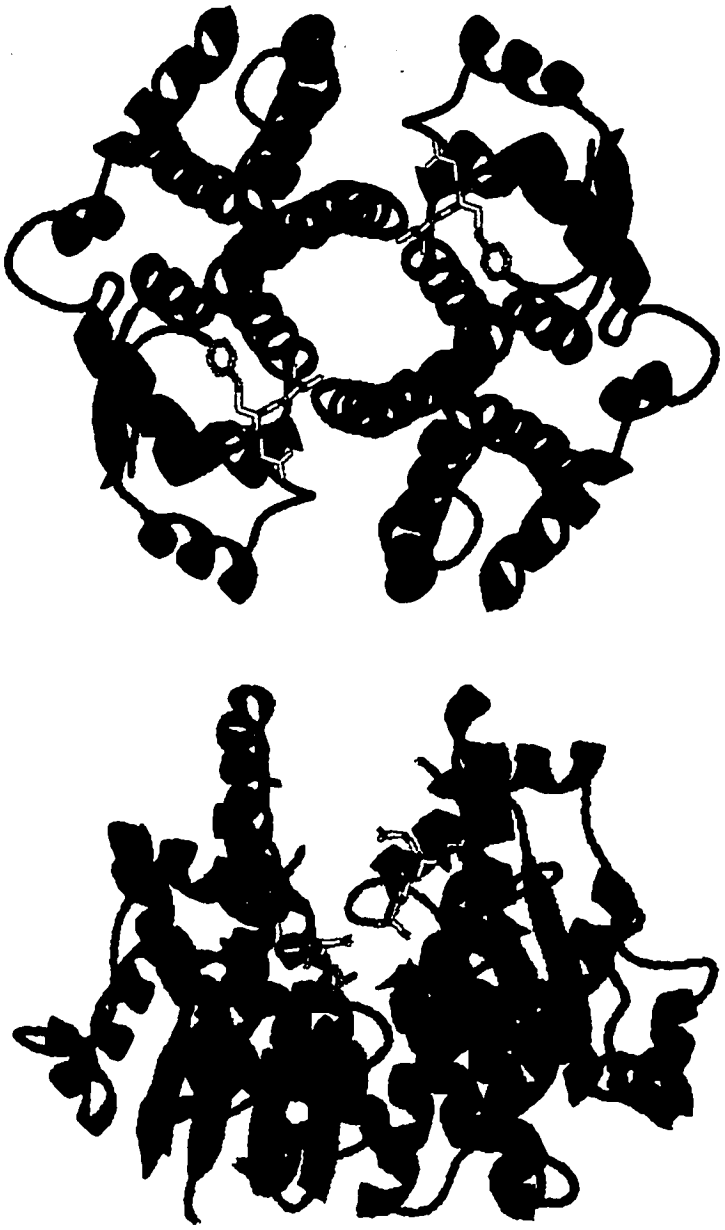

Figure 3.1. Two views of the GST A1-1 dimer (33). One molecule of S-benzylglutathione (yellow) is shown bound at each active site. The side chains of cysteine 112 A and B (red) are shown inserting into the intersubunit cleft.

stress. Glutathiolation may thus represent a common molecular switch in proteins relevant to cellular defenses against oxidative stress. Given the recognized role of GSTs in detoxifying electrophilic species, including lipid peroxides, epoxides, and other reactive oxygen species, these enzymes clearly play a significant role in responding to oxidative stress (Zhao *et al.*, 1999). Glutathiolation has been documented for two glutathione S-transferases, the cytosolic rat M4-4 isozyme and the human microsomal GST isozyme, with activation of glutathione conjugation activity demonstrated for the latter enzyme (Cheng *et al.*, 2001; Dafré *et al.*, 1996). GST A1-1 is subject to induction through the antioxidant response elements AP-1 and NF-κB by a variety of chemical agents which are either oxidants themselves or which are converted to reactive oxidative metabolizes by phase I xenobiotic metabolizing enzymes (Ramos-Gomez *et al.*, 2001; Pinkus *et al.*, 1996). We hypothesized that glutathiolation may be a further mechanism by which GST A1-1 is recruited to respond to oxidative stress.

The insertion of two highly charged and hydrophilic glutathione moieties into the intersubunit cleft would certainly be expected to alter the binding affinity of hydrophobic ligands if indeed they bind in this region. To further perturb the intersubunit cleft, we have exploited the proximity of the two equivalent cysteine residues of the dimer by crosslinking them with several different agents, thus imposing a direct blockade of the intersubunit cleft. Here we report the results of kinetic studies with cys 112 glutathiolated GST A1-1 and cys 112 crosslinked enzyme which strongly argue against the intersubunit cleft as the non-substrate ligand binding site. Moreover, a rigorous kinetic analysis of classical non-substrate ligands suggests that in many cases they may

act as simple competitive inhibitors, rather than non-competitively as previously considered. Together, these results prompt a reassessment of the 'ligandin' activity of GST A1-1.

3.2 Experimental Procedures

3.2.1 Materials

Reduced glutathione, ethacrynic acid, chloro-2,4-dinitrobenzene, β-estradiol-3,17-disulfate, hematin, and lithocholic acid, were purchased from Sigma. The crosslinking agents BMOE, BMB, BMPEO3, and BMPEO4 were purchased from Pierce. The glutathione-ethacrynic acid conjugate was prepared as described previously (Ploemen *et al.*, 1990).

Recombinant human glutathione S-transferase A1-1 was expressed in E. *coli* and purified as described previously (Ibarra *et al.*, 2001). The enzyme was incubated with 10mM dithiothreitol to ensure complete reduction of cysteine residues, followed by extensive dialysis to remove the reducing agent.

3.2.2 Chemical modification of GST

Glutathiolation incubations contained 1 μM GST in 100 mM phosphate buffer, pH 8.0. As a glutathiolation agent, 1 mM GSSG was added. Enzyme to be used for the

kinetic studies was shaken at 25°C until no native enzyme was detectable by electrospray mass spectrometry; that is, complete glutathiolation of the GST monomers was achieved. Native enzyme to be used as a control for the kinetic studies was incubated under the same conditions but without GSSG. Monitoring the extent of glutathiolation was achieved by LC-MS, using a 5 cm Poros R2 column (elution by a fast linear gradient from 5% AcCN / 0.05% TFA to 60 % AcCN / 0.05% TFA in 7 minutes) coupled to a Fisons VG Quattro II mass spectrometer fitted with a Z-spray ESI source. Electrospray mass spectrometry data were deconvoluted using the Maximum Entropy utility of the MassLynx software package.

To assess the intracellular glutathiolation of GST, HepG2 cells (an immortalized hepatocyte cell line) were grown and exposed to 50 μM H_2O_2 6 hours prior to harvesting. Cells were harvested, centrifuged, and sonicated immediately to preserve the existing glutathiolation state. Cellular extracts were quickly applied to glutathione affinity resin in a micro-column, washed, and eluted with S-hexyl glutathione. GST purified by this method was then assayed by mass spectrometry as described in the preceding paragraph.

Crosslinkage with various *bis*-maleimides was achieved by incubation of 10 μM GST in 100 mM phosphate buffer, pH 7.2, with the appropriate crosslinking agent. Stocks of the crosslinking agent were prepared in DMSO and added in aliquots of 0.5 equivalents. After each addition, the vial was shaken for 30 minutes at 25°C and the extent of the reaction determined by LC-MS as above. Additional crosslinker was aliquoted until the intensity of the unmodified enzyme peak in the mass spectrum represented less than 5 % of the intensity of the crosslinked dimer. Typically, this

required the addition of 2 to 3 equivalents of crosslinker (total incubation time 2 to 3 hours). Native enzyme to be used as a control was incubated under the same conditions but without any crosslinking agent.

3.2.3 GST assays

Activity of glutathiolated and native GST with chloro-2,4-dinitrobenzene (CDNB) as the electrophilic substrate was determined at 20 nM GST with 3 mM glutathione and variable CDNB concentration or 2 mM CDNB and variable GSH concentration. Rates were determined by measuring absorption at 340 nm (λ_{max} of glutathione-dinitrobenzene) for 1 minute on a Beckman DU 7400 spectrophotometer. For activity with 4-hydroxynonenal (HNE), 50 nM GST was incubated with 3 mM glutathione and 10 μM HNE, and the reaction monitored by absorption of HNE at 224 nm. Data were fit to the Michaelis-Menten equation using Graphpad Prism 3.0 to determine Km and Vmax. The activity of the crosslinked enzymes was determined at a single substrate concentration (3 mM GSH, 750 μM CDNB) and compared to unmodified control.

For inhibition assays with glutathiolated and native enzyme, GST concentration was 10 nM and CDNB concentrations of 250 μM, 500 μM, 1 mM, and 2 mM were paired with variable inhibitor concentrations as follows. For hematin, 0, 100 nM, 200 nM, 400 nM, 800 nM, 1.6 μM, 3.2 μM; lithocholic acid, 0, 2.5 μM, 5 μM, 10 μM, 20 μM; estradiol disulfate, 0, 25 μM, 50 μM, 100 μM, 400 μM, 800 μM; and glutathione-

ethacrynic acid, 0, 500 nM, 2 μM, 4 μM, 8 μM. Data were analyzed by global non-linear regression using Microcal Origin.

For inhibition assays with the crosslinked enzymes, GSH concentration was 3 mM and CDNB concentration was 750 μM. IC_{50}s were determined by varying the concentration of hematin.

3.3 Results

3.3.1 Preparation of Modified Enzymes

Figure 3.1 illustrates the location of the two equivalent cysteine 112 residues within the overall architecture of the GST A1-1 dimer. This residue lies in the loop region between helix 4 and helix 5, and its side chain thiol protrudes into the large, V-shaped intersubunit cleft. As seen in the lower panel of Figure 3.1, this cleft is roughly 'V' shaped and approximately 27 Å in depth. The side chain of cysteine 112 resides about 10 Å from the top of the cleft, while the span separating the cysteinyl thiols of the two monomers varies from 14.6 Å to 18.3 Å in the four published crystal structures (Sinning *et al.*, 1993; Cameron *et al.*, 1995). This difference is largely due to varying orientations of the side chain, as the distance between the alpha carbons of the two residues varies by less than 1 Å. We have prepared enzyme in which both of the cysteine residues are coupled to glutathione via disulfide bonds ('glutathiolated'). By reference to the two glutathione moieties of the bound S-benzyl glutathione in Figure 3.1, the amount

of space they would occupy within the cleft can be appreciated at a glance. We have also crosslinked these cysteine residues using four *bis*-maleimides whose lengths vary from 8 Å to 18 Å (Figure 3.2). While two of these agents appear to be shorter than the span between the cysteinyl thiols, the crystallographic B-values indicate that cysteine 112 resides within a very dynamic region of the protein. We therefore employed these short crosslinking agents to probe the stability of the intersubunit cleft as it is observed in crystal structures.

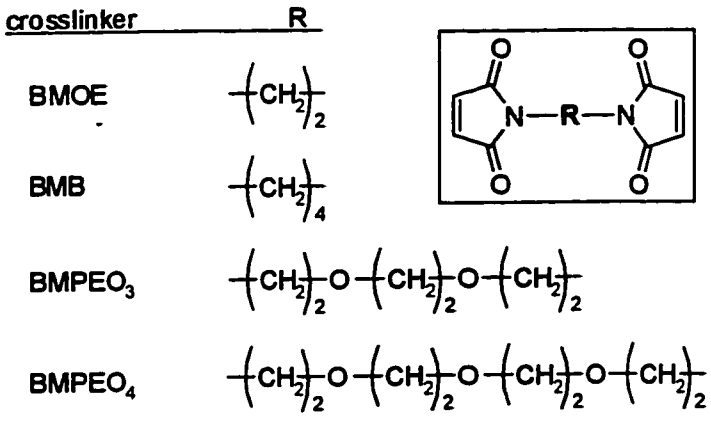

Figure 3.2. General structure of bis-maleimides used to crosslink GST A1-1. Lengths of the individual crosslinking agents vary and are specified in Table 2.

The progress of the chemical modifications made at cysteine 112 was followed by electrospray mass spectrometry. Maleimides react very selectively with cysteine residues at pH 7.2, and the formation of glutathione mixed disulfides is of course specific to cysteine residues. As this protein contains only a single cysteine residue per monomer, peptide mapping was not necessary to localize the modifications to cysteine 112. Since

the LC-MS process dissociates the dimer into its equivalent subunits, the mass spectrum of the wild type enzyme consists of a single peak at M_R 25500. Enzyme which has been crosslinked with *bis*-maleimides results in the appearance of a peak at 51000 + M_R of the crosslinking agent. This is illustrated in Figure 3.3 with the crosslinking agent BMB, which has a molecular weight of 250.

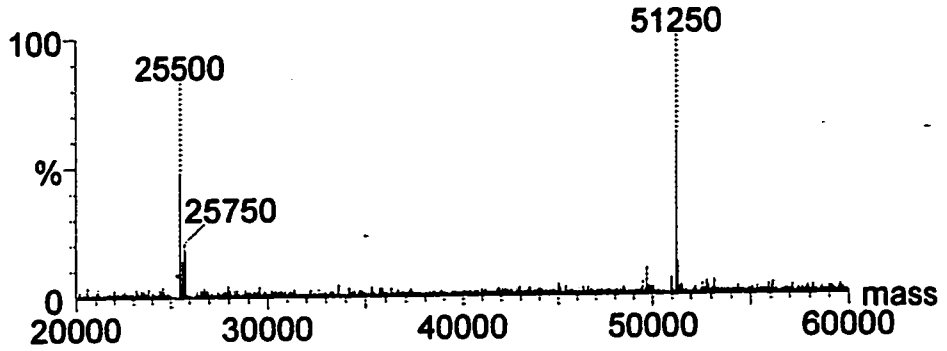

Figure 3.3. Deconvoluted electrospray mass spectrum of GST A1-1 partially crosslinked with the bis-maleimide BMB. At this early time point in the crosslinkage reaction, unmodified monomer is still present (M_R 25500) along with crosslinked dimer (M_R 51250). The reaction intermediate in which only one monomer has reacted with the crosslinker (M_R 25750) is observed only with the short crosslinkers BMB and BMOE.

Also visible in this spectrum are unmodified monomer (M_R 25500) and monomer which has reacted with one end of the crosslinker, but which has not yet been coupled to the other subunit (M_R 25750) . Interestingly, this intermediate species in the crosslinkage reaction (25500 +M_R of the crosslinker) is observed only with the relatively short crosslinking agents BMB and BMOE, whose lengths are shorter than the span between

the cysteine residues observed in the crystal structures. This is consistent with a scheme in which the second reaction step is too fast to observe when the geometry of the crosslinker is ideal. Even with the shortest crosslinker, however, nearly complete crosslinkage is observed in a 3 hour incubation.

Incubation with excess GSSG leads to formation of glutathiolated enzyme (M_R 25805), while incubation with DTT restores native enzyme (M_R 25500, Figure 3.4). The kinetics of this reaction are quite slow, requiring hours at 25°C to achieve complete glutathiolation as judged by mass spectrometry.

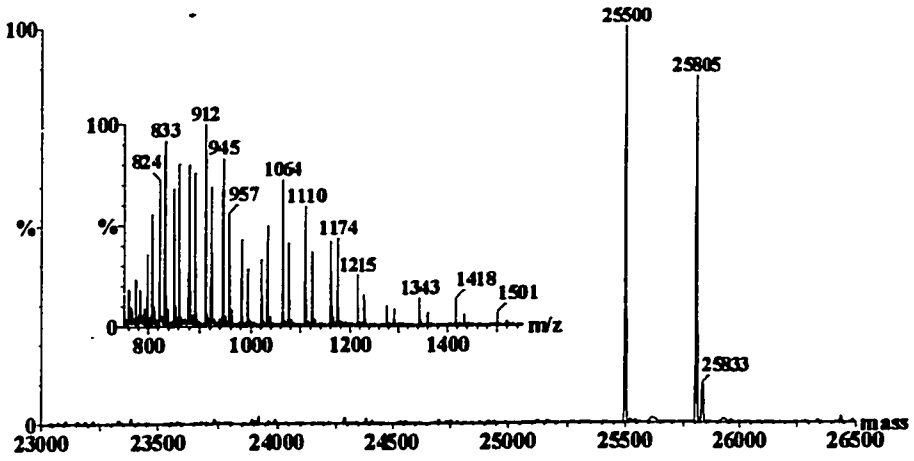

Figure 3.4. Electrospray mass spectrum of partially glutathiolated GST A1-1. The deconvoluted spectrum reveals native (25500 Da) and glutathiolated (25805 Da) monomers. Inset, the raw data illustrating the two envelopes of multiply charged ions arising from the two monomeric states.

To determine whether glutathiolation of GST occurs under cellular conditions (particularly under oxidative stress), HepG2 cells were grown in the presence and absence of H_2O_2. These cells were lysed and crude GST was prepared by the abbreviated purification described in section 3.2.2. In this purification, only the redox-inactive species S-hexyl glutathione is used to elute the GST from the glutathione affinity resin. This procedure eliminates the possibility of glutathiolation occurring during the purification as a result of exposure to GSH. Although active GST was isolated by this procedure, the quantity of protein recovered was of such a small order that the signal-to-noise ratio of the mass spectra of these samples did not provide conclusive evidence regarding the glutathiolation state of the enzyme. Therefore, a small fermentation of over-expressing *E. coli* cells were subjected to the same procedure. The enzyme from these cells was clearly native as determined by mass spectrometry; no glutathiolated enzyme was detectable (data not shown). When a portion of the GST from these cells was purified using GSH as the affinity eluent, substantial amounts of glutathiolated enzyme were observed by mass spectrometry. It therefore appears likely that the glutathiolation which we have observed in other enzyme preparations occurs during purification, and there is no evidence that this occurs intracellularly.

Since glutathiolation has gained recent attention as a potential regulatory mechanism, we considered that mass spectrometry may provide a rapid, sensitive means of determining the glutathiolation state of proteins. Indeed, emerging proteomics efforts rely heavily on mass spectrometry. Small-molecule glutathione conjugates exhibit a well characterized fragmentation in electrospray mass spectrometry involving cleavage of the

γ-glu-cys linkage. Using glutathiolated GST A1-1 as a test case, we performed tandem mass spectrometry to determine if a similar cleavage is observed in glutathiolated proteins. Such a spectrometric 'signature' could be used to identify glutathiolated proteins in a high-throughput environment. However, neither neutral-loss nor daughter ion scans revealed γ-glu-cys cleavage occurring in the glutathiolated protein.

3.3.2 Kinetics of Native and Glutathiolated GST A1-1

The glutathione conjugation activity of native and glutathiolated GST A1-1 was determined using variable concentrations of the diagnostic substrate chloro-2,4-dinitrobenzene (CDNB). Michaelis-Menten plots generated from these kinetic data are superimposable for the two forms (Figure 3.5), indicating that glutathiolation has no significant effect on glutathione conjugation activity. The kinetic parameters V_{max} and K_m were determined by non-linear regression of the Michaelis-Menten plots, and are tabulated within Figure 3.5. Using a fixed concentration of CDNB, a second set of assays was performed with variable GSH concentrations, which demonstrated that the K_m for GSH was also unchanged by glutathiolation (Figure 3.5, inset). Enzyme activity was also assayed with the long-chain substrate 4-hydroxynonenal, and was again found to be unaffected by glutathiolation (data not shown).

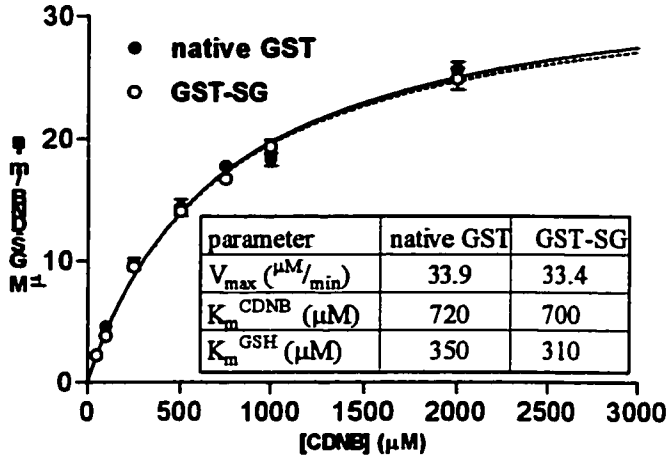

Figure 3.5. Overlaid Michaelis-Menten plots of CDNB turnover by native (closed circles) and glutathiolated (GST-SG, open circles) GST A1-1. The kinetic parameters derived from these plots are tabulated in the inset. Also included in the table is the K_m for glutathione of each enzyme form, derived from the corresponding experiment with variable GSH concentrations.

To assess the effect of glutathiolation on the binding of non-substrate ligands in the ligandin site, three such endogenous ligands were assayed for their inhibition of the enzyme activity: lithocholic acid (LCA, a bile acid), estradiol-3,17-disulfate (EDS), and hematin. The inhibition data were analyzed by global non-linear regression, which is a more robust analysis method than the linear regressions which have previously been used to characterize inhibition of GST by non-substrate ligands. Nonlinear regression is superior to linear regression as it does not require linear transformations which introduce distortions into the data set. Further, the global fitting method seeks to find the best fit to all of the data simultaneously rather than treating the data set from each concentration

condition independently, which effectively decreases the weight of any single data point on the overall fit. Our data were fit to the rate equation

$$v = \frac{V_{max} \cdot [S]}{K_m \cdot \left(1 + \frac{[I]}{K_i}\right) + [S] \cdot \left(1 + \frac{[I]}{\alpha \cdot K_i}\right)}$$

which is derived from the general inhibition expression shown in Scheme 1.

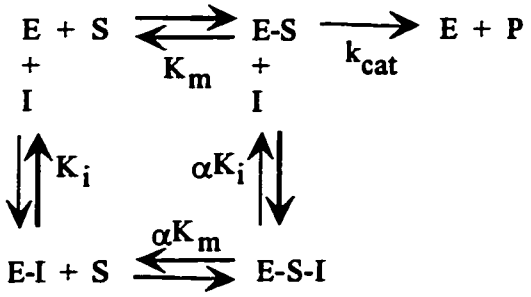

Scheme 1

This rate equation is noncommittal with respect to inhibition mechanism; rather, the regression routine is permitted to vary the factor α to achieve the best fit. If the best fit is obtained by expanding α to infinity, the iterations stop and the user can fix its value at some suitably large number; the equation then reduces to the rate equation for a competitive inhibitor. Convergence on an α value of 1 produces the rate equation for a non-competitive inhibitor. Values between 0 and 1 or between 1 and infinity imply mixed inhibition with positive or negative cooperativity, respectively, in the binding of substrate and inhibitor. Fitting data to this equation therefore provides a quantitative measure of the mechanism along the continuum from pure competitive to pure

noncompetitive inhibition. The kinetic parameters resulting from this analysis are shown in Table 3.1, along with results for the classical competitive GST inhibitor glutathione-ethacrynic acid (GS-EA). Again, no significant differences were seen between the native and glutathiolated enzymes. Unexpectedly, the parameter α, which provides a quantitative measure of the inhibition mechanism (α = 1 for non-competitive inhibitors, α = ∞ for competitive inhibitors) expanded to infinity for LCA and EDS suggesting that they, like GS-EA, are in fact competitive inhibitors with respect to CDNB. Only hematin produced an α indicative of an inhibitor possessing substantial non-competitive character.

Table 3.1. Comparative kinetic parameters of GST A1-1 inhibitors. Values for K_i and α were determined by global non-linear regression for native and glutathiolated (GST-SG) enzyme; α represents a measure of the inhibition mechanism (see text).

Inhibitor		Native GST	GST-SG
GS-EA	Ki (μM)	1.2 (0.1)	0.94(0.04)
	α	∞	∞
EDS	Ki (μM)	105 (9)	130 (10)
	α	∞	∞
LCA	Ki (μM)	7.3 (0.5)	5.5 (0.5)
	α	∞	∞
Hematin	Ki (μM)	0.20 (0.01)	0.24 (0.010)
	α	3.4	5.0

3.3.3 Kinetics of Crosslinked GST A1-1

For each of the crosslinked enzymes, CDNB conjugation activity at a single substrate concentration was determined relative to unmodified control (Table 3.2).

Table 3.2. Kinetic parameters of crosslinked GST A1-1.

Crosslinker	length (Å)	% activity	hematin IC_{50} (nM)
none (control)	-	100	200
BMOE	8.0	89	280
BMB	10.9	103	250
$BMPEO_3$	14.7	86	260
$BMPEO_4$	17.8	99	280

Again, it is evident that modification at cysteine 112 has little effect on the catalytic turnover of CDNB. Because the previous inhibition studies with non-substrate ligands revealed that only hematin was in fact a non-competitive inhibitor, this was the only compound assayed for its inhibition of the crosslinked enzymes. The hematin concentration required for 50% inhibition at a single substrate concentration (IC_{50}) was determined for each crosslinked enzyme and unmodified control, and the results are included in Table 2. As with glutathiolation, crosslinkage of these two residues across the intersubunit cleft has little effect upon the inhibition of GST A1-1 by hematin.

3.4 Discussion

These studies were initiated after mass spectrometry studies revealed that recombinant GST A1-1 produced in our laboratory was substantially glutathiolated in many of our enzyme preparations. This observation raised the possibility that glutathiolation may regulate GST A1-1 as it has been reported to regulate other enzymes,

including other GST isoforms. Given the multifunctional nature of GST A1-1, we hypothesized that glutathiolation may represent a means of 'switching' these functions on and off. Specifically, the location of the glutathiolated cysteine residue in the intersubunit cleft suggested that this modification may destroy this putative binding site of non-substrate ligands. Such an effect would represent a 'molecular switch' between the ligandin and glutathione conjugation activities, since ligand binding inhibits the enzyme but glutathiolation does not. This scheme would be consistent with the role of GST in the detoxification of lipid hydroperoxides and other reactive species generated under oxidative stress, since these conditions would be more likely to result in glutathiolated protein. By other mechanisms, glutathiolation may also alter the substrate specificity to favor detoxification of reactive oxygen species. Although the results of our studies with glutathiolated enzyme were contrary to our hypotheses , they were nonetheless intriguing from the more limited standpoint of the 'ligandin' function of GST A1-1. This prompted us to prepare the cross-linked enzyme as a further probe of our findings.

Cysteine 112 is not an active site residue in GST A1-1, however several nearby residues on helix 4 are directly involved in substrate binding. The adjacent residue, val 111, comprises the "top" of the hydrophobic substrate binding site (H-site). When substrate is bound, the highly dynamic C-terminal helix closes over the active site and contacts val 111 and pro 110. On the next turn of helix 4, three consecutive residues with aliphatic side chains (leu 108, leu 107, and ile 106) comprise the side of the H-site, providing direct hydrophobic contacts with the electrophilic substrate. Because of the

proximity and connectivity of these residues to cys 112, it is reasonable to expect that perturbations of the protein structure caused by modification of this residue may have implications for substrate binding and catalysis. Moreover, the orientation of the cysteinyl side chain into the intersubunit cleft suggests that adducts of this residue would insert into the space postulated to be the binding site of non-substrate ligands.

To determine the effect of glutathiolation upon the glutathione conjugation activity of GST A1-1, kinetic experiments were conducted with two structurally dissimilar substrates. The glutathiolated enzyme used in these experiments was completely glutathiolated as judged by mass spectrometry, such that both subunits of the GST dimer were glutathiolated at cys 112. The Michaelis Menten plots in Figure 3.5 illustrate that the native and glutathiolated forms of this enzyme are kinetically indistinguishable with chloro-2,4-dinitrobenzene (CDNB) as the substrate. Using a fixed concentration of CDNB, a second set of assays was performed with variable GSH concentrations, which demonstrated that the K_m for GSH was also unchanged by glutathiolation. The second substrate which we employed was 4-hydroxy-nonenal (HNE), which is a product of lipid peroxidation and is therefore physiologically relevant in cells under oxidative stress. Although HNE has been reported to be a relatively poor substrate for GST A1-1(Ålin, 1985), we speculated that if glutathiolation of this enzyme is indeed a regulatory event occurring during oxidative stress, its selectivity for oxidatively generated substrates such as this may increase. However, we again found indistinguishable kinetics between the native and glutathiolated enzymes (data not shown). Therefore, we have found no evidence that glutathiolation of cys 112 affects

substrate binding or catalytic turnover of this enzyme. In light of the protein architecture described above, this result is somewhat surprising. It thus appears that the addition of the large and highly hydrophilic glutathione moiety to cys 112 has no major effect on the conformation of the nearby hydrophobic residues which contribute to electrophilic substrate binding. The lack of structural perturbation upon glutathiolation has been confirmed by crystallography of partially glutathiolated protein (Le Trong, 2002). In these structures, the subunits which have been glutathiolated retain their native confirmation, while only the cysteinyl side chain of the attached glutathione is crystallographically observed, indicating the glutathione moiety is unstructured and highly dynamic.

Upon observing the somewhat surprising result that glutathione conjugation activity is unaffected by this modification, we assessed its impact upon the binding of non-substrate ligands. Glutathiolation of the two equivalent cys 112 residues effectively puts a cap on the intersubunit cleft, hindering the movement of bulky solutes from the top of the cleft. Modeling suggests that there may be enough space beneath the glutathiolated residues for relatively small ligands (e.g., steroids) to bind, but not for larger ligands such as porphyrins. Moreover, the highly charged nature of these glutathione moieties (totaling four free carboxylates and two amines) makes the chemical environment of the cleft region considerably more hydrophilic, and would certainly alter the affinity of hydrophobic ligands for this site. For these reasons, we postulated that glutathiolation of cys 112 may destroy the ligandin binding site of GST A1-1. However, the global non-linear analysis of our inhibition data with three non-substrate ligands

demonstrates that their binding is not significantly altered by glutathiolation of cys 112 (Table 3.1). Furthermore, this analysis indicates that two of the non-substrate ligands, the steroid derivative EDS and the bile acid LCA, inhibit the native enzyme competitively, suggesting that they bind in the H-site. To illustrate the ability of this analytical method to determine inhibition mechanism, Figure 3.6 presents the LCA inhibition data and

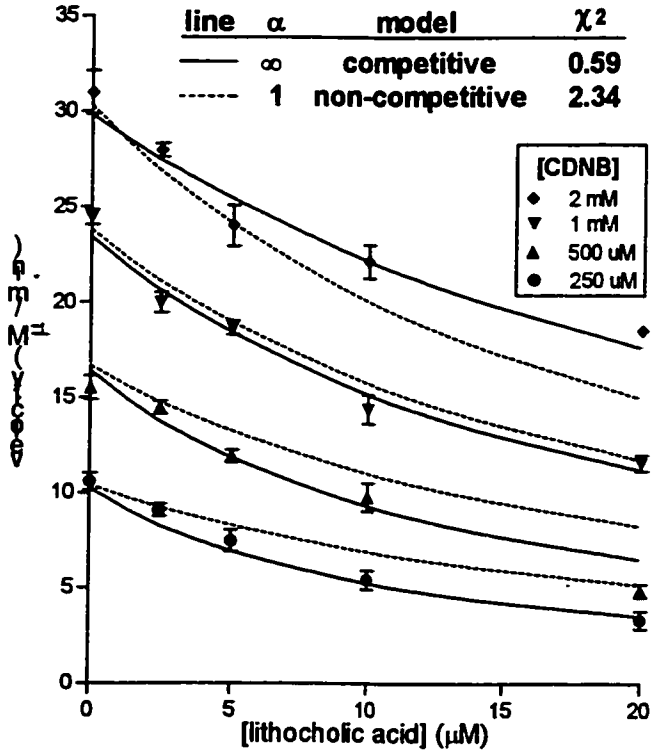

Figure 3.6. Comparative fitting of the LCA inhibition data when forced to fit the competitive ($\alpha = \infty$, solid lines) and non-competitive ($\alpha = 1$, dashed lines) inhibition equations, graphically illustrating the superiority of the competitive model to this system. When α is allowed to vary as a fitting parameter, the best fit is indeed achieved by expanding this factor to infinity.

compares the quality of the non-linear fits when forced to adhere to the competitive versus non-competitive models (fixed at ∞ or 1, respectively). The competitive model clearly produces a better fit of the data, as evidenced by the 4-fold greater value of χ^2 (sum of squares difference) for the non-competitive fit. Notice that at an intermediate CDNB concentration of 1 mM (near the K_m) the competitive and non-competitive fits yield similar curves. However, at substrate concentrations above this, the non-competitive model consistently predicts reaction velocities which are lower than those actually observed, while at lower substrate concentrations this model predicts velocities which are too high. Thus Figure 3.6 graphically illustrates the importance of performing inhibition assays over a wide substrate concentration range (above and below the K_m) to enable discrimination of the inhibition mechanism.

To further probe for binding in the intersubunit cleft, we employed the *bis*-maleimide crosslinking agents shown in Figure 3.2 to perturb the local structure and physically block entry of potential ligands. The lengths of these agents vary by a factor of greater than 2, covering a length range from 8 Å to 18 Å. The length of the shortest of these agents, BMOE, is about half the distance between the cysteinyl thiols observed in the available crystal structures (14.6 Å to 18.3 Å). Despite this, the two monomers of GST A1-1 are readily crosslinked even by BMOE, with only slightly longer incubation times required to achieve complete crosslinkage with the short crosslinkers BMB and BMOE. This effect is illustrated by mass spectrometry of an intermediate time point of the GST – BMB incubation (Figure 3.3), wherein three molecular species are clearly observable: monomer (M_R 25500), monomer-crosslinker (M_R 25750), and monomer-

crosslinker-monomer (M_R 51250). The rate of the initial reaction (monomer → monomer-crosslinker), which can be monitored by the disappearance of unmodified monomer, is similar for all of the crosslinkers tested. The longer crosslinkers $BMPEO_3$ and $BMPEO_4$ then react quickly with the second monomer to form the crosslinked dimer; the intermediate monomer-crosslinker species is not observed when these incubations are carried out at 25°C. This intermediate species accumulates to a small extent with the shorter crosslinkers, as the second reaction (monomer-crosslinker → monomer-crosslinker-monomer) is dependent upon the dynamics of the protein, requiring partial closing of the intersubunit cleft. That this reaction occurs at only a slightly slower rate with the shortest crosslinker is a testament to the mobility of this region of the protein.

Upon verification of complete crosslinkage of the enzyme by mass spectrometry, activity assays were conducted at a single substrate concentration and compared to unmodified control. As seen in Table 3.2, crosslinkage had minimal effect upon glutathione conjugation activity. It is remarkable that even crosslinkage with BMOE, which holds the intersubunit cleft about halfway closed relative to its crystallographic conformation, has little effect on catalytic activity. To assess the effect of crosslinkage on non-substrate ligand binding, the IC_{50} of hematin with of the crosslinked enzymes (plus unmodified control) was determined. Only hematin was assayed as an inhibitor since LCA and EDS both exhibited competitive inhibition with the native enzyme (Table 3.1), indicating that they bind in the H-site. These IC_{50} (Table 3.2) data indicate that, as with glutathiolation, crosslinkage of the enzyme at cys 112 does not affect the inhibition by hematin.

Much of the interest of enzymologists in the non-substrate ligand binding of GST A1-1 lies in the ability of these compounds to elicit non-competitive inhibition. We therefore employed inhibition kinetics (rather than direct binding measurements) to probe the effect of chemical modifications of cysteine 112. Our results suggest that LCA and EDS are simple competitive inhibitors, while hematin seems to fit the classical criterion of L-site ligands, non-competitive inhibition. However, the inhibition which it exhibits is not achieved by binding at the intersubunit cleft; that is, the 'L-site' must lie elsewhere on the enzyme. As we have not measured direct binding to the enzyme, it remains possible that hematin (or the other ligands) could bind at the intersubunit cleft of the native enzyme without catalytic consequence.

The fact that large, structurally diverse hydrophobic compounds bind to GST A1-1 is unsurprising given that its catalytic function is to conjugate glutathione to xenobiotics. Indeed, the primary difference between a substrate for the enzyme and a non-substrate ligand may simply be the presence or absence of an electrophilic center suitable for reaction with glutathione. Given the lack of substrate specificity which this enzyme exhibits (and which is necessary to fulfill its role as a xenobiotic detoxification enzyme), one might reasonably expect that a variety of hydrophobic but unreactive compounds would bind in the active site and act as competitive inhibitors. Due to the inherent lack of specificity of this enzyme, the binding modes of substrates and non-substrate ligands alike are probably very dynamic, with small free energy differences between multiple bound conformations. However, the reports that certain hydrophobic compounds (particularly endogenous anions such as porphyrins and bile acids) act as

non-competitive inhibitors led to the assumption that they bind at a discrete site. In the crystal structure of a cytosolic GST from *Schistozoma japonicum*, the antihelmenthitic drug praziquantel was observed to be bound within the solvent-accessible intersubunit cleft region, which became a candidate for the ligandin site (McTigue *et al.*, 1995). However, it is notable that praziquantel has been reported not to be an inhibitor of this enzyme (Sluis-Cremer *et al.*, 1996; Walker *et al.*, 1993), suggesting that binding within the cleft as observed in the crystal structure does not interfere with catalytic activity. The *S. japonicum* enzyme contains a prominent tyrosine residue (tyr 104) within the cleft which makes hydrophobic contacts with praziquantel along the entire length of its side chain. The authors of this paper, however, note that mammalian GSTs of known structure lack a tyrosine residue at this position. The equivalent residue in human GST A1-1 is glu 104, which is involved in a salt bridge with arg 15. In fact, there are no aromatic residues within the intersubunit cleft of GST A1-1, and the environment there is not particularly hydrophobic. Interestingly, no crystal structures have emerged of GST A1-1 in the presence of non-substrate ligands despite the fact that this isoform is most closely associated with the ligandin function.

In a very recent thermodynamic study (Sayed *et al.*, 2002), other workers demonstrated that 8-anilino-1-naphthalene sulfonate (ANS) binds to GST A1-1 with a stoichiometry of 2 per dimer. Moreover, they showed conclusively that hydrophobic interactions with phenylalanine 222 contribute significantly to ANS binding. This residue, which lies at the end of the C-terminal helix, closes over the H-site when substrate is bound. For example, in the crystal structure of the GST A1-1 - ethacrynic

acid complex (Sinning *et al.*, 1993), this residue contributes aromatic interactions with the bound substrate. Although the authors of this study concluded that ANS binds at the edges of the intersubunit cleft, their results are perhaps more consistent with ANS binding independently at the two H-sites of the GST A1-1 dimer. One difficulty in comparing the results of this thermodynamic study with those of other workers using different methods is that different ligands were employed in each case. Our kinetic results with native, unmodified enzyme indicate that non-substrate ligands have different inhibition mechanisms (Table 3.1), and there is no compelling reason to believe that they all bind at the same site. Questions of the binding site, binding stoichiometry, and inhibition mechanism must be considered on a case by case basis for each non-substrate ligand; that is, it cannot be assumed that all hydrophobic anions interact with GST in the same manner.

A variety of organic anions including dyes and acidic drugs have been characterized as inhibitors of different GST isoforms. Two such examples are cibacron blue (discussed in Chapter 2) and bromosulfophthalein, both of which are non-substrate ligands which have been reported to be non-competitive inhibitors of GST P1-1. In a recent crystallographic study, however, these ligands were clearly localized to the hydrophobic substrate binding site; the observation of non-competitive inhibition appears to be due to the large size of this site which can be simultaneously occupied by substrate and inhibitor (Oakley *et al.*, 1999). GST A1-1 has a similarly large hydrophobic substrate site, and the fact that nearly all investigators use the relatively small substrate CDNB makes it distinctly possible that dual occupancy occurs in this

isoform as well. Non-competitive inhibition by ligands bound in the H-site may be elicited by several mechanisms. For example, it may change the bound conformation of CDNB such that the electrophilic center is improperly oriented for conjugation, or prevent the proper alignment of the catalytic tyrosine residue with GSH, or prevent product release by holding the C-terminal helix in a 'closed' position. Moreover, glutathione conjugation of larger substrates which occupy more of the H-site may be inhibited competitively by compounds which exhibit non-competitive inhibition of CDNB turnover. We note that researchers in the cytochrome P450 field have recently observed dual occupancy in the active sites of these xenobiotic metabolizing enzymes, producing inhibition profiles which vary when different substrates are employed (Shou *et al.*, 1994; Wang *et al.*, 2000). Indeed it may be a general phenomenon that in the presence of multiple potential ligands and substrates, enzymes with large, non-specific active sites produce atypical kinetics in which classical enzymological considerations may not apply.

Upon examination of the available crystal structures of GST A1-1 (Sinning *et al.*, 1993; Cameron *et al.*, 1995), it is immediately clear that the intersubunit cleft can be viewed as a channel between the two active sites of the dimer. Indeed, the two H-sites and the intersubunit cleft together form a roughly S-shaped, solvent-filled channel in the enzyme, which presents very hydrophobic environments at the ends of the 'S' (the two H-sites), but which transitions through a rather more hydrophilic environment within the cleft (Figure 3.7). Glutathiolation or crosslinkage of cys 112 effectively cuts this 'S' in half by blocking the cleft near the twofold symmetry axis. It appears plausible that

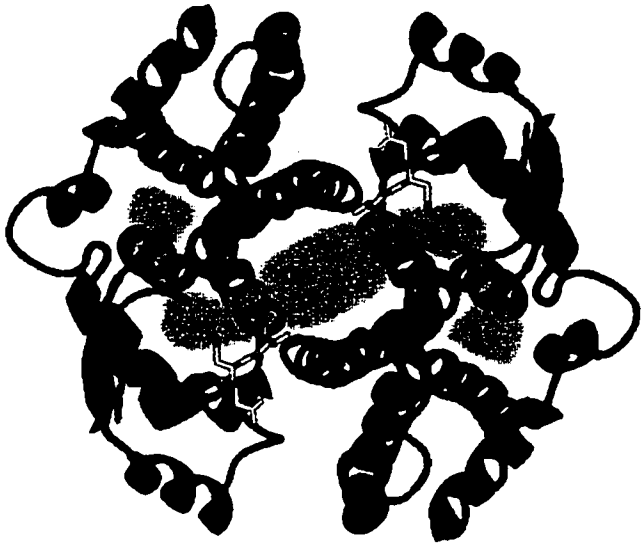

Figure 3.7. View of the GST A1-1 dimer along the 2-fold symmetry axis. The shaded area represents the continuous, solvent-filled S-shaped channel which defines potential binding sites to this enzyme. S-benzylglutathione (yellow) and cysteine 112 (red) are highlighted for reference. This channel is constricted between met 208 and pro 110 at the H-site, but expands into a broad, hydrophobic region at the ends of the S-curve.

amphipathic compounds could bind by hydrophobic interactions at the edge of one of the H-sites, but spill out into the cleft to retain solvation of its polar functional groups. The H-site has been recognized as the hydrophobic region adjacent to the thiol function of bound glutathione, and is comprised largely of aliphatic residues from helix 4 (leu 107, leu 108, pro 110, val 111), met 208, and several residues of the highly dynamic C-terminal helix which begins at glu 210. There is a constriction between met 208 and pro

110, but on the other side of that constriction the protein architecture expands again into a broad hydrophobic cavity. This region is bounded by helices 4, 5, and 7, and the loop region preceding the C-terminal helix. As shown in Figure 3.8, hydrophobic residues from each of these structural elements line the sides of this cavity. In the crystal structure

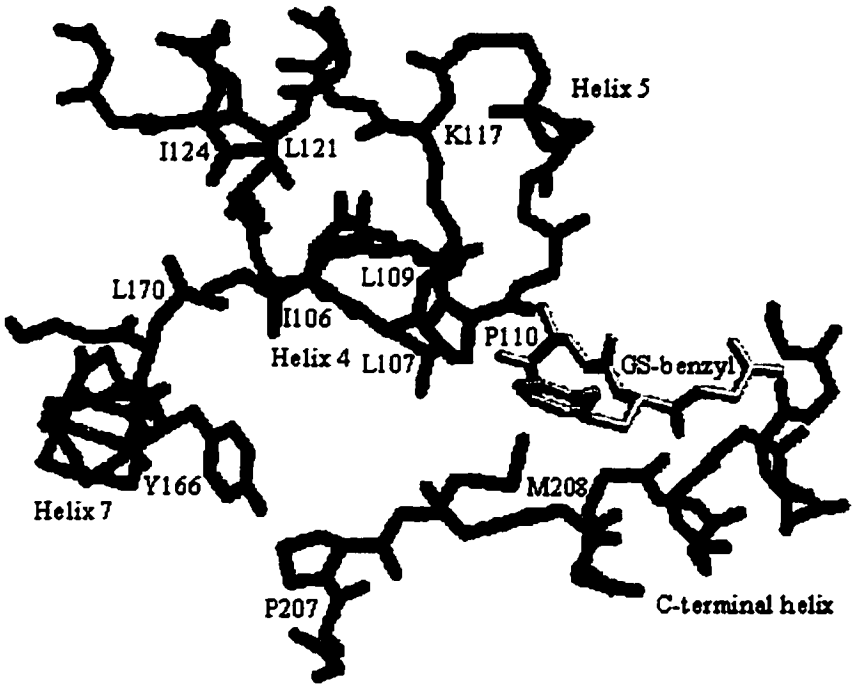

Figure 3.8. Inspection of hydrophobic residues (gray) in the cavity adjacent to the H-site; S-benzylglutathione (yellow) is included for reference. These residues are located on helices 4, 5, and 7, and the loop region preceding the C-terminal helix. Lysine 117 (blue) is located on helix 5 and its cationic side chain lies at the top of the cavity. Note the constriction between met 208 and pro 110 which partially separates this cavity from the H-site.

of the apo enzyme, as well as in complex with ethacrynic acid and its glutathione conjugate, this cavity is open to bulk solvent and contains multiple crystallographically observed water molecules (Sinning *et al.*, 1993; Cameron *et al.*, 1995). Lysine 117 from helix 5 lies at the top of this hydrophobic region, and its side chain is not involved in any salt bridges within the enzyme. An unpaired positively charged residue adjacent to a large, solvent-accessible hydrophobic pocket immediately suggests a potential binding site for organic anions which typify the non-substrate ligands of this enzyme. We believe that the hydrophobic nature of this site with its proximity to the sidechain of lys 117 makes this a more plausible binding site for organic anions such as hematin than the relatively hydrophilic intersubunit cleft. It may be noteworthy that the loop region between helices 4 and 5 (in which lys 117 resides) is reported to be involved in crystallographic interactions (Cameron *et al.*, 1995), suggesting that the involvement of these residues in protein-ligand interactions may alter the crystallization properties of the enzyme. Indeed, we have tried to obtain diffractable crystals in the presence of hematin with no success and have little doubt that others have tried as well; yet no crystal structures of this high-affinity enzyme-ligand complex have been published to date. This newly described site is separated from the established H-site by a narrow gap between met 208 and pro 110. The Cα-Cα distance between these residues varies from 7.4 to 8.4 Å in the available crystal structures, which may restrict direct passage of bound ligands or substrates from one site to the other. However, both of these residues occur in dynamic regions of the protein, with the B-factors of the α-carbons of met 208 and pro 110 reported as 50 $Å^2$ and 47 $Å^2$, respectively, in the apo enzyme with a global average

B-factor of 26 $Å^2$ (Cameron *et al.*, 1995). Given this mobility, it is difficult to assert whether this second hydrophobic pocket should be viewed as a discrete potential binding site or rather as simply an extension of the H-site.

Notes to Chapter 3

1) The work described in this chapter has been previously published:

Lyon, Robert P. and Atkins, William M. (2002) Kinetic Characterization of Native and Cysteine 112-Modified Glutathione S-Transferase A1-1: Reassessment of Nonsubstrate Ligand Binding. *Biochemistry* **41**, 10920-10927.

2) Residue numbering reflects the presence of the transcription initiator codon for an N-terminal methionine residue. Although mass spectrometry indicates that this residue is not present in our protein preparations, we retain the numbering convention to maintain consistency with other literature.

CHAPTER 4

Self-Assembly of Glutathione Disulfide in Organic Solvents[1]

4.1 Introduction

Considerable attention has been given to polymers and small molecules capable of self-assembly into extended non-covalent structures such as nanotubes and tapes (Voyer, 1997; Hartgerink *et al.*, 1996; Aggeli *et al.*, 1997). Under appropriate conditions, these assembled arrays are often observed to trap bulk solvent and result in the formation of transparent gels (Aggeli *et al.*, 1997b; Hanabusa *et al.*, 1993; Wang *et al.*, 1999). Such gels constructed of biocompatible materials have been sought by researchers in fields such as biomaterials, biosensors, tissue engineering, and drug delivery (Holmes *et al.*, 2000; Tan *et al.*, 1998). For these applications, peptides and proteins have emerged as ideal gelling agents. Numerous proteins and peptides, both natural and synthetic, have been shown to produce aggregates and gels in various solvent systems (Aggeli *et al.*, 1997; Aggeli *et al.*, 1997b; Tan *et al.*, 1998; Kirschner *et al.*, 1987). While large proteins in denaturing conditions can cause gelation by non-specific tangling of the protein backbones, the formation of gels by small proteins and peptides is often the result of highly specific interactions to form long, non-covalent supramolecular assemblies. Considerable work has focused on engineering peptides to manipulate these interactions and control their gelation properties (Aggeli *et al.*, 1997; Osterman and Kaiser, 1985; Krejchi *et al.*, 1994). A common structural motif of the peptides which

have resulted from these efforts is the antiparallel β-sheet. Several peptides have been designed to form extended intermolecular β-sheets in appropriate solvents, causing gelation at sufficiently high concentrations (Aggeli *et al.*, 1997; Aggeli *et al.*, 1997b). A set of design principles has emerged from these studies for the engineering of peptides which form β-sheet arrays. These principles include: a minimum of six residues per strand; strong attractive forces between the side chains of adjacent strands (hydrophobic, hydrogen bonding, and electrostatic); an element of lateral recognition to configure adjacent strands in an antiparallel fashion; and solvent interactions to maintain solubility in the desired solvent (Aggeli *et al.*, 1997; Aggeli *et al.*, 1997b).

The self-assembled β-sheets of these engineered peptides resemble the abnormal protein aggregates characteristic of numerous diseases, including the prion rods of spongiform encephalopothies, polyglutamine fibrils of Huntington's disease, and amyloid plaques of Alzheimer's disease (AD) (Aggeli *et al.*, 1997b). Indeed, a fragment consisting of residues 1-28 of the AD amyloid β-protein has been reported to form gels in aqueous solutions (Kirschner *et al.*, 1987). The interactions which produce aggregates and gels of peptides in various solvent systems may thus represent models of pathological *in vivo* protein aggregation and abnormal protein folding. Recent observations that many unrelated proteins may form amyloid fibrils under appropriate conditions has suggested that the ability to adopt an amyloidogenic conformation is independent of sequence, being rather a characteristic of the conserved polypeptide backbone (Chiti *et al.*, 1999; Guijarro *et al.*, 1998; Gross *et al.*, 1999).

The ubiquitous tripeptide glutathione (γ-glu-cys-gly, GSH) is present in nearly all known aerobic organisms. Glutathione concentrations in human tissues are typically in the 1 – 10 mM range (Slivka *et al.*, 1987; Meister, 1991).. The multiple, well-characterized functions of GSH include detoxification of exogenous electrophiles and reactive oxygen species, maintenance of cellular thiol status, and serving as a cofactor in the biosynthesis of endogenous compounds (Meister, 1991; Hayes and McLellan, 1999; Seis, 1999). Additionally, there is indirect evidence that glutathione may have roles in protein folding, signaling, and regulation via thiol-disulfide exchange (Cotgreave and Gerdes, 1998; Darby *et al.*, 1994). Its role as an antioxidant is mediated by recycling of glutathione between its reduced form as a free thiol (GSH) and its oxidized disulfide (GSSG) form. Glutathione is an unconventional peptide in that the glu-cys linkage is via the side chain carboxylate of glutamate (see Figure 4.1).

We have observed that GSSG produces transparent, thermoreversible gels in dimethylsulfoxide (DMSO) and in aqueous solutions of dimethylformamide (DMF) and methanol. By electron microscopy, these gels appear as a fibrous network of filaments approximately 75 nm wide. The filaments stain with Congo Red and exhibit strong green birefringence, suggestive of a crossed β-sheet structure similar to β-amyloid. Analog studies indicate that the γ-glu-cys peptide linkage of glutathione is a structural motif critical to the gelation behavior. GSSG is considerably smaller than other natural peptides which have been shown to adopt an amyloidogenic configuration, and its peptide backbone is unique due the γ-glu-cys linkage. Previous spectroscopic studies suggest that in aqueous solution, GSSG adopts an intramolecular, antiparallel β-sheet

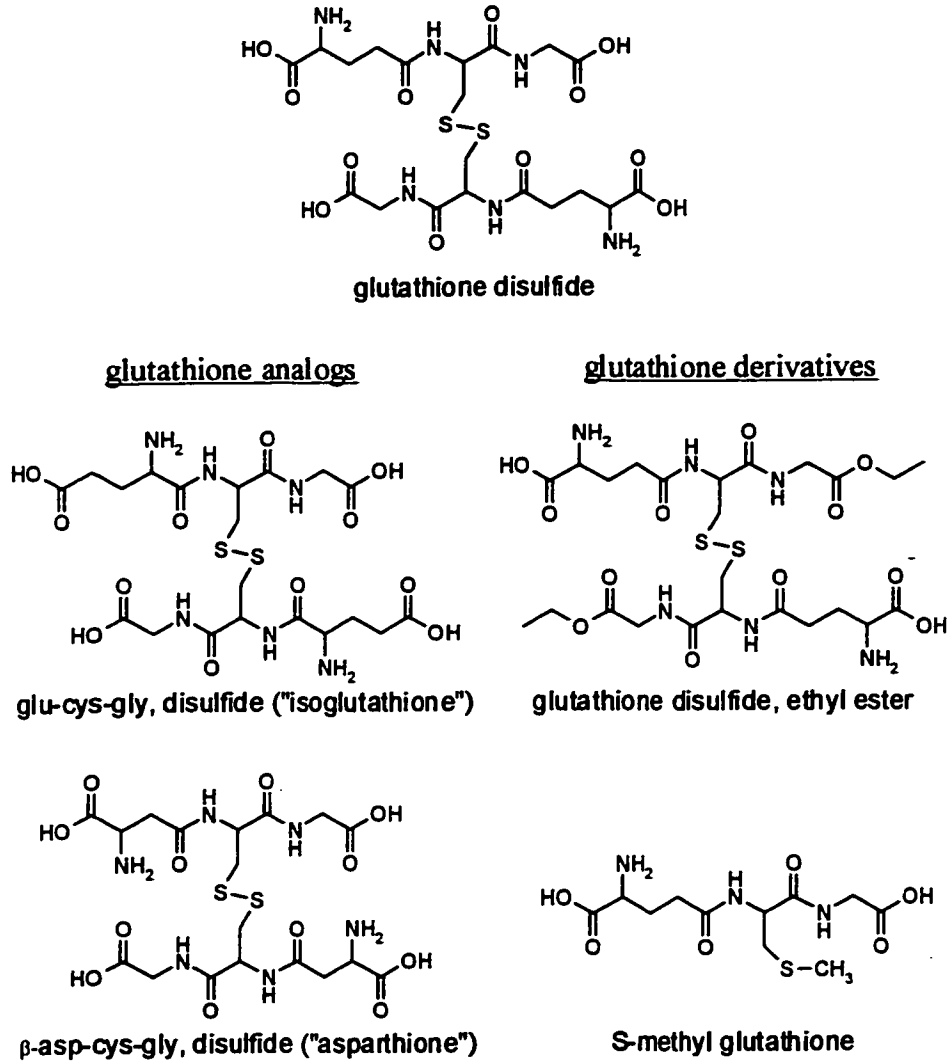

Figure 4.1: Structures of glutathione disulfide (GSSG) and the glutathione analogs and derivatives discussed in this chapter.

type conformation stabilized by the restricted rotation about the disulfide bond (Howarth and Lian, 1982; Schwartz and Cutnell, 1983). We propose that in appropriate organic solvents, these stable β-sheet units self-assemble into an extended network of intermolecular, antiparallel sheets. This network immobilizes bulk solvent and results in

the formation of transparent gels. It is interesting to speculate that this unexpected self-recognition behavior of such an abundant and multifunctional peptide may have physiological consequences for protein regulation, aggregation, and folding.

4.2 Experimental Procedures

4.2.1 Materials

Glutathione (reduced and disulfide), glutathione ethyl ester, and S-methyl glutathione were purchased from Sigma. The tripeptides glu-cys-gly and β-asp-cys-gly were purchased from Synpep. Other reagents and solvents were purchased from Aldrich.

4.2.2 Preparation of Gels

Gels in DMSO were prepared by dissolution of glutathione with gentle heating to about 60°C. Gels in aqueous DMF and methanol were prepared by addition of the organic solvent to concentrated aqueous solutions of glutathione; aqueous fractions less than 10% are required for gelation. For glutathione derivative and analog studies, solutions of 10 $^{mg}/_{mL}$ were prepared and observed for 1 month for gelation behavior.

4.2.3 Visible and Polarization Microscopy

Firm gels of GSSG in DMSO (65 mM) were sliced with a razor into thin sections and placed on microscope slides. To 1 mL of a stock solution of 80% ethanol / 20% DMSO saturated with Congo Red and sodium chloride were added 10 μL of 1% NaOH. Alkaline stain solution was applied to the slide for 2 minutes then poured off, and the gei sections rinsed with several portions of 80% ethanol / 20% DMSO. Stained sections were air dried overnight to remove excess DMSO. Drying was necessary to make the sections suitably thin for polarization microscopy. Dried gel samples were visualized at 40x or 100x magnification, and birefringence determined between crossed polarizers. Two control slides were also prepared. These consisted of 65 mM glu-cys-gly ("isoglutathione") plus Congo Red in DMSO, and 65 mM GSSG plus Congo Red in 50/50 water / DMF (neither of these solutions produce gels). In each case, the solution was applied to a slide and allowed to dry prior to microscopy observations.

4.2.4 Electron Microscopy

For transmission electron microscopy, Formvar® coated copper grids (200 mesh, Fullam, Inc., Latham, NY) were touched to the surface of the gel, then washed with ethanol and negatively stained with uranyl acetate in 95% ethanol. TEM was performed on a JEOL electron microscope with an acceleration potential of 80 keV.

4.2.5 Spectroscopy

Proton NMR: Glutathione (GSH or GSSG) was dissolved at 3 mg/mL in either d_6-DMSO or 90% H_2O / 10% D_2O. Spectra were obtained on a Varian INOVA 500 MHz NMR.

Circular dichroism: Spectra of GSSG in 90% methanol were obtained in 5 mm path length cells on a Jasco J-720 spectropolarimeter.

Mass spectrometry: Gel samples were dissolved in water and analyzed by direct injection ESI-MS on a Fisons VG Quattro II mass spectrometer.

4.3 Results

4.3.1 General Observations

Glutathione solutions up to 80 mM have been prepared by heating DMSO to 60°C. Upon cooling, the rate of gelation is dependent upon glutathione concentration and whether the starting material was reduced (GSH) or disulfide (GSSG) glutathione. In the case of GSSG, increased viscosity is immediately observed at concentrations above 16 mM. At 8 mM, formation of rigid transparent gels is observed within 1 week. No gelation is observed at concentrations below 8 mM (4.9 mg/mL). However, if GSH is dissolved in DMSO, gelation is noticeably slower, requiring several days at 32 mM and up to 2 weeks at 16 mM (note that upon oxidation, GSSG molar concentration is half that of original GSH concentration). However, the gels which eventually result from GSH solutions are qualitatively stiffer than those from GSSG solutions, perhaps due to

aggregates assembling from fewer nucleation sites and thus forming fewer, but more extensive intermolecular arrays. The gelation of GSH / DMSO solutions can be accelerated by bubbling compressed air through the solution, while gelation time is increased approximately threefold by the addition of one molar equivalent of dithiothreitol (DTT). Collectively, these observations indicate that GSSG is the active gelling agent rather than GSH. These gels are thermostable to about 50°C, becoming transparent fluids above this temperature, and re-gelling upon cooling. Upon standing at room temperature, GSSG / DMSO gels are stable for months to years, while addition of one molar equivalent of DTT causes dissolution within 24 hours. The transparency of the gel is slowly lost, however; Figure 4.2 shows a gel prepared at 20 mg/mL GSH after 1 week (Figure 4.2 A) and 6 months (Figure 4.2 B). The culture tube shown in this figure in which the gel was prepared is inverted on the benchtop to illustrate the rigidity of the gel. The black background highlights the appearance of small 'pockets' of semitransparency which appear within the gel matrix after several weeks. In gels prepared from GSH, this state of mixed semitransparency exists indefinitely; as of this writing, the tube shown in Figure 4.2 still appears as in the right frame of the figure after sitting on the bench for nearly two years. In gels prepared from GSSG, however, the appearance of opaque pockets progresses to the formation of solid aggregates within the pockets over the course of weeks to months. This effect is illustrated in Figure 4.3, which compares gels prepared from GSH and GSSG at 20 mg/mL side-by-side. The 'aged' gel prepared from GSH (Figure 4.3, left) resembles the partly cloudy gel shown in Figure 4.2 B; the GSSG gel, however, has produced solid aggregates which have fallen

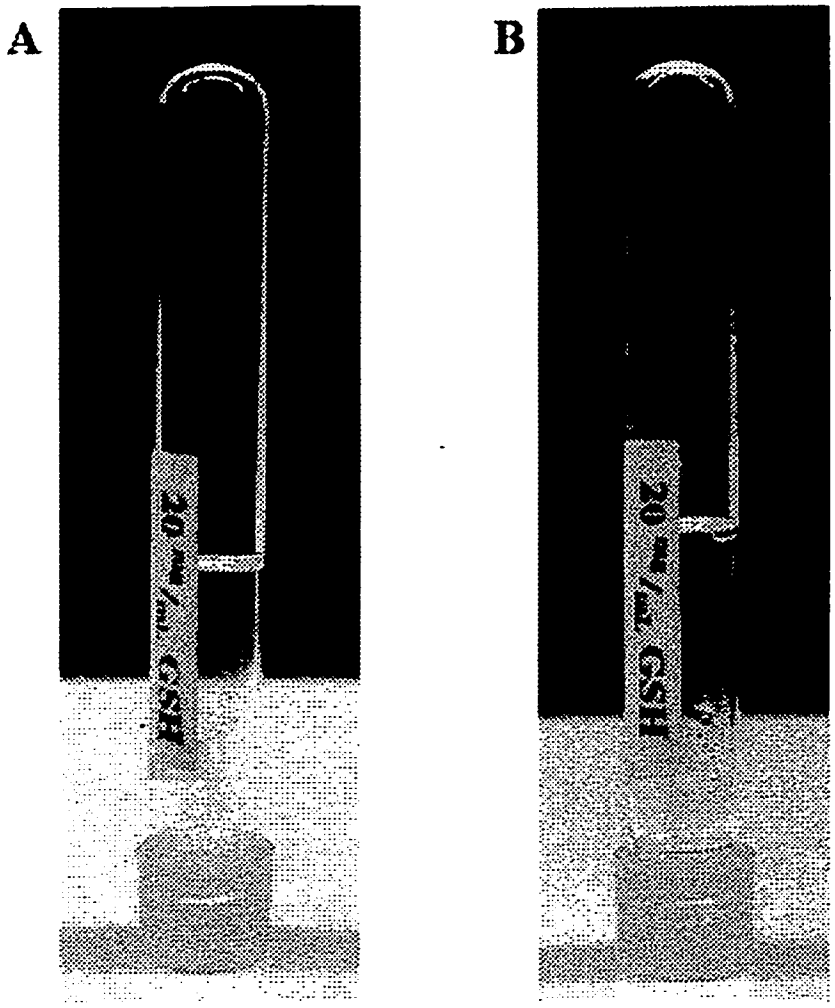

Figure 4.2: Photographs of 'fresh' and 'aged' gel prepared at 20 mg/mL GSH in DMSO. 4.2 A, after 1 week the gel appears completely transparent; the tube is inverted for the photograph to demonstrate the rigidity of the gel. 4.2 B, after 24 weeks, numerous small pockets of semi-transparency have appeared giving the gel a partly cloudy appearance; integrity of the gel, however, is not compromised.

to the bottom of the vial, restoring fluidity to the DMSO solution. These aggregates are remarkably spherical in their morphology; under a low-power visible microscope (Figure

4.4), they appear as clusters of separate spheres.

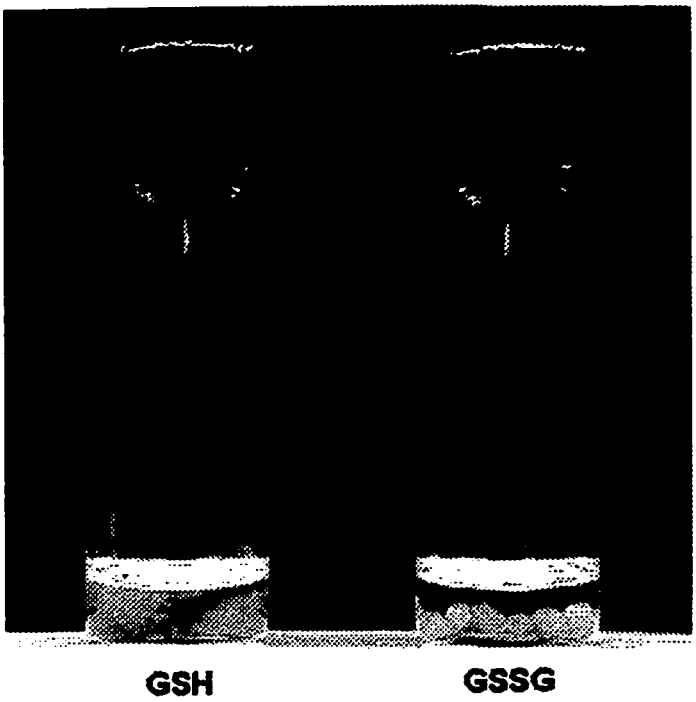

Figure 4.3: Comparison of 'aged' gels prepared from GSH and GSSG in DMSO. While the gel prepared from GSH (left) produces diffuse regions of semitransparency, the gel prepared from GSSG (right) produces pockets which are both more numerous and more dense, and which develop into solid aggregates.

Solutions prepared by adding DMF to aqueous GSSG solutions produce gels within minutes at concentrations as low as 5 mM (3 mg/mL) in 90% DMF. These gels are thermostable to about 65°C. Above this temperature, they produce a milky white suspension which, upon cooling, clarifies nearly completely and re-gels. Solutions prepared by adding methanol to aqueous GSSG solutions require cooling to about 0°C to

Figure 4.4: A cluster of aggregates from an aged GSSG / DMSO gel viewed under a low-power visible microscope. The spherical morphology of the individual aggregates is evident in this micrograph, as is their tendency to clump together.

produce transparent gels at concentrations as low as 1.5 mM (0.9 mg/mL) in 90% methanol. In some cases, the solution remains gelled after warming to room temperature. In all solvent systems, gels form with up to 20% water, although the minimum GSSG concentration necessary to form gels increases with increasing aqueous fraction. It is notable that GSSG forms gels in both polar aprotic (DMSO and DMF) and protic (methanol) organic solvents.

4.3.2 Behavior of Glutathione Analogs and Derivatives

The glutathione analogs and derivatives illustrated in Figure 1 were assayed for their ability to produce gels in 90% methanol, 90% DMF, and DMSO. Because of its inability to form a disulfide, S-methyl glutathione was selected to verify that the disulfide is required for gelation. 'Isoglutathione' and 'asparthione' were chosen to test the relevance of the unusual geometry of the γ-glutamyl function of glutathione to the gelation behavior. Glutathione ethyl ester was selected to assess the importance of the hydrogen bond-donating and ionizable terminal carboxylic acid function. Of these analogs and derivatives, only the disulfide form of glutathione ethyl ester was found to exhibit any gelation activity, forming transparent gels in 90% methanol and 90% DMF. The reduced thiol form of the ethyl ester is readily soluble in DMSO, but surprisingly the disulfide is practically insoluble, and does not form gels. Neither 'isoglutathione' nor 'asparthione' displayed any gelation activity, suggesting that the γ-glutamyl structural element is critical for gelation.

4.3.3 Spectroscopy

Two-dimensional NMR was employed to determine the chemical shifts of each of the glutathionyl protons. The resulting COSY spectrum of GSH in d_6-DMSO is shown in Figure 4.5; the expansion in the figure excludes the amide region. The resulting peak assignments are summarized in Figure 4.6 and Table 4.1, and are in agreement with the

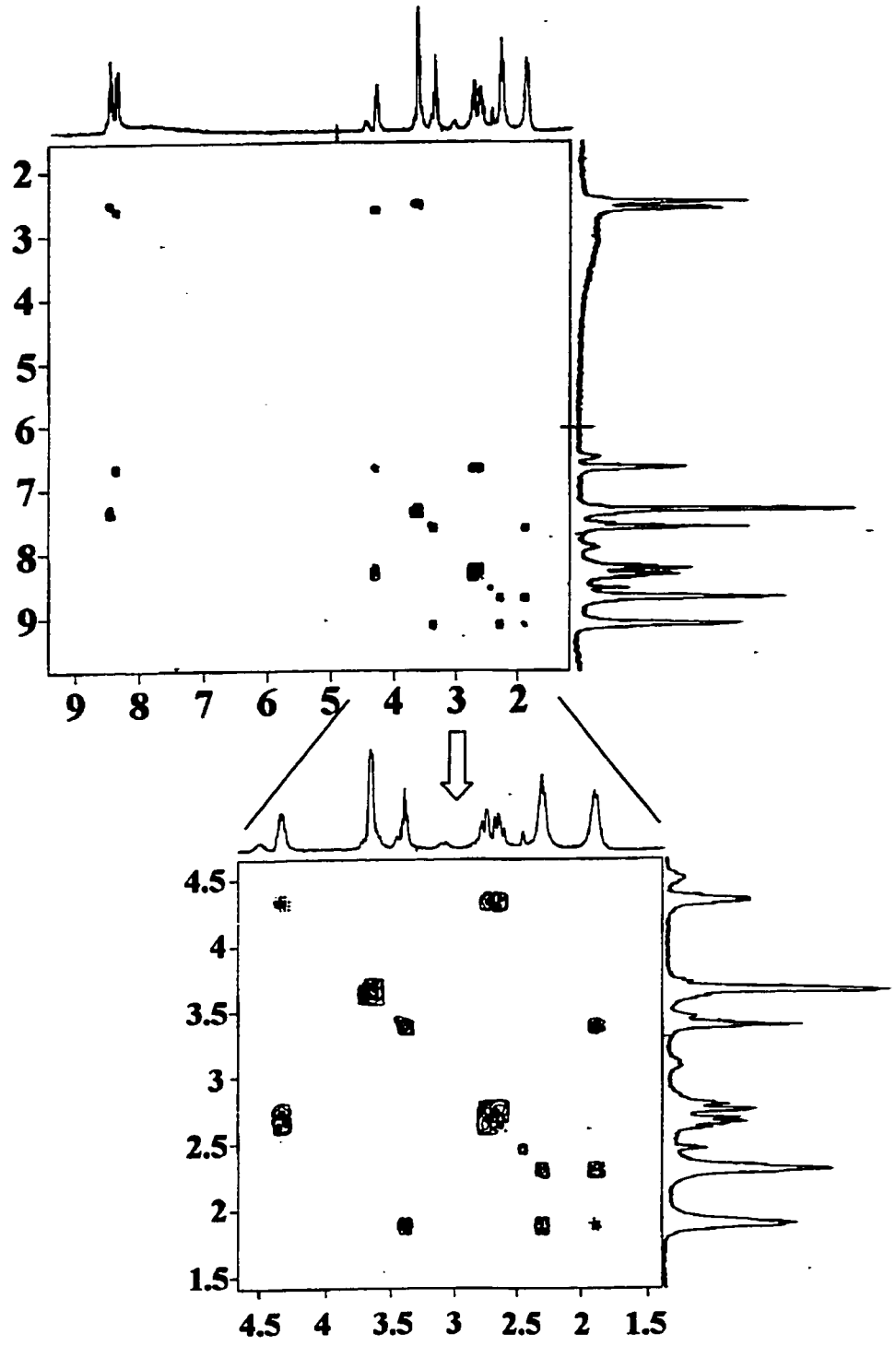

Figure 4.5. COSY NMR spectrum of GSH in d_6-DMSO. Enlargement of the 1.5 – 4.5 ppm region omits the amide peaks, but clarifies the congested region of the spectrum.

Table 4.1. ^{1}H NMR chemical shift data of GSH and GSSG in H_2O and DMSO. The rows labeled Δδ represent the change in the chemical shift of each proton in each solvent upon oxidation of GSH to GSSG. Shift data (and protons in the structure) are presented in one of three colors to represent their change in behavior between the two compounds in the two solvents. Protons in green exhibit little change upon GSH ⇒ GSSG oxidation in either solvent; protons in blue exhibit significant changes in both solvents; protons in red exhibit significant changes only in DMSO.

Sample	Glu α	Glu β_1	Glu β_2[a]	Glu γ	Cys N-H	Cys α	Cys β_1	Cys β_2	Gly N-H	Gly α
GSH/H_2O	3.80	2.15	-	2.53	8.46	4.55	2.94	2.94	8.50	3.95
GSSG/H_2O	3.80	2.14	-	2.52	8.58	4.65	2.96	3.26	8.53	3.95
Δδ	0	-0.01	-	-0.01	+0.12	+0.10	+0.02	+0.32	+0.03	0
GSH/DMSO	3.33	1.85	1.93	2.32	8.37	4.36	2.69	2.82	8.68	3.70
GSSG/DMSO	3.47	1.94	-	2.35	8.56	4.52	2.89	3.15	8.62	3.71
Δδ	+0.14	+0.09	+0.01	+0.03	+0.19	+0.16	+0.20	+0.33	-0.06	+0.01

[a] the two β protons of glu are nonequivalent, and in some cases are resolvable.

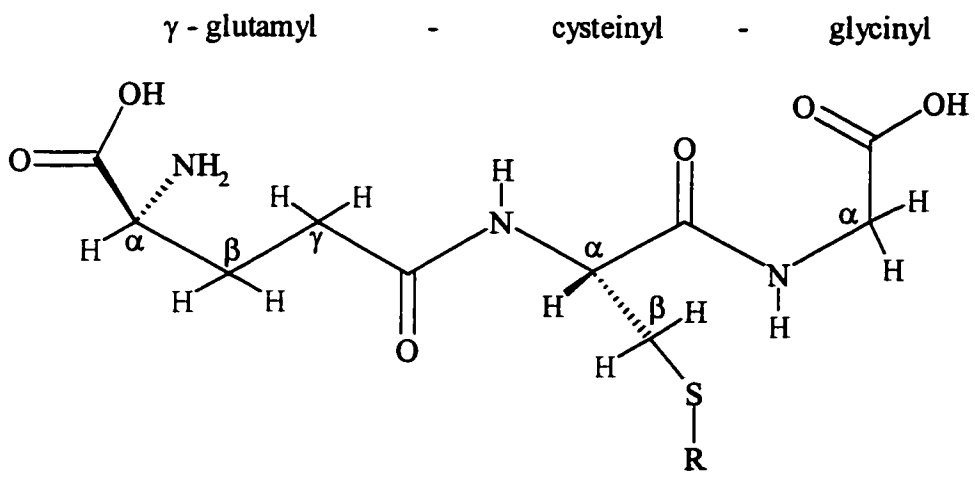

Figure 4.6. Structure of glutathione, color coded to match the NMR chemical shift data in Table 4.1. For GSH, R = H; for GSSG, R = a second, equivalent glutathione moiety.

literature. To probe for conformational differences between GSH and GSSG which may exist in organic solvents but not in water, spectra were obtained for the reduced and disulfide forms of glutathione in d_6-DMSO and in 90% H_2O / 10% D_2O. Figure 4.6 and Table 4.1 also include the chemical shifts obtained from these studies, along with changes in chemical shift which occur upon oxidation of GSH to GSSG within each solvent system. The structure of glutathione and the coloring scheme are included to help illustrate which atoms appear to experience changes in their chemical environment upon the GSH $\Rightarrow$ GSSG conversion. Upon oxidation, the glycinyl protons and one of the non-equivalent γ-glutamyl β- protons (green) did not exhibit any significant change in either solvent. However, significant changes in the chemical shift of 3 of the 4 cysteinyl protons (blue) occurred within both solvent systems, while the fourth cysteinyl proton and the γ-glutamyl α- and β- protons (red) exhibited significant changes only in DMSO. To illustrate the quality of the NMR data used for this analysis, the spectrum of GSH in d_6-DMSO is shown in Figure 4.7. This particular spectrum was chosen for illustration as it also visually demonstrates the observed chemical shift changes upon the GSH $\Rightarrow$ GSSG conversion. Although the sample used to acquire this spectrum was prepared from GSH, the rate of oxidation in DMSO is sufficiently high that peaks arising from the disulfide are clearly visible in the spectrum. For example, the proton in GSH resonates at 4.36 ppm, but the equivalent proton in GSSG is shifted to 4.52 ppm; this is shown in the figure. To illustrate these effects across the entire spectrum, the enlargements of the spectrum are shown in Figure 4.8.

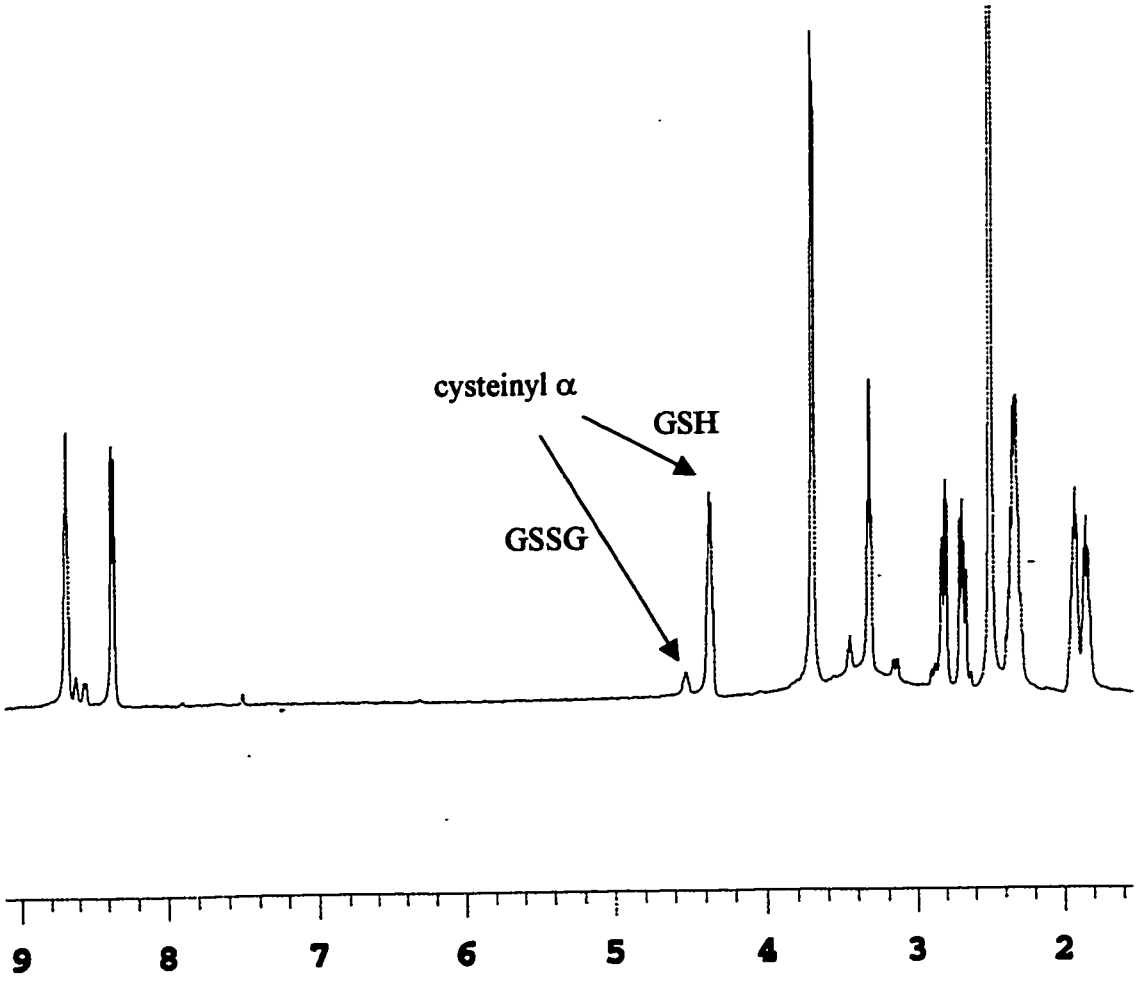

Figure 4.7. 500 MHz NMR spectrum of GSH in d_6-DMSO.

Circular dichroism spectra of GSSG in 90% methanol were obtained at variable temperature and concentration (Figure 4.9) to probe conformational changes occurring upon gelation. These spectra are similar to those of GSSG in aqueous solutions which have been published previously (Coleman and Blout, 1968; Ottnad *et al.*, 1973). These authors have assigned the negative bands (212 nm and 270 nm) to disulfide transitions and the positive band at 230 nm to the cys-gly peptide bond. A fourth band near 240 nm is clearly present in our spectra, but is nearly absent in aqueous solutions (Coleman and

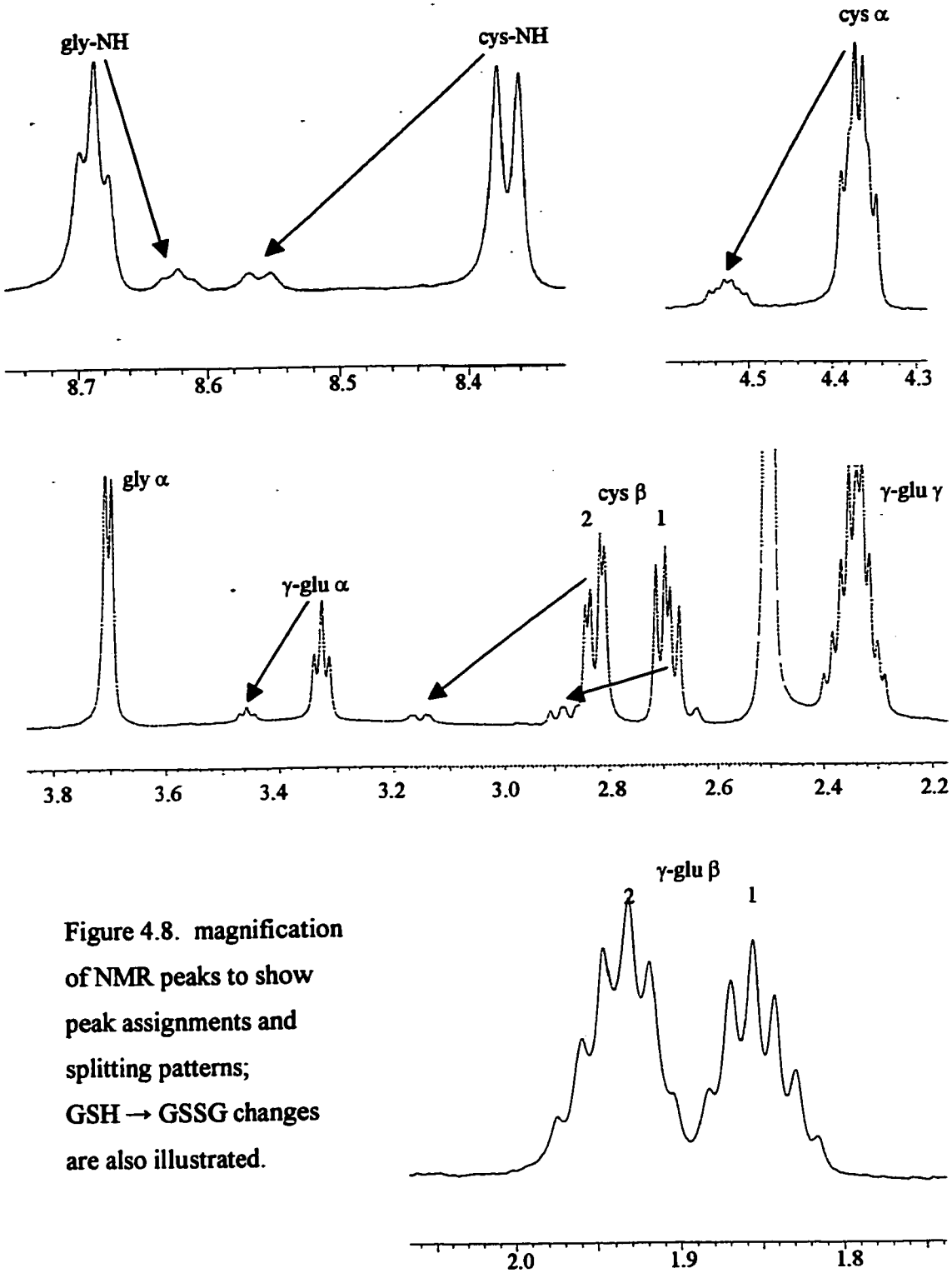

Figure 4.8. magnification of NMR peaks to show peak assignments and splitting patterns; GSH → GSSG changes are also illustrated.

Blout, 1968). Figure 4.9 A illustrates the concentration dependence of the CD spectrum at -10°C, a temperature which results in gelation at concentrations of 1 mM and above.

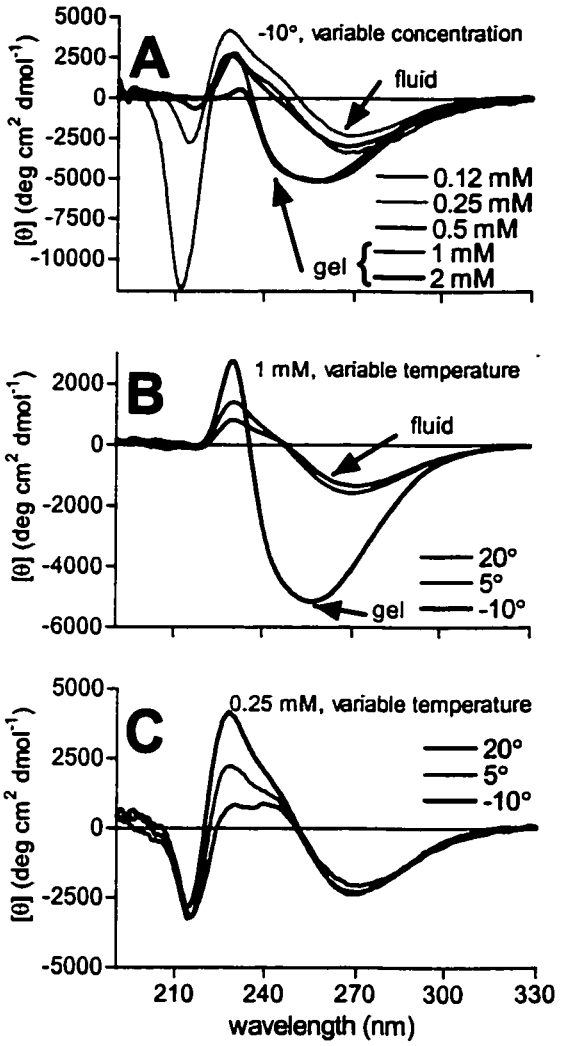

Figure 4.9. Circular dichroism spectra of GSSG in 90% methanol as a function of temperature and concentration. **A**, variable GSSG concentration at a constant temperature of -10°C; 1 mM and 2 mM samples are in gel phase, others are fluid. **B**, variable temperature at a constant GSSG concentration of 1 mM; again, -10°C sample in gel phase. **C**, variable temperature at a constant concentration of 0.25 mM; all samples are fluid.

The intensity of the disulfide band at 212 nm decreases dramatically with increasing concentration, and is completely absent in the gelled samples at 1 mM and 2 mM. By contrast, the disulfide band at 270 nm is relatively unaffected by variations in concentration below the threshold for gelation, but in the gelled samples the intensity of this band increases significantly and it appears to blue-shift. The maxima of this peak is difficult to discern, however, because the sign of the band at 240 nm appears to invert in the gelled samples, becoming negative and coalescing with the disulfide band. These long-wavelength changes are also observed in Figure 4.9 B, which illustrates the temperature dependence of the spectrum at 1 mM. The fluid → gel transition between 5°C and -10°C again produces a marked increase in the intensity of the long-wavelength disulfide band and an inversion of the sign of the 240 nm band. At 0.25 mM (Figure 4.9 C), below the gelation threshold, temperature has little influence on these bands, with the greatest impact being seen on the cys-gly peptide bond transition at 230 nm. Collectively, these results indicate that gelation is coupled to an alteration of the local structure of the disulfide, and further suggests involvement of the γ-glutamyl moiety.

4.3.4 Polarization Microscopy

To determine if the GSSG aggregates which produce gels can be characterized as amyloid, we stained gel slices with an alkaline Congo Red solution and observed them between crossed polarizers. The staining and subsequent appearance of green birefringence is considered the most specific method for the determination of amyloid

(Westermark *et al.*, 1999). Briefly, the incoming light is polarized by a filter beneath the microscope stage; a second polarizer lies between the sample and the viewing lens. With the polarizers in parallel, the sample appears red; when they are perpendicular ('crossed'), all wavelengths are blocked by the second polarizer *unless they are rotated by the sample*. Those wavelengths which are rotated by the dye are complimentary to the reflected wavelengths. Congo Red therefore rotates green light, and the phenomenon is called green birefringence. If the molecules of dye are randomly ordered on the slide, no birefringence will be observed; a positive result from the birefringence assay requires that the dye molecules are arranged in an ordered fashion across the surface of the stained material. This is the basis for the specificity of the assay, as Congo Red has been found to bind amyloid fibrils in an ordered, repeating fashion along the length of the fibril, although the specific binding contacts are unknown.

GSSG / DMSO gel slices stained readily with Congo Red, and when partially dried appear pale red in color with darker red fibers visible as shown Figure 4.10 A. As the polarizers are crossed and the angle between them approaches 90°, the thin sections begin to exhibit strong green birefringence (Figure 4.10 B). At a polarization angle of 90°, only the birefringent regions are visible (Figure 4.10 C). This effect is even more dramatic at a higher magnification (Figure 4.11). These results are classic indicators of Congo Red binding to a cross-β sheet fibril structure. None of the control slides exhibited any birefringence (not shown).

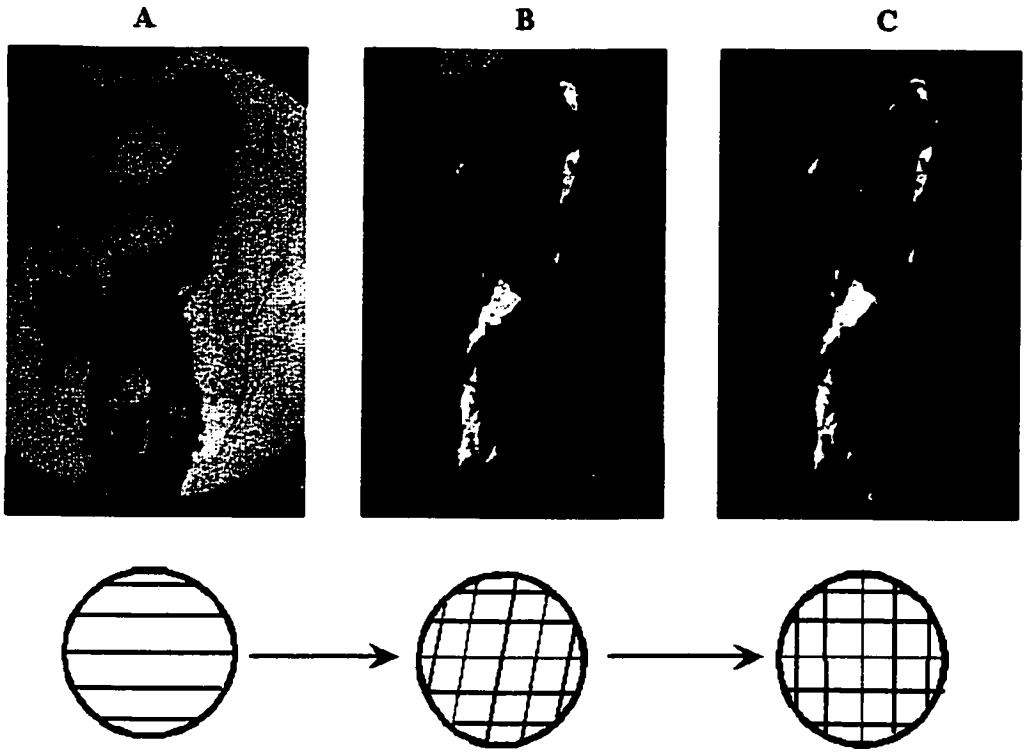

Figure 4.10: GSSG / DMSO gel slices stained with Congo Red. The cartoon below each slide represents the angle between the two polarizers. From **A** to **B** this angle approaches 90°, causing red color to diminish and regions of green birefringence to appear. At 90° (**C**), only the green birefringent regions are observed, with the second polarizer blocking all other light.

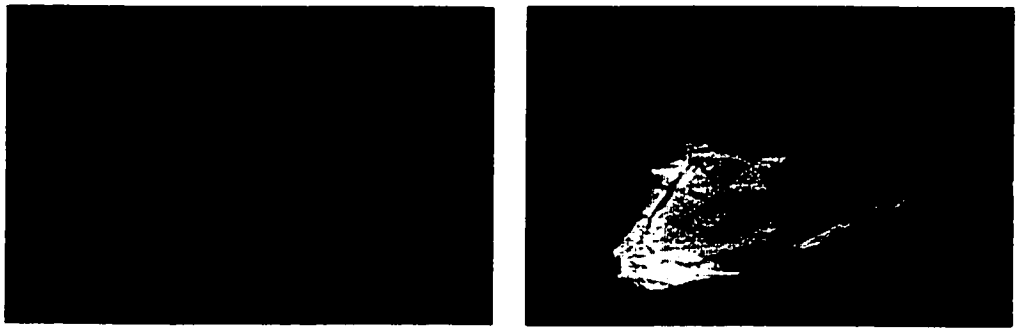

Figure 4.11: Congo-Red stained gel at high magnification. In these samples the fibrous appearance of the gel is evident; under crossed polarizers (left), strong green birefringence is observed along the lengths of the fibrous structures.

4.3.5 Electron Microscopy

TEM images revealed tangles of fibrous structures approximately 75 nm in diameter. The structures appeared to consist of straight fibers with multiple branching "nodes," which intersect and tangle to form a 3-dimensional web-like fiber network. Examples illustrating these structures are shown in Figure 4.12. The morphology of these structures appears distinct from typical unbranched amyloid fibrils.

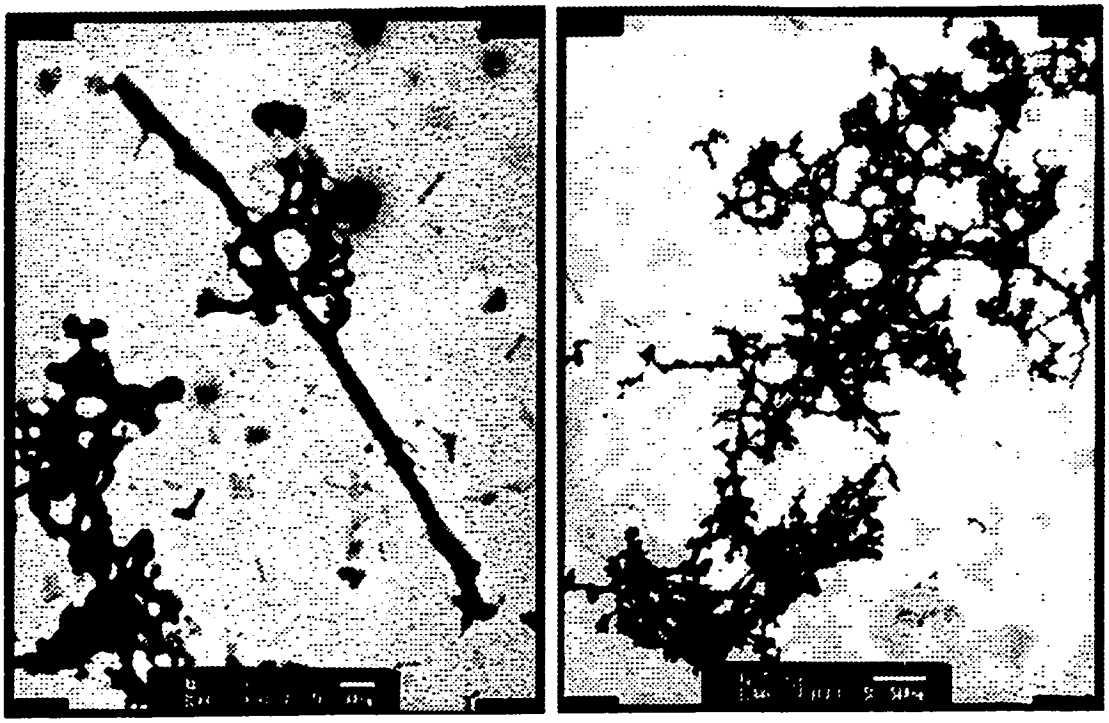

Figure 4.12: Electron micrographs of GSSG / DMSO gel. Left, fiber about 2 μm in length with minimal branching nodes (25,000x; bar = 200 nm). Right, tangle of fibers of varying lengths, with multiple nodes producing web-like network (15,000x; bar = 500 nm).

4.4 Discussion

Previous NMR studies of GSSG in aqueous media have indicated that its two tripeptide strands adopt an antiparallel, extended conformation (Howarth and Lian, 1982; Schwartz and Cutnell, 1983). This conformation is stabilized by hydrogen bonding between the glycyl amide nitrogens and the γ-glutamyl amide carbonyls, as well as the restricted rotation of the disulfide bond. Although the hydrogen bonding pattern is typical of an antiparallel β-sheet, the disulfide between the strands distinguishes this structure from a "true" β-sheet. Because of this, one would not necessarily expect GSSG to exhibit the spectroscopic signatures of a classic β-sheet. However, similar antiparallel β-like conformations have been reported for other small acyclic peptides with a central cystine residue (Raj *et al.*, 1990; Ueyama and Araki, 1978). Furthermore, the CD spectrum of GSSG is similar to that of a cystine peptide which has been shown by NMR and x-ray crystallography to adopt an antiparallel intramolecular β-type conformation (Raj *et al.*, 1990). This β-type intramolecular conformation thus appears to be a common structural motif among small acyclic cystine peptides. However, GSSG is the first such peptide to be reported to self-assemble into extended intermolecular aggregates in organic solvents, and our studies suggest that the γ-glu-cys bond is required for this unique behavior.

Many peptides and proteins have been observed to form gels in denaturing organic solvents. However, glutathione is an unusual and interesting case for several reasons. First, it is significantly smaller than most peptide gelling agents. It has been

suggested that the minimum required peptide length to produce stable extended β-sheet structures is six residues (Aggeli *et al.*, 1997; Osterman and Kaiser, 1985; Krejchi *et al.*, 1994). While GSSG satisfies this stipulation, its nonlinear geometry dictates that each strand is only three residues long. Because of this small size, the extended intermolecular array is assembled by remarkably few contacts. Second, glutathione represents an atypical peptide structure. In addition to its nonlinearity by virtue of a central cystine residue, GSSG also possesses two side-chain peptide bonds (the γ-glu-cys linkages). The results from our analog studies indicate that the gelation behavior is highly specific to this structure. The disulfide forms of the glutathione isomer glu-cys-gly as well as the analog β-asp-cys-gly failed to exhibit gelation in any of the solvents tested. These stringent structural requirements for gelation suggest that GSSG gels are stabilized by highly ordered and specific intra- and intermolecular interactions. Finally, the ubiquitous nature of glutathione in biological systems and its high concentrations (up to 10 mM) in our own cells make it a particularly relevant peptide for study.

Our initial observation was that reduced glutathione, GSH, produces gels in DMSO over a period of several days. However, three lines of evidence demonstrate that it is GSSG which is responsible for gelation. First, the S-methyl conjugate of glutathione, which cannot oxidize to GSSG, does not exhibit gelation. Second, mass spectra (not shown) of gels prepared with GSH indicate the presence of substantial quantities of GSSG, confirming that the oxidation occurs over the time scale of gelation. Acceleration of this oxidation by bubbling air through GSH / DMSO solutions also accelerates gelation, while addition of DTT slows gelation considerably and causes the

dissolution of preexisting gels. Finally, solutions prepared with GSSG produce gels much more quickly than solutions prepared with GSH. Thus, oxidation represents a 'molecular switch' which converts soluble GSH into a species capable of self-assembly into non-covalent arrays. The redox environment therefore presents an opportunity for control or regulation of the gelation process.

Several qualitative observations suggest that the self-assembly which results in gelation follows a classical 'seeding' process, similar to amyloid deposition. In this process, a threshold concentration must be exceeded for the formation of 'nano-aggregate' nuclei consisting of a few molecules to occur (a slow process); once this condition is met, additional molecules can rapidly add to the growing non-covalent polymer. In DMSO, this threshold appears to be around 5 mg/mL (a molar ratio of about 1600 solvent molecules per molecule of GSSG), and even lower in DMF and MeOH. The fact that gels prepared from GSH are more rigid than gels from GSSG may be explained by the fact that in DMSO, GSH is slowly oxidized to GSSG; when the threshold concentration of GSSG is reached, seeding occurs at relatively few distinct points. As more GSSG is produced, it adds to one of these few but growing non-covalent arrays, creating long polymers which create tangles capable of efficiently trapping solvent. Conversely, when GSSG is added directly, the threshold concentration is immediately reached resulting in nucleation at many sites. This results in the formation of more, but shorter, fibers of assembled GSSG. Intuitively, these shorter fibers would be more mobile and have fewer intersection points with other fibers, thus trapping solvent less effectively. This effect is also likely responsible for the different

'aging' processes of gels prepared from GSH and GSSG. While aged gels prepared from GSH exhibit diffuse cloudiness and regions of semitransparency for indefinite periods (Figures 4.2, 4.3), gels prepared from GSSG produce solid aggregates within a period of months (Figure 4.3). The distinctly spherical appearance of these aggregates (Figure 4.4) is intriguing; presumably this is due to the fact that a sphere is the shape with the greatest ratio of volume to surface area. By forming spheres, then, the aggregates of GSSG minimize their exposure to DMSO and maximize intermolecular interactions with other molecules of GSSG. The fact that these individual spheres form clumps further expels solvent from contact with GSSG. It may be the case that the center of each of these spheres represents a nucleation site in the seeding process of aggregate formation.

In aqueous media, NMR studies suggest that the terminal groups of GSSG have minimal interactions with each other (Howarth and Lian, 1982), and it appears probable that these groups would be highly solvated. In organic solvents, a cross-strand interaction between these terminal groups may become more favorable than solvation. Indeed, our NMR data of the glutamyl α- and β-protons (Table 1) suggest that in DMSO, there is a change in the environment of the N-terminus upon oxidation of GSH to GSSG. These protons (red) are shifted downfield by 0.14 ppm and 0.09 ppm, respectively. Given the distance of these protons from the site of the oxidative modification (and the fact that the intervening γ-protons are unaffected), the change in the chemical environment of these protons must be due to an indirect effect such as a change in geometry or solvation, rather than a direct interaction with the disulfide. In aqueous media, these protons do not exhibit any significant shift upon oxidation of GSH to GSSG.

In water, only the cysteinyl protons (blue) exhibit large changes upon oxidation, which is unsurprising given their proximity to the redox-active thiol. The N-termini of GSSG differ from typical cystine peptides due to the γ-glu-cys linkage, which creates an unusually long distance between this bond and the N-terminus. How this affects the conformation of the N-termini is unclear, but its presence is critical for the gelation behavior, as demonstrated by the analog studies. It may also be significant that the NMR chemical shifts of both cysteinyl β-protons are affected by the GSH ⇒ GSSG conversion in DMSO, while only one of these protons exhibits a significant change in aqueous solution (Table 1). In summary, the NMR data point to the N-terminus and perhaps the disulfide as regions which may be responsible for the unusual behavior of glutathione in DMSO.

Previous studies in aqueous solutions suggest that GSSG has three CD bands: two associated with the disulfide and one arising from the cys-gly peptide bond (Coleman and Blout, 1968; Ottnad *et al.*, 1973). Due to the long distance from the chiral glutamyl α-carbon to the γ-glu-cys peptide bond, it is not believed that this chromophore is a significant source of asymmetry in the CD spectrum. The work of Coleman and Blout (Coleman and Blout, 1968) with derivatives of L-cystine revealed that GSSG gives rise to an anomalously broad long-wavelength disulfide band in aqueous media, and they suggested that this may be due to an unidentified fourth band of negative sign near 240 nm. This band is clearly present in our spectra (Figure 4.9), and we propose that this relatively weak band may be assigned to the γ-glu-cys peptide bond; the weakness of the band is likely due to the distance of this chromophore from the chiral center of the

glutamyl residue. In the transition from fluid to gel in 90% methanol, this band reverses in sign from positive to negative and increases in magnitude (Figures 4.9 A and 4.9 B), suggesting a major perturbation in the geometry of its associated chromophore. If our assignment of this band to the γ-glu-cys peptide bond is correct, the observed perturbation further implicates the γ-glu-cys moiety in the gelation process. The other significant change which occurs in the CD spectrum upon gelation is the increase in intensity and the blue shift of the long wavelength disulfide transition ($\pi \rightarrow \sigma^*$). The disulfide group possesses inherent asymmetry due to the fact that it can adopt a left- or right-handed screw sense, with a significant barrier to rotation between the two. This arrangement arises from mutual electronic repulsions between the nonbonding electrons of the two sulfur atoms, such that two degenerate S-S dihedral angles exist at approximately 90° and 270°. The presence of nearby asymmetric centers breaks the degeneracy of the two senses, so in derivatives of L-cystine such as GSSG one screw sense is energetically favored over the other. However, solutions typically contain a mixture of the two rotamers, so intensities of this band are usually very low. The observation that the intensity of this band increases upon gelation suggests that the energy differential between the two rotamers becomes greater in the gel phase. This suggests that only one rotamer is responsible for self-assembly, thus introducing a further element of specificity. Unfortunately, there is disagreement in the literature as to whether the sign of the long-wavelength disulfide band can be reliably used to determine absolute screw sense, so we make no attempt to do so here. There is also disagreement as to whether the short-wavelength disulfide band arises from a $\pi \rightarrow \sigma^*$ or $\sigma \rightarrow \sigma^*$ transition.

Our data indicate that in 90% methanol, this band is highly sensitive to concentration (Figure 4.9A), and is completely absent under gel-forming conditions. The significance of this spectral change is not clear at present. Regardless of this uncertainty, the CD data demonstrate that the local chirality of the disulfide bond and possibly also the γ-glu-cys peptide bond are coupled to intermolecular self-assembly, as manifested in gelation. Therefore, both CD and NMR implicate the geometries of the disulfide bond and the terminus of the γ-glutamyl residue in the gelation behavior.

It is notable that the barrier to rotation about the disulfide bond results in minimal entropic cost for the formation of the proposed intramolecular interactions within the antiparallel strands of GSSG. Because the strands are already effectively "locked" into a β-type conformation, the entropy loss associated with assembly into an extended intermolecular β-sheet is lower than it would be for conformationally unrestricted tripeptides. We presume that this allows the formation of stable intermolecular sheets with peptide strands which are shorter than would be possible with linear peptides. The observed Congo Red birefringence (Figures 4.10, 4.11) suggests that the extended GSSG structure is very similar to amyloid, with extended sheets running perpendicular to the direction of the strands. A model which illustrates an extended GSSG β-sheet is shown in Figure 4.13. This model shows all of the terminal groups in an unionized state, although we have not elucidated their protonation state in each of the solvent systems which produce gels. However, the observation that the glycyl ethyl ester of GSSG is capable of forming gels indicates that gelation does not require the C-terminus to act as a hydrogen bond donor or to form a salt bridge. Thus our proposed model suggests that the

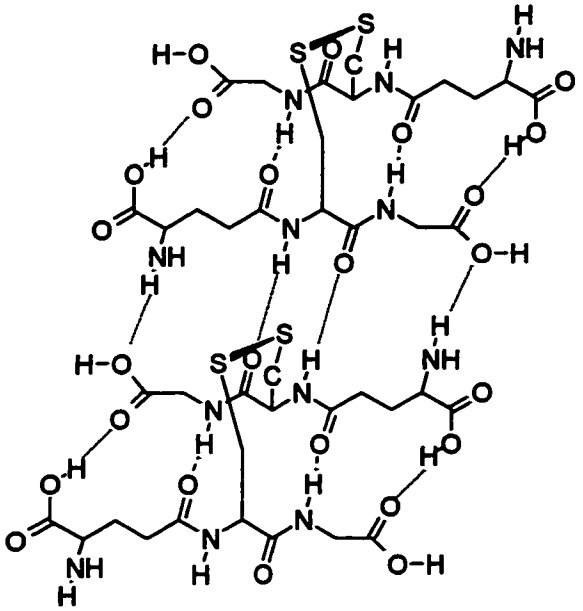

Figure 4.13: Model of intra- and intermolecular hydrogen bonding which could stabilize an extended GSSG β-sheet-like structure in organic solvents.

glycyl carboxyl group acts only as a hydrogen bond acceptor. The design principles of cross-strand attractive forces and lateral strand recognition which have been proposed by Aggeli *et al.* (Aggeli *et al.*, 1997) for engineering β-sheet peptides are uniquely addressed by this model. The disulfide can be considered as an extremely strong (and conformationally restricted) cross-strand attraction within each GSSG unit, and the geometry of the γ-glutamyl residue allows for specific intermolecular recognition. Indeed, the γ-glu-cys linkage appears to be a requirement for intermolecular assembly. The observation that the unique structural features of GSSG allows its aggregation into supramolecular structures may provide additional design principles for the engineering of self-assembling peptides.

The ubiquitous nature and multiple functions of glutathione in biological systems raise questions about possible physiological significance of its self-assembly behavior. Concentrations required for localized microscopic effects of such behavior may be significantly lower than those required for a macroscopic event such as gel formation. Partially folded or unfolded proteins may be expected to have exposed sections of uncharged amino acid residues which resemble the low-dielectric conditions of polar organic solvents such as methanol and DMF. It is interesting to speculate that the self-recognition properties of glutathione within such an environment may have functional implications, for example in the pathogenesis of diseases associated with abnormal protein aggregation. Indeed, many such diseases, including Alzheimer's Disease and other amyloid diseases, have been correlated with oxidative stress, a condition which may result in increased GSSG concentrations (White *et al.*, 1986; Seis, 1983). It is currently believed that endogenous factors may mediate amyloid deposition by altering the stability of amyloidogenic folding intermediates or by acting as 'seeds' for amyloid plaques. Our Congo Red birefringence results suggest that GSSG may possess a face complimentary to amyloid aggregates, and thereby interact with unfolding intermediates of β-amyloid protein. It is conceivable that such an interaction could help to solubilize the amyloid protein, thus serving as a defense mechanism against protein aggregation; alternatively, the interaction could promote aggregation. Interestingly, GSSG forms insoluble complexes with some physiologically relevant metals which have been suggested to promote aggregation of amyloid β-peptide (Mantyh *et al.*, 1993; Garzon-Rodriguez *et*

al., 1999; Postal *et al.*, 1985; Krezel and Bal, 1999), and at least one such GSSG-metal complex has been isolated from human tissue (Marzullo and Friedhoff, 1977).

There is also increasing interest in the function of transiently formed glutathione mixed disulfides in protein folding, which serve to direct the formation of appropriate protein disulfides in a process mediated by protein disulfide isomerase (Cotgreave and Gerdes, 1998). However, the mechanistic details of how glutathione performs this function are poorly understood. The interactions which we propose to stabilize an extended GSSG sheet (Figure 4.13) could also be formed by two glutathione-protein mixed disulfides, with the two glutathionyl moieties presenting complementary hydrogen bonding and electrostatic sites. In this manner, glutathiolation of two protein cysteine residues may provide a handle for molecular recognition of each other, in a manner analogous to the self-recognition which drives the intermolecular assembly of GSSG reported here. Human lens proteins are also frequently glutathiolated (Cotgreave and Gerdes, 1998), and the role of glutathione in the process of cataract formation and lens opacification is an area of intense research. In light of the ubiquitous nature of glutathione and its extraordinary range of physiological functions, it is possible that the remarkably specific self-assembly properties described here serve important roles in biological systems.

Notes to Chapter 4

1) The work described in this chapter has been previously published:

Lyon, Robert P. and Atkins, William M. (2001) Self-Assembly and Gelation of Oxidized Glutathione in Organic Solvents. *J. Am. Chem. Soc.* **123**, 4408-4413.

REFERENCES

Aggeli, A., Bell, M., Boden, N., Keen, J.N., McLeish, T.C.B., Nyrkova, I., Radford, S.E., & Semenov, A. (1997) Engineering of peptide β-sheet nanotapes. *J. Mater. Chem.* **7**, 1135-1145.

Aggelli, A., Bell, M., Boden, N., Keen, J.N., Knowles, P.F., McLeish, T.C.B., Pitkeathly, M., & Radford, S.E. (1997) Responsive gels formed by the spontaneous self-assembly of peptides into polymeric β-sheet tapes. *Nature* **386**, 259-262.

Ålin, P., Danielson, H., and Mannervik, B. (1985) 4-hydroxyalk-2-enals are substrates for glutathione transferase. *FEBS* **179**, 267-270.

Armstrong, R. N. (1994) Glutathione S-transferases: Structure and mechanism of an archetypical detoxication enzyme. *Adv. Enzymol. Rel. Areas Mol. Biol.* **69**, 1-44.

Armstrong, R. N. (1997) Structure, catalytic mechanism, and evolution of the glutathione transferases. *Chem. Res. Tox.* **10**, 2-18.

Barycki, J. J. and Colman, R. F. (1997) Identification of the nonsubstrate steroid binding site of rat liver glutathione S-transferase, isozyme 1-1, by the steroid affinity label, 3β-(iodoacetoxy)dehydroisoandrosterone. *Arch. Biochem. Biophys.* **345**, 16-31.

Bhargava, M. M., Listowsky, I., and Arias, I. M. (1978) Ligandin: bilirubin binding and glutathione S-transferase activity are independent processes. *J. Biol. Chem.* **253**, 4112-4115.

Cabiscol, E. and Levine, R.L. (1996) The phosphatase activity of carbonic anhydrase III is reversibly regulated by glutathiolation. *Proc. Natl. Acad. Sci. USA* **93**, 4170-4174.

Cameron, A. D., Sinning, I., L'Hermite, G., Olin, B., Board, P. G., Mannervik, B., and Jones, T. A. (1995) Structural analysis of human alpha-class glutathione transferase A1-1 in the apo-form and in complexes with ethacrynic acid and its glutathione conjugate. *Structure* **3**, 717-727.

Cheng, H., Tchaikovskaya, T, Tu, Y. L., Chapman, J., Qian, B., Ching, W-M., Tien, M., Rowe, J. D., Patskovsky, Y. V., Listowsky, I., and Tu, C-P. D. (2001) Rat glutathione S-transferse M4-4: an isoenzyme with unique structural features including a redox-reactive cysteine-115 residue that forms mixed disulphides with glutathione. *Biochem. J.* **356**, 403-414.

Cheng, Y-C. and Prusoff, W. H. (1973) Relationship between the inhibition constant (K_i) and the concentration of inhibitor which causes 50 per cent inhibition (I_{50}) of an enzymatic reaction. *Biochem. Pharm.* **22**, 3099-3108.

Chiti, F., Webster, P., Taddei, N., Clark, A., Stefani, M., Ramponi, G., and Dobson, C. M. (1999) Designing conditions for *in vitro* formation of amyloid protofilaments and fibrils. *Proc. Natl. Acad. Sci. USA* **96**, 3590-3594.

Chu, F., Ward, N. E., and O'Brian, A. (2001) Potent inactivation of representative members of each PKC isozyme subfamily and PKD via S-thiolation by the tumor-promotion/progression antagonist glutathione but not by its precursor cysteine. *Carcinogenesis* **22**, 1221-1229.

Coleman, D.L. & Blout, E.R. (1968) The optical activity of the disulfide bond in L-cystine and somre derivatives of L-cystine. *J. Am. Chem. Soc.* **90**, 2405-2415.

Come, J.H., Fraser, P.E., & Lansbury, P.T., Jr. (1993) A kinetic model for amyloid formation in the prion diseases: importance of seeding. *Proc. Natl. Acad. Sci. USA* **90**, 5959-5963.

Cotgreave, I.A. & Gerdes, R.G. (1998) Recent trends in glutathione biochemistry—glutathione-protein interactions: a molecular link between oxidative stress and cell proliferation? *Biochem. Biophys. Res. Commun.* **242**, 1-9.

Dafré, A.L., Sies, H., and Akerboom, T. (1996) Protein S-thiolation and regulation of microsomal glutathione transferase activity by the glutathione redox couple. *Arch. Biochem. Biophys.* **332**, 288-294.

Darby, N.J., Freedman, R.B., & Creighton, T.E. (1994) Dissecting the mechanism of protein disulfide isomerase: catalysis of disulfide bond formation in a model peptide. *Biochemistry* **33**, 7937-7947.

Demasi, M., Shringarpure, R., and Davies, K. J. (2001) Glutathiolation of the proteasome is enhanced by proteolytic inhibitors. *Arch. Biochem. Biophys.* **389**, 254-263.

Dirven, H. A. A. M., van Ommen, B., and van Bladeren, P. J. (1996) Glutathione conjugation of alkylating cytostatic drugs with a nitrogen mustard group and the role of glutathione S-transferases. *Chem. Res. Tox.* **9**, 351-360.

Flatgaard, J. E., Bauer, K. E., and Kauvar, L. M. (1993) Isozyme specificity of novel glutathoine S-transferase inhibitors. *Cancer Chemother. Pharmacol.* **33**, 63-70.

Garzon-Rodriguez, W., Yatsimirsky, A.K., & Glabe, C.G. (1999) Binding of Zn(II), Cu(II), and Fe(II) ions to Alzheimer's aβ peptide studied by fluorescence. *Bioorg. Med. Chem. Let.* **9**, 2243-2248.

Greco, W. R. and Hakala, M. T. (1979) Evaluation of methods for estimating the dissociation constant of tight binding enzyme inhibitors. *J. Biol. Chem.* **254**, 12104-12109.

Groß, M., Wilkins, D.K., Pitkeathly, M.C., Chung, E.W., Higham, C., Clark, A., & Dobson, C.M. (1999) Formation of amyloid fibrils by peptides derived from the bacterial cold shock protein CspB. *Protein Sci.* **8**, 1350-1357.

Guijarro, J. I., Sunde, M., Jones, J. A., Campbell, I. D., and Dobson, C. M. (1998) Amyloid fibril formation by an SH3 domain. *Proc. Natl. Acad. Sci. USA* **95**, 4224-4228.

Hanabusa, K., Miki, T., Taguchi, Y., Koyama, T., & Shirai, H. (1993) Small molecular gelling agents to harden organic liquids: alkylamide of N-benzyloxycarbonyl-L-valyl-L-valine. *J. Chem. Soc. Chem. Commun.*, 390-392.

Harper, J.D. & Lansbury, P.T., Jr. (1997) Models of amyloid seeding in Alzheimer's disease and scrapie: mechanistic truths and physiological consequences of the time-dependent solubility of amyloid proteins. *Annu. Rev. Biochem.* **66**, 385-407.

Hartgerink, J.D., Granja, J.R., Milligan, R.A., & Ghadiri, R. (1996) Self-Assembling Peptide Nanotubes. *J. Am. Chem. Soc.* **118**, 43-50.

Hayes, J.D. & McLellan, L.I. (1999) Glutathione and glutathione-dependent enzymes represent a co-ordinately regulated defence against oxidative stress. *Free Rad. Res.* **31**, 273-300.

Holmes, T.C., de Lacalle, S., Su, X., Liu, G., Rich, A., & Zhang, S. (2000) Extensive neurite outgrowth and active synapse formation on self-assembling peptide scaffolds. *Proc. Natl. Acad. Sci. USA* **97**, 6728-6733.

Howarth, O.W. & Lian, L.Y. (1982) Resolved librational motions of gramicidin-S and glutathione dimer as studied by nuclear magnetic resonance spectroscopy. *J. Chem. Soc. Perkin. Trans. II*, 263-267.

Ibarra, C., Nieslanik, B. S., and Atkins, W. M. (2001) Contribution of Aromatic-Aromatic Interactions to the Anomalous pKa of Tyrosine-9 and the C-Terminal Dynamics of Glutathione S-Transferase A1-1. *Biochemistry* **40**, 10614-10624.

Jarrett, J.T. & Lansbury, P.T., Jr. (1993) Seeding "one-dimensional crystallization" of amyloid: a pathogenic mechanism in Alzheimer's disease and scrapie? *Cell* **73**, 1055-1058.

Kamisaka, K., Listowsky, I., Gatmaitan, Z., and Arias, I. M. (1975) Interactions of bilirubin and other ligands with ligandin. *Biochemistry* **14**, 2175-2180.

Ketley, J. N., Habig, W. H., and Jakoby, W. B. (1975) Binding of nonsubstrate ligands to the glutathione S-transferases. *J. Biol. Chem.* **250**, 8670-8673.

Kirschner, D.A., Inouye, H., Duffy, L.K., Sinclair, A., Lind, M., & Selkoe, D.J. (1987) Synthetic peptide homologous to β protein fromAlzheimer disease forms amyloid-like fibrils *in vitro*. *Proc. Natl. Acad. Sci. USA* **84**, 6953-6957.

Klatt, P., Molina, E.P., and Lamas, S. (1999) Nitric oxide inhibits c-Jun DNA binding by Specifically targeted S-glutathionylation. *J. Biol. Chem.* **274**, 15857-15864.

Krejchi, M.T., Atkins, E.D.T., Waddon, A.J., Fournier, M.J., Mason, T.L., & Tirrell, D.A. (1994) Chemical sequence control of β-sheet assembly in macromolecular crystals of periodic polypeptides. *Science* **265**, 1427-1432.

Krezel, A. & Bal, W. (1999) Coordination chemistry of glutathione. *Acta Biochim. Pol.* **46**, 567-580.

Kuzmič, P., Sideris, S., Cregar, L. M., Elrod, K. C., Rice. K. D., and Janc, J. W. (2000) High-throughput screening of enzyme inhibitors: Automatic determination of tight-binding inhibition constants. *Anal. Biochem.* **281**, 62-67.

Le Trong, I., Stenkamp, R. E., Ibarra, C, Atkins, W. M., and Adman, E. T. (2002) 1.3 Å resolution structure of human glutathione S-transferase with S-hexyl glutathione bound reveals possible new binding site. *Prot. Struct. Func. Genet.*, in press.

Litwack, G., Ketterer, B., and Arias, I. M. (1971) Ligandin: a hepatic protein which binds steroids, bilirubin, carcinogens and a number of exogenous organic anions. *Nature* **234**, 466-467.

Lyttle, M. H., Hocker, M. D., Hui, H. C., Caldwell, C. G., Aaron, D. T., Engqvist-Goldstein, A., Flatgaard, J. E., and Bauer, K. E. (1994) Isozyme-specific glutathione S-transferase inhibitors: Design and synthesis. *J. Med. Chem.* **37**, 189-194.

Mannervik, B. (1985) The isoenzymes of glutathione transferases. *Advan. Enzymol. Rel. Areas Mol. Biol.* **57**, 657-417.

Mannervik, B., Awasthi, Y. C., Board, P. G., Hayes, J. D., Di Ilio, C., Ketterer, B., Listowsky, I., Moergenstern, R., Muramatsu, M., Pearson, W. R., Pickett, C. B., Sato, K., Widersten, M., and Wolf, C. R. (1992) Nomenclature for human glutathione transferases. *Biochem. J.* **282**, 305-308.

Mannervik, B. and Danielson, U.H. (1988) Glutathione transferases—structure and catalytic activity. CRC *Crit. Rev. Biochem.* **23**, 283-337.

Mantyh, P.W., Ghilardi, J.R., Rogers, S., DeMaster, E., Allen, C.J., Stimson, E.R., & Maggio, J.E. (1993) Aluminum, iron, and zinc ions promote aggregation of physiological concentrations of β-amyloid peptide. *J. Neurochem.* **61**, 1171-1174.

Marshall, A. D., Darbyshire, J. F., Hunter, A. P., McPhie, P., and Jakoby, W. B. (1997) Control of activity through oxidative modification at the conserved residue cys^{66} of aryl sulfotransferase IV. *J. Biol. Chem.* **272**, 9153-9160.

Marzullo, G. & Friedhoff, A.J. (1977) An inhibitor of opiate receptor binding from human erythrocytes identified as a glutathione-copper complex. *Life Sci.* **21**, 1559-1568.

McDuffee, A. T., Senisterra, G., Huntley, S., Lepock, J. R., Sekhar, K. R., Meredith, M. J., Borrelli, M. J., Morrow, J. D., and Freeman, M. L. (1997) Proteins containing non-native disulfide bonds generated by oxidative stress can act as signals for the induction of the heat shock response. *J. Cell. Phys.* **171**, 143-151.

McTigue, M. A., Williams, D. R., and Tainer, J. A. (1995) Crystal structures of a schistosomal drug and vaccine target: glutathione S-transferase from *Schistosoma japonica* and its complex with the leading antischistosomal drug praziquantel. *J. Mol. Biol.* **246**, 21-27.

Meister, A. (1991) Glutathione deficiency produced by inhibition of its synthesis, and its reversal; applications in research and therapy. *Pharmacol. Ther.* **51**, 155-194.

Morgan, A. S., Ciaccio, P. J., Tew, K. D., and Kauvar, L. M. (1996) Isozyme-specific glutathione S-transferase inhibitors potentiate drug sensitivity in cultured human tumor cell lines. *Cancer Chemother. Pharmacol.* **37**, 363-370.

Niitsu, Y., Takahashi, Y., Ban, N., Takayama, T., Saito, T., Katahira, T., Umetsu, Y., Nakajima, T., Ohi, M., Kuga, T., Sakamaki, S., Matsunaga, T., Hirayama, Y., Kuroda, H., Homma, H., Kato, J., and Kogawa, K. (1998) A proof of glutathione S-transferase pi-related multidrug resistance by transfer of antisense gene to cancer cells and sense gene to bone marrow stem cells. *Chem. Biol. Interact.* **24**, 325-332.

Oakley, A. J., Lo Bello, M., Nuccetelli, M., Mazzetti, A. P., and Parker, A. W. (1999) The ligandin (non-substrate) binding site of human pi class glutathione transferase is located in the electrophile binding site (H-site). *J. Mol. Biol.* **291**, 913-926.

Ohl, V. S. and Litwack, G. (1977) Selective inhibition of glutathione S-transferases by 17β-estradiol disulfate. *Arch. Biochem. Biophys.* **180**, 186-190.

Okamoto, T., Akaike, T., Sawa, T., Miyamoto, Y., van der Vliet, A., and Maeda, H. (2001) Activation of matrix metalloproteinases by peroxynitrite-induced protein S-glutathiolation via disulfide S-oxide formation. *J. Biol. Chem.* **276**, 29596-29602.

Osterman, D.G. & Kaiser, E.T. (1985) Design and characterization of peptides with amphiphilic β-strand structures. *J. Cell. Biochem.* **29**, 57-72.

Ottnad, M., Ottnad, C., Hartter, P., & Jung, G. (1973) in *Glutathione: Proceedings of the 16th Conference of the German Society of Biological Chemistry*; Flohe, L., Benohr, H.Ch., Sies, H., Waller, H.D., & Wendel, A., ed. (Georg Thieme Verlag, Stuttgart), pp. 20-28.

Pang, Y-P., Quiram, P., Jelacic, T., Hong, F., and Brimijoin, S. (1996) Highly potent, selective, and low cost bis-tetrahydroaminacrine inhibitors of acetylcholinesterase. *J. Biol. Chem.* **271**, 23646-23649.

Pinkus, R., Weiner, L. M., and Daniel, V. (1996) Role of oxidants and antioxidants in the induction of AP-1, NF-κB, and glutathione S-transferase gene expression. *J. Biol. Chem.* **271**, 13422-13429.

Ploemen, J. H. T. M., Van Ommen, B., and Van Bladeren, P. (1990) Inhibition of rat and juman glutathione S=transferase isoenzymes by ethacrynic acid and its glutathione conjugate. *Biochem. Pharmacol.* **40**, 1631-1635.

Postal, W.S., Vogel, E.J., Young, C.M., & Greenaway, F.T. (1985) The binding of copper(II) and zinc(II) to oxidized glutathione. *J. Inorg. Biochem.* **25**, 25-33.

Raj, P.A., Soni. S.D., Ramasubbu, N., Bhandary, K.K., & Levine, M.J. (1990) Crystal structure and solution conformation of S,S'-bis(BOC-cys-ala-OME): intramolecular antiparellel β-sheet conformation of an acyclic cystine peptide. *Biopolymers* **30**, 73-85.

Ramos-Gomez, M., Kwak, M., Dolan, P. M., *et al.* (2001) Sensitivity to carcinogenesis is increased and chemoprotective efficacy of enzyme inducers is lost in nrf2 transcription factor-deficient mice. *Proc. Natl. Acad. Sci. USA* **98**, 3410-3415.

Rao, J., Lahiri, J., Weis, R. M., and Whitesides, G. M. (2000) Design, synthesis, and characterization of a high-affinity trivalent system derived from vancomycin and L-lys-D-ala-D-ala. *J. Am. Chem. Soc.* **122**, 2698-2710.

Sayed, Y., Hornby, J. A. T., Marimar, L., and Dirr, H. (2002) Thermodynamics of the ligandin function of human class alpha glutathione transferase A1-1: energetics of organic anion ligand binding. *Biochem. J.* **363**, 341-346.

Schaschke, N., Matschiner, G., Zetl, F., Marquardt, U., Bergner, A., Bode, W., Sommerhoff, C. P., and Moroder, L. (2001) Bivalent inhibition of human β-tryptase. *Chem. & Biol.* 8, 313-327.

Schwartz, A.L. & Cutnell, J.D. (1983) One- and two-dimensional NMR studies of exchanging amide protons in glutathione. *J. Magn. Reson.* **53**, 398-411.

Seis, H. (1983) in *Oxidative Stress*, ed. Seis, H. (Academic Press, London), pp. 73-90.

Seis, H. (1999) Glutathione and its role in cellular functions. *Free Rad. Biol. Med.* **27**, 916-921.

Shou, M., Grogan, J., Mancewicz, J. A., Krausz, K. W., Gonzalez, F. J. Gelboin, H. V., and Korzekwa, K. R. (1994) Activation of CYP3A4: Evidence for the Simultaneous Binding of Two Substrates in a Cytochrome P450 Active Site. *Biochemistry* **33**, 6450-6455.

Sinning, I., Kleywegt, G. J., Cowan, S. W., Reinemer, P., Dirr, H. W., Huber, R., Gilliland, G. L., Armstrong, R. N., Ji, X., Board, P. G., Olin, B., Mannervik, B., and Jones, T. A. (1993) Structure determination and refinement of human alpha class glutathione transferase A1-1, and a comparison with the mu and pi class enzymes. *J. Mol. Biol.* **232**, 192-212.

Slivka, A., Spina, M.B., & Cohen, G. (1987) Reduced and oxidized glutathione in human and monkey brain. *Neurosci. Let.* **74**, 112-118.

Sluis-Cremer, N., Naidoo, N. N. Kaplan, W. H., Manoharan, H., Fahl, W. E., and Dirr, H. W. (1996) Determination of a binding site for a non-substrate ligand in mammalian cytosolic glutathione S-transferases by means of fluorescence-resonance energy transfer. *Eur. J. Biochem.* **241**, 484-488.

Tan, M.M., Corley, C.A., & Stevenson, C.L. (1998) Effect of gelation on the chemical stability and conformation of leuprolide. *Pharm. Res.* **15**, 1442-1448.

Tew, K. D. (1994) Glutathione-associated enzymes in anticancer drug resistance. *Cancer Res.* **54**, 4313-4320.

Tew K. D., Monks A., Barone L., Rosser D., Akerman G., Montali J. A., Wheatley J. B., and Schmidt D. E. Jr. (1996) Glutathione-associated enzymes in the human cell lines of the National Cancer Institute drug screening program. *Mol. Pharmacol.* **50**, 149-159.

Ueyama, N. & Araki, T. (1978) Two antiparallel tripeptide chains stabilized by an SS unit: S,S'-bis(CBZ-L-ala-L-cys-L-ala-Ome) in chloroform solution. *J. Am. Chem. Soc.* **100**, 4603-4605.

Vander Jagt, D. L., Wilson, S. P., Dean, V. L., and Simons, P. C. (1982) Bilirubin binding to rat liver ligandins (glutathione S-transferases A and B) *J. Biol. Chem.* **257**, 1997-2001.

Vargo, M. A. and Colman, R.F. (2001) Affinity labeling of rat glutathione S-transferase isozyme 1-1 by 17β-iodoacetoxy-estradiol-3-sulfate. *J. Biol. Chem.* **276**, 2031-2036.

Voyer, N. (1997) The development of peptide nanostructures. *Topics Curr. Chem.* **184**, 1-37.

Walker, J., Crowley, P., Moreman, A. D., and Barrett, J. (1993) Biochemical properties of cloned glutathione S-transferases from *Schistosoma mansoni* and *Schistosoma japonicum*. *Mol. Biochem. Parasitol.* **61**, 255-264.

Wang, C., Stewart, R.J., & Kopecek, J. (1999) Hybrid hydrogels assembled from synthetic polymers and coiled-coil protein domains. *Nature* **397**, 417-420.

Wang, R. W., Newton, D. J., Liu, N., Atkins, W. M., and Lu, A. Y. H. (2000) Human cytochrome P450 3A4: *in vitro* drug-drug interaction patterns are substrate-dependent. *Drug Metab. Disp.* **28**, 360-366.

Wang, T., Arifoglu, P., Ronai, Z., and Tew, K. D. (2001) Glutathione S-transferase P1-1 (GSTP1-1) inhibits c-Jun N-terminal kinase (JNK1) signaling through interaction with the C terminus. *J. Biol. Chem.* **276**, 20999-21003.

Ward, N.E., Pierce, D.S., Chung, S.E., Gravitt, K.R., and O'Brian, C.A. (1998) Irreversible inactivation of protein kinase C by glutathione. *J. Biol. Chem.* **273**, 12558-12566.

Waxman, D. J. (1990) Glutathione S-transferases: role in alkylating agent resistance and possible target for modulation chemotherapy—a review. *Cancer Res.* **50**, 6449-6454.

Westermark, G.T., Johnson, K.H., & Westermark, P. (1999) Staining methods for indentification of amyloid in tissue. *Methods Enzymol.* **309**, 3-25.

White, C.W., Mimmack, R.F., & Repine, J.E. (1986) Accumulation of lung tissue oxidized glutathione (GSSG) as a marker of oxidant induced lung injury. *Chest* **89** suppl., 111-113.

Wilce, M. C. J. and Parker, M. W. (1994) Structure and function of glutathione S-transferases. *Biochim. et Biophys. Acta* **1205**, 1-18.

Williams, J. W. and Morrison, J. F. (1979) The kinetics of reversible tight-binding inhibition. *Meth. Enzymol.* **63**, 437-467.

Yin, Z., Ivanov, V. N., Habelhah, H., Tew, K., and Ronai, Z. (2000) Glutathione S-transferase p elicits protection against H2O2-induced cell death via coordinated regulation of stress kinases. *Cancer Res.* **60**, 4053-7405.

Zhao, T., Singhal, S. S., Piper, J. T., Cheng, J., Pandya, U., Clark-Wronski, J., Awasthi, S., and Awasthi, Y. C. (1999) The role of human glutathione S-transferases hGSTA1-1 and hGST A2-2 in protection against oxidative stress. *Arch. Biochem. Biophys.* **367**, 216-224.

ROBERT LYON

University of Washington
Dept. of Medicinal Chemistry
Mail Stop 357610
Seattle WA 98105
206-543-0237

6826 16th Ave NE
Seattle WA 98115
206-525-9515

rplyon@u.washington.edu

EDUCATION

Ph.D., Medicinal Chemistry, University of Washington, September 2002
Dissertation title: "Enzymology at the dimer interface of glutathione S-transferase"
Advisor: Dr. William M. Atkins

B.S., Chemistry, Western Washington University, (GPA 3.5), 1995
Undergraduate research advisor: Dr. Mark Wicholas

RESEARCH EXPERIENCE

1995 – present Graduate Research Assistant, University of Washington
Advisor: Dr. William M. Atkins

- Designed, synthesized, and assayed high affinity enzyme inhibitors, including a novel class of *bis*-glutathione conjugates
- Characterized peptides and proteins by electrospray mass spectrometry, fluorescence spectroscopy, circular dichroism, and NMR

1994 – 1995 Undergraduate Research Assistant, Western Washington University
Advisor: Dr. Mark Wicholas

- Synthesized stable copper-semiquinone complexes from highly air-sensitive precursors

1994 Summer Intern, Dow Corning Corporation, Midland MI
Supervisor: Dr. Loren Durfee

- Developed method for quantification of silicone polymers in biological tissues by atomic absorption spectroscopy

AWARDS

- Recipient of National Institutes of Health Pharmacological Sciences Training Grant (1999 – present)

AFFILIATIONS

- American Chemical Society

PUBLICATIONS

Lyon, Robert P. and Atkins, William M. Novel, High Affinity Bivalent Inhibitors of Glutathione S-Transferase Isoforms A1-1 and P1-1. Manuscript in Preparation.

Lyon, Robert P. and Atkins, William M. (2002) Kinetic Characterization of Native and Cysteine 112-Modified Glutathione S-Transferase A1-1: Reassessment of Nonsubstrate Ligand Binding. *Biochemistry* **41**, 10920-10927.

Lyon, Robert P. and Atkins, William M. (2001) Self-Assembly and Gelation of Oxidized Glutathione in Organic Solvents. *J. Am. Chem. Soc.* **123**, 4408-4413.

Nieslanik, Brenda S., Dabrowski, Michael J., Lyon, Robert P., and Atkins, William M. (1999) Stopped-Flow Kinetic Analysis of the Ligand-Induced Coil-Helix Transition in Glutathione S-Transferase A1-1: Evidence for a Persistent Denatured State. *Biochemistry* **38**, 6971-6980.